

# **THE DOSIMETRY OF IONIZING RADIATION**

**Volume I**

Edited by KENNETH R. KASE

*Joint Center for Radiation Therapy  
Harvard Medical School  
Boston, Massachusetts*

**BENGT E. BJÄRNGARD**

*Joint Center for Radiation Therapy  
Harvard Medical School  
Boston, Massachusetts*

**FRANK H. ATTIX**

*Department of Medical Physics  
University of Wisconsin Medical School  
Madison, Wisconsin*



**1985**

**ACADEMIC PRESS, INC.**

**Harcourt Brace Jovanovich, Publishers**

**Orlando San Diego New York Austin**

**London Montreal Sydney Tokyo Toronto**

# Contents

LIST OF CONTRIBUTORS	vii
PREFACE	ix

## 1. Theoretical Basis for Dosimetry

*Gudrun Alm Carlsson*

I. Introduction	2
II. Energy Imparted: The Fundamental Quantity of Radiation Dosimetry	4
III. Absorbed Dose	13
IV. Detector Response	15
V. Radiometric Quantities: Mean Energy Imparted and Absorbed Dose in Terms of Vectorial Energy Fluence	19
VI. Absorbed Dose in Terms of Scalar Radiometric Quantities and Interaction Coefficients	36
VII. Cavity Theory	67
References	71

## 2. Fundamentals of Microdosimetry

*Albrecht M. Kellerer*

I. Introduction	78
II. General Concepts and Basic Quantities	79
III. The Compound Poisson Process in Microdosimetry	97
IV. Determination and Utilization of the Microdosimetric Parameters	113
V. The Straggling Problem and the Single-Event Spectrum	125
VI. Geometric Aspects of the Inchoate Distribution	137
Appendix: Algorithm for the Compound Poisson Process	154
References	158

## 3. Dosimetry for External Beams of Photon and Electron Radiation

*Andrée Dutreix and André Bridier*

I. The Detector	164
II. Dosimetry for Photon Beams	181

III. Dosimetry for Electron Beams	202
IV. Uncertainties	216
References	223
 4. Dosimetry of External Beams of Nuclear Particles	
<i>Johan J. Broerse, John T. Lyman, and Johannes Zoetelief</i>	
I. Introduction	230
II. Beam Characteristics	232
III. Dosimetry Methods	238
IV. Radiation Quality	250
V. Determination of Absorbed Dose at a Reference Point	252
VI. Treatment Planning for External Beam Therapy	264
VII. Response of Biological Dosimeters	268
VIII. <i>In Vivo</i> Dosimetry	275
IX. Conclusions	278
References	281
 5. Measurement and Dosimetry of Radioactivity in the Environment	
<i>Kurt Lidén and Elis Holm</i>	
I. Introduction	292
II. Sources of Environmental Radioactivity	294
III. General Aspects of Measurement Methods	305
IV. Analytical Procedures and Measurement of Radioactivity	310
V. Nonconventional Methods for Assessment of Radionuclides	351
VI. Discussion of Errors and the Need for Uniformity in Gathering and Reporting Data	353
VII. Estimation of Radiation Levels Received by Human Beings	357
References	364
 6. Internal Dosimetry for Radiation Protection	
<i>John R. Johnson</i>	
I. Introduction	369
II. Basic Concepts	370
III. Specific Effective Energy	376
IV. Models of Radionuclide Transport in Humans	380
V. Individual Monitoring and Dose Assessment	388
VI. Summary	406
References	406
INDEX	411

## 2

**Fundamentals of Microdosimetry***ALBRECHT M. KELLERER*

INSTITUT FÜR MEDIZINISCHE STRAHLENKUNDE  
 JULIUS-MAXIMILIANS-UNIVERSITÄT WÜRZBURG  
 WÜRZBURG, FEDERAL REPUBLIC OF GERMANY

I.	Introduction	78
II.	General Concepts and Basic Quantities	79
A.	Nature of the Problem	79
B.	Conventional Parameters	81
C.	Two Aspects of Microdosimetry	87
D.	The Inchoate Distribution of Energy Transfers	88
E.	The Stochastic Quantities and Their Distributions	90
F.	The Single-Event Distribution	93
III.	The Compound Poisson Process in Microdosimetry	97
A.	The Double Role of the Compound Poisson Process	97
B.	The Basic Equation	99
C.	An Additivity Relation and the Resulting Solution	105
D.	Relations for the Moments	107
IV.	Determination and Utilization of the Microdosimetric Parameters	113
A.	Aspects of Dosimetric and Microdosimetric Measurements	113
B.	Application of Microdosimetric Data in Radiation Protection	117
C.	Biophysical Implications of Microdosimetric Data	120
V.	The Straggling Problem and the Single-Event Spectrum	125
A.	Energy-Loss Straggling	126
B.	Comparison of the Various Random Factors	132
VI.	Geometric Aspects of the Inchoate Distribution	137
A.	Uniform and Weighted Random Sampling	137
B.	Formulas for the Associated Volume and for the Unweighted Averages	141
C.	The Random Intercept of Two Geometric Objects	143
D.	Application to Microdosimetry	146
E.	A Biophysical Model	152
	Appendix: Algorithm for the Compound Poisson Process	154
A.	Solution by Successive Convolutions	154
B.	Simulation of Specific Energy Distributions	157
	References	158

## I. Introduction

The remarkable feature of ionizing radiations is their discontinuous interaction with matter. However, absorbed dose and absorbed dose rate are defined as statistical averages that disregard the resulting random fluctuations [1]. For most radiobiological considerations these quantities therefore lose all direct meaning. The knowledge of absorbed dose may permit no statement on energy actually imparted to individual cells or to subcellular structures. The deviations are most substantial for small volumes, for small doses, or for densely ionizing radiations; in many cases the energy imparted at a given absorbed dose can be zero or it can exceed the expectation value by orders of magnitude. Additional concepts and quantities are therefore required to specify the energy concentrations in microscopic regions. This is the subject matter of microdosimetry.

The random nature of energy deposition attracted considerable attention early in the history of radiation biology; this led to the *target theory* and various related approaches. These approaches were aimed at an explanation of the shape of dose–effect relations in terms of the statistics of energy deposits that were termed *hits* and that were alternatively thought to be single ionizations [2], or events of *point heat* [3]. As a heuristic principle this interpretation was useful. The first monograph on the subject [4] still deserves attention, and some principles of target theory will be considered in Section IV. In many applications, however, the approach failed because it made only limited use of physics data or the general tools of probability theory. Absorbed dose remained the sole reference quantity. The parameters of actual interest were derived from simple formulae based on the Poisson statistics for assumed identical and statistically independent events of energy deposition.

A far more realistic treatment emerged in the work of Lea, who attempted a more detailed description of the random configurations of energy deposition in the tracks of charged particles. His monograph “Actions of Radiations on Living Cells” [5] is still a classic; the premature death of Lea (1947) interrupted a promising development.

Microdosimetry in its present sense was, however, not the result of a gradual development. Instead it is founded entirely on an original approach introduced by H. H. Rossi when he recognized the fundamental difference between absorbed dose and the corresponding random variables that need to be described by probability distributions. He and his colleagues proceeded then to develop techniques for measuring the random fluctuations of energy deposition, to construct a novel conceptional and mathematical framework, and to apply the new concepts and methods to radiobiology (see, e.g., [6–9]).

The theoretical basis of microdosimetry is treated in this chapter. Experimental techniques, numerical data, and applications are referred to for illustration of essential concepts and results. A recent report of the ICRU [10] can be consulted for additional details, for technical aspects, and for a compilation of nu-

merical data. The chapter by Rossi in the earlier, related monograph [8] retains special value as an overall introduction and as a synopsis of the essentials of the field.

## II. General Concepts and Basic Quantities

### A. NATURE OF THE PROBLEM

The theory of radiation quality has a twofold aspect. The physicist asks for a precise description of a radiation field; the biophysicist requires information on the energy distributions in microscopic structures, or on the local concentrations of the radiation-induced ionizations and subsequent radiation products.

For a description of a radiation field one can employ *radiometric quantities*, such as the fluences of the different particles and their spectral distributions in energy and direction. The computation or the experimental determination of these quantities will usually be complex, and even if they are fully known a complete description of the radiation field is not attained. Such a description would require additional information on the spatial and temporal correlation of the fluence of different secondary particles that always occurs when a primary ionizing particle interacts with matter.

To obtain information on the energy distribution in the exposed medium one requires *material constants*, such as cross sections and stopping powers, in addition to the radiometric quantities. The necessary computations may be difficult, but—provided the input information is sufficient—they are always possible, for example, by Monte Carlo simulation. A far more fundamental problem is the inherent complexity of the resultant information. The microscopic patterns of energy deposition differ so widely with different types of radiation and on different levels of spatial resolution that even the most detailed description or simulation may contribute little toward the recognition of those features and parameters that are critical for the biological effect. The purpose of microdosimetry is therefore not the unlimited generation of data, but their deliberate reduction to the most essential parameters.

The radiobiologist has always used highly simplified parameters to elucidate the role of the microscopic distribution of energy and the effectiveness of different types of ionizing radiations. The treatment in terms of linear energy transfer (LET) is an extreme simplification, but is very widely utilized and, in view of its simplicity, it has been remarkably successful. The treatment in terms of microdosimetry is more complex and far more realistic. However, it too rests on various approximations. Such approximations are acceptable when they bring out those aspects that differ for the different types of ionizing radiation; they need not take full account of features that are common to different radiations. For this reason quantities can be employed that are linked to the energy imparted without specific regard to the nature of the electronic alterations; the latter can

be assumed to be largely similar for different types of ionizing radiations. For example, there is reason to assume that excitations contribute little to the action of ionizing radiations on the cell, but this need not be reflected in the definition of microdosimetric quantities. The definitions refer only to total energy imparted. Nevertheless, the quantities remain valid because the ratio of excitations to ionizations and their spatial interrelation are similar for different radiations. Furthermore, one may note that, in contrast to their definitions, the microdosimetric quantities are experimentally determined by ionization measurements in gas. This leads to inaccuracies that are usually not critical. The spatial distribution of ionizations produced by a charged particle in tissue-equivalent gas is largely representative also of the distribution of all energy transfers along the particle's track in tissue.

A further simplification in microdosimetry results from the fact that only the tracks of *charged* particles need to be considered. All ionizing radiations work ultimately through charged particles. Electromagnetic radiations release in matter electrons and positrons, and neutrons release nuclear recoils or nuclear fragments. These charged particles produce the majority of electronic excitations and ionizations that are responsible for the biological effect. It is, therefore, sufficient to treat only the *directly ionizing*, charged particle radiation field. Because the mean free path of photons or neutrons is larger than the structures of interest in microdosimetry, it is possible to disregard any spatial correlation of charged particles even if they are produced by the same uncharged particle. An important exception is the multiplicity of electrons released in an Auger cascade. Other exceptions are  $\alpha$ - or  $\beta$ -emitting hot spots. These exceptional cases (see, e.g., [11-13]) are not treated in this chapter, but they can be of considerable radiobiological interest.

Figure 1 serves as a rough illustration of the configuration of charged particle tracks. The dots symbolize individual ionizations in tracks that are computed on the basis of random numbers. The diagrams are somewhat simplified. In particular, the track of the densely ionizing 500-keV proton is actually considerably more narrow than indicated in the diagram, where an attempt has been made to resolve the individual ionizations. Furthermore, it will be noted that the diagram fails to indicate the complex spatial orientation of tracks that occur randomly in the exposed medium. An essential point, however, is the substantial increase of the ionization density with decreasing velocity of the particle. This increase leads to considerable differences in the concentration of the energy transferred to the cell and it has evident implications for the biological effectiveness of ionizing radiations. The local fluctuations of energy deposition and the resultant complexities of energy distribution are equally important and they are the objective of the microdosimetric analysis.

There is, at present, no satisfactory method for obtaining images of tracks experimentally. Nuclear emulsions have been employed for studies of track struc-

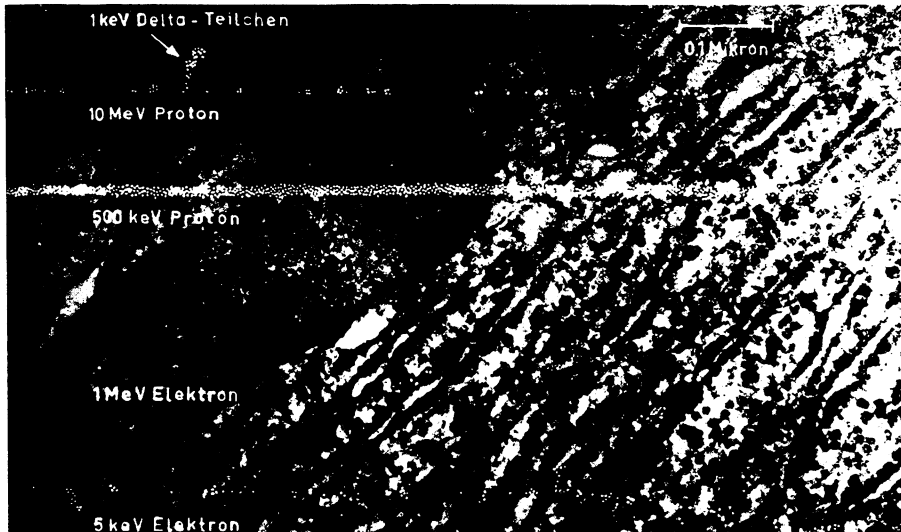


**Fig. 1.** Diagram of track segments in tissue of electrons and protons with various energies. The dots represent ionizations. The lateral extension of the track core is somewhat enlarged to permit the resolution of individual energy transfers. The length of the track segments is 1  $\mu\text{m}$ .

ture [14, 15], but they do not have sufficient resolution to represent individual ionizations. Somewhat better resolution has been obtained with the more sensitive cloud chamber, which permits a fairly accurate visualization of the tracks, at least of sparsely ionizing particles [16]. However, the only common and practicable method for obtaining geometric representations of charged particle tracks is Monte Carlo simulation on the basis of known and interpolated collision cross sections. Such studies have provided the basis for a quantitative evaluation of particle tracks. In view of the available computer codes and their descriptions (see, e.g., [17–19]) it will not be necessary to give details here. The simulated charged particle tracks can be considered as available input information.

## B. CONVENTIONAL PARAMETERS

Certain basic features of the microdistribution of energy deposition by ionizing radiations can be described in terms of conventional parameters; this facilitates the subsequent introduction of the microdosimetric concepts and their interpretation.

### 1. *Fluence*

The most important radiometric quantity is the fluence  $\phi$  of a specified type of particle. It is defined as the mean number (expectation value) of particles entering a sphere of unit cross section (diameter:  $d = 2/\sqrt{\pi}$ ). The definition is equivalent to the statement that, on the average,  $\phi/2$  particles traverse a unit

plane surface area randomly oriented, or, in a unidirectional field,  $\phi$  particles traverse a unit surface element orthogonal to the direction of the field. Another equivalent statement is that the fluence is equal to the mean total length of particle trajectories per unit volume.

Figure 2 gives the fluence per unit absorbed dose in water for monoenergetic photons, neutrons, and charged particles. The diagram shows that the fluence of uncharged particles, necessary to deliver a given dose, exceeds that of charged particles very substantially. However, a cell or a subcellular structure can be traversed by many uncharged particles without any interaction, and it is therefore the fluence of charged particles that is directly relevant to microdosimetry.

## 2. Mean Free Path and Range

Figure 3 gives the range of charged particles and the mean free path of uncharged particles in water. The mean free path of photons and neutrons is large compared to cells and cellular structures, i.e., to sites of interest in microdosimetry. The spatial correlation of charged particles set in motion by the same un-

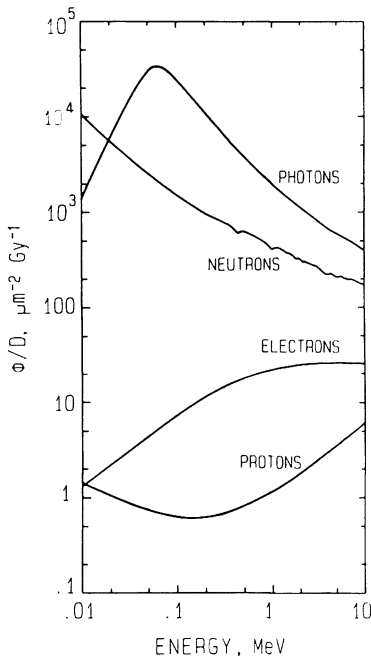


**Fig. 2.** Fluence per unit absorbed dose in water for charged and uncharged particles with specified initial energies. The fluence of the uncharged particles is always considerably larger than the fluence of the charged secondaries, for equal doses. Charged particle equilibrium is assumed to exist for the uncharged particle fields.

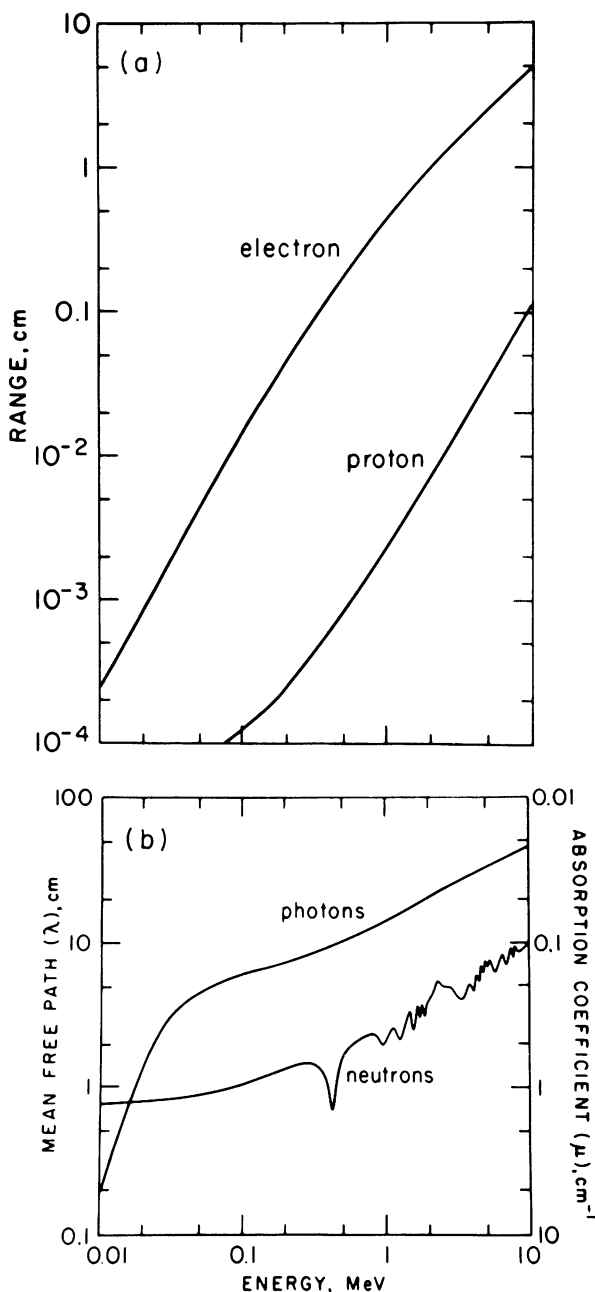


**Fig. 3.** (a) Range of electrons and protons and (b) mean free path of photons and neutrons of specified energy in water. (From Kellerer and Rossi [41].)

charged particle can therefore, as stated in the preceding paragraph, be disregarded in most microdosimetric considerations. The plot of the ranges of charged particles can be utilized to judge whether the particle ranges are large compared with the structures of interest, a condition of considerable importance for the considerations of Section V.

There are various definitions of the range of charged particles; they differ most substantially for electrons, because electrons are subject to considerable energy-loss straggling and angular scattering. The range in Fig. 3 is an integrated range, i.e., the mean total length of the trajectory of the particle.

### 3. Linear Energy Transfer (LET)

Linear energy transfer (LET), or collision stopping power, is defined as  $L = dE/dx$ , where  $dE$  is the mean energy lost by a charged particle in electronic collisions along an element  $dx$  of its trajectory. The value of  $L$  depends on the energy of the particle (see Fig. 4), and in the usual case of a mixed radiation field one deals with a distribution of  $L$  in the exposed material. To characterize a radiation by a single parameter one has to utilize a mean value of LET, but such a mean value may provide little useful information on the radiation field. Moreover there are two common ways to specify LET distributions, and accordingly two different mean values. It is instructive to consider the distinction because it has its correspondence with microdosimetric functions (see Section II, F).

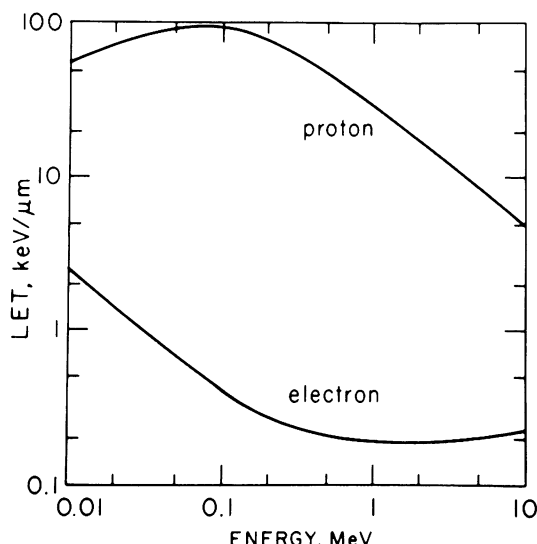


**Fig. 4.** Linear energy transfer (LET) for electrons and protons in water as a function of their energy. (From Kellerer and Rossi [41].)

The *frequency distribution* of LET is defined in terms of total track length of the charged particles or, equivalently, in terms of the particle fluence. The *distribution function* (or *sum distribution*)  $F(L)$  is the fraction of total track length, i.e., the fraction of fluence, that is associated with linear energy transfer not larger than  $L$ :

$$F(L) = \phi_L / \phi \quad (1)$$

where  $\phi$  is the total fluence and  $\phi_L$  is the fluence of particles with LET not exceeding  $L$ .

For electrons there is the obvious difficulty that it is unclear whether secondary electrons, i.e.,  $\delta$  rays, are to be included in the definitions. A possible convention is to include only those electrons, regardless of whether they are primaries or secondaries, that exceed a certain threshold energy. A suitably restricted LET value must then be applied. This will be considered later in this subsection, where it will also be pointed out that the LET concept is, for additional reasons, particularly problematic for electrons.

The density of LET in track length or fluence is denoted by  $f(L) = dF(L)/dL$ . The *track (or frequency) average* is the mean value that corresponds to the distribution:<sup>\*</sup>

$$\bar{L}_F = \int L f(L) dL = \int [1 - F(L)] dL \quad (2)$$

The *dose distribution* (or *weighted distribution*) of LET is defined in terms of the absorbed dose delivered by particles of specified LET. The distribution function  $D(L)$  is the fraction of absorbed dose due to particles with linear energy transfer not larger than  $L$ :

$$D(L) = D_L / D \quad (3)$$

where  $D$  is the total absorbed dose, and  $D_L$  is the absorbed dose due to particles with LET not exceeding  $L$ .

The corresponding density of LET in dose is denoted by  $d(L) = dD(L)/dL$ . The *dose average* (or *weighted average*) is

$$\bar{L}_D = \int L d(L) dL = \int (1 - D(L)) dL \quad (4)$$

The dose distribution of LET is related to the frequency distribution:

$$d(L) = L f(L) / \bar{L}_F \quad (5)$$

\*The indices F and D are used in this chapter for *frequency* averages and *dose* (or *energy*)-weighted averages of various distributions. The densities and weighted densities are designated by  $f(\cdot)$  and  $d(\cdot)$ . This notation is a compromise with common usage. In the more mathematical treatment of Section III, D and in the discussion of the straggling problem a different notation is used; for example, the frequency mean and the weighted mean of the collision spectrum are denoted by  $\delta_1$  and  $\delta_2$  rather than by  $\delta_F$  and  $\delta_D$ .

Accordingly one can express the dose average LET in terms of the first two moments of  $f(L)$ :

$$\bar{L}_D = \overline{\bar{L}_F^2} / \bar{L}_F \quad (6)$$

For any distribution the variance equals the second moment minus the square of the first moment. Thus one obtains for the variance and for the relative variance:

$$\sigma_L^2 = \overline{\bar{L}_F^2} - \bar{L}_F^2 \quad (7)$$

$$V_L = \sigma_L^2 / \bar{L}_F^2 = (\bar{L}_D / \bar{L}_F) - 1 \quad (8)$$

It follows that the dose average is always larger than the frequency average, the difference being proportional to the variance of  $f(L)$ :

$$\bar{L}_D - \bar{L}_F = (\overline{\bar{L}_F^2} - \bar{L}_F^2) / \bar{L}_F = \sigma_F^2 / \bar{L}_F \quad (9)$$

In spite of its complexities the LET concept can, at best, provide a crude characterization of the charged particle tracks that occur in the exposed medium. Three features are essential in describing charged particle tracks:

- (1) The finite range of the particles and the change of LET along the track.
- (2) The lateral extension of the particle tracks due to the finite range of  $\delta$  rays.
- (3) The statistical fluctuation of energy loss along the particle track, often termed *energy-loss straggling*.

All three features, and others, e.g., the angular scattering, are disregarded in the LET concept. Only the second point is sometimes taken into account by consideration of a restricted LET, i.e., a stopping power that includes only collisions with energy transfer below a specified cutoff [21]. However, this modification is of doubtful value; one requires a set of LET distributions that belong to different cutoff values but one gains little information about the actual structure of particle tracks.

If a charged particle traverses a spherical reference volume of diameter  $d$ , the mean chord length is  $2d/3$  and one would, therefore, expect the energy loss  $\frac{2}{3}Ld$ . However, the actual energy losses can deviate substantially from this value. A quantitative evaluation [22] shows that the LET concept is never adequate for electrons; there are no sites sufficiently small to disregard the finite range of the electrons and at the same time sufficiently large to discount the energy-loss straggling and lateral escape of  $\delta$  rays. For heavy ions, on the other hand, there are site sizes and particle energies for which the LET concept predicts adequately the energy deposition. But even in this case the LET is of limited value since it permits no statement on the energy distribution within the sites, although this distribution can differ substantially for particles that have the same LET but different velocities.

These limitations of the LET concept illustrate the need for a treatment that is based on random variables rather than statistical expectation values. This has been the historical root of microdosimetry. The spherical proportional counters that are now the main tool of microdosimetry were first utilized in the attempt to measure LET spectra in various radiation fields. In the course of these experiments Rossi realized the inherent impossibility of determining exact LET distributions. Microdosimetry originated when he recognized that the seemingly inadequate response of the detectors was, in fact, superior to the information originally sought. Not the values of LET, but the actual energy concentrations determine the biological effect. These energy concentrations need therefore to be analyzed.

### C. TWO ASPECTS OF MICRODOSIMETRY

The spatial patterns of energy deposition in the tracks of charged particles and the resulting biological effectiveness of radiations can be regarded from two different points of view. This needs to be explained before the definitions of basic quantities are considered.

The concept that has been utilized first and that is still most familiar involves certain sensitive structures (*sites*) in the cell, and postulates that the biological effect is determined by the amount of energy deposited in these structures. In a first approximation the spatial distribution of energy within the site is often disregarded, although it must evidently codetermine the effectiveness of the energy imparted. For any considerations in terms of the site concept one requires the probability distribution, and certain expectation values, of energy imparted in the specified structures (see Section II, E). Of equal importance is the probability distribution of energy imparted if exactly one particle and/or its associated particles affect the site (see Section II, F). The probability distributions of energy imparted depend on size and shape of the structure and on the type of radiation.

Energy imparted and its probability distributions can be determined, for any radiation field, with walled or wall-less proportional counters developed for this purpose. Such detectors, termed *Rossi counters*, simulate spherical or cylindrical tissue regions with linear dimensions not less than fractions of a micrometer (see, e.g., [10, 23]). It is essential that microdosimetry has been developed in terms of quantities that are readily measurable, even for an unknown radiation field. These quantities have remained the conventional basis of microdosimetry. In the present chapter, too, most definitions and a major part of the theoretical considerations relate to functions and parameters linked to the *site concept*.

Microdosimetry and microdosimetric quantities are, however, not limited to the site concept or to the notion of energy imparted to certain structures. With the advancement of computational methods and the availability of Monte Carlo simulations of charged particle tracks a more general view has been adopted and

new methods were sought to quantitate or parametrize the microgeometric patterns of energy deposition. While there is, of course, an unlimited variety of possible approaches, one can make the rough distinction between methods that relate the random pattern of energy deposits to a site, i.e., a spatial "probe," and methods that characterize the pattern in terms of spatial interrelations that do not refer to a reference geometry but only to the spatial structure of the track itself. Parameters obtained by this latter method remain meaningful even in a uniform extended medium.

The site concept and the measurements with microdosimetric detectors correspond to the first class of approaches. The LET concept is perhaps the simplest example of the second method. More sophisticated descriptions in terms of the *proximity concept* utilize the notion of the distribution of distances between energy transfers. It is evident that the spatial proximity of energy transfers governs the probabilities of interactions, according to the lifetime and the mobility of radiation products such as free radicals or, on a more complex scale, of macromolecular lesions. Concepts, such as the *proximity function* [10, 24], have therefore extended the application of microdosimetry to radiation chemistry [25] and radiation biology [26, 27]. The novel approaches cannot be adequately treated within this chapter—and some of the results still lack a satisfactory mathematical basis. Some essentials are, however, explained in Section VI. The same section gives the fundamental interrelation that links essential quantities for the site and the proximity concepts.

#### D. THE INCHOATE DISTRIBUTION OF ENERGY TRANSFERS

For all geometric considerations in microdosimetry the notion of the *inchoate distribution of energy transfers* is essential. It can also help to clarify the definition of the conventional microdosimetric quantities, and it is therefore introduced here.

A convention on terminology is required first. The term *ionizing particle* is subsequently used for a particle with kinetic energy exceeding a specified threshold. The threshold energy will depend on the type of particle and the exposed material, but the choice of the numerical value is not of concern for the present considerations. It is sufficient that appropriate values can be selected for specific circumstances, and one may note that the selected value need not strictly conform to the actual threshold for ionizations in the material.

Ionizing charged particles undergo interactions and lose energy at certain points in the exposed medium. The point of interaction is termed a *transfer point*. The particle of kinetic energy  $E_1$  can be stopped at the transfer point or it can emerge with reduced kinetic energy  $E_2$ . It will be treated as an emerging particle only if its kinetic energy still exceeds the specified cutoff. The interaction may also produce one or more secondary ionizing particles with kinetic

energies  $E_3$ ,  $E_4$ , etc. If no ionizing particle emerges from the point of interaction, the point is the end of a charged particle track or of one of its branches. The various possibilities are exemplified in the diagram of Fig. 5.

At any transfer point  $T_i$ , the *energy transfer*  $\epsilon_i$  is the energy that has left the field of ionizing radiations, i.e., it equals the kinetic energy of the incoming particle minus the kinetic energy of all emerging ionizing particles.\*

In an exposed medium a random configuration of transfer points occurs. The term *particle track* is used for the configuration of transfer points and of associated charged particles. The entire constellation of transfer points in the exposed medium has been called the *inchoate distribution* (of *energy transfers*) [24]. The term *inchoate* refers to the fact that this is the incipient distribution before the subsequent processes of further energy degradation.

The notion of the inchoate distribution of energy transfers is particularly pertinent to microdosimetric computations, because any microdosimetric variable and its probability distribution can be determined from repeated random realizations of inchoate distributions or from multiple sampling of a sufficiently extended inchoate distribution. This will be dealt with in Section VI.

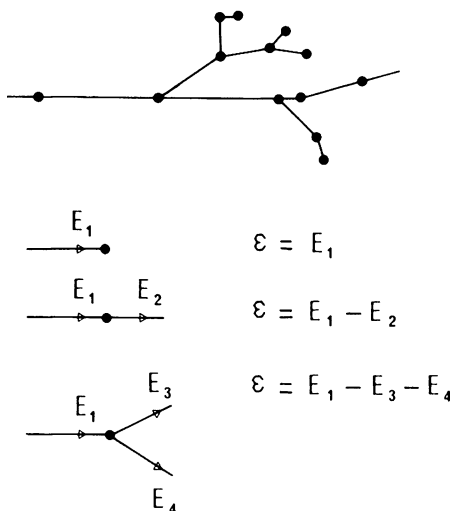


**Fig. 5.** Schematic diagram of a segment of a charged particle track with indication (●) of the transfer points and the corresponding energy transfers ( $\epsilon_i$ ).

\*A rigorous definition has to account also for possible changes of rest mass. In the interest of brevity it is here omitted; it is sufficient to note that it is analogous to the formulation in the definition of absorbed dose [1, 28].

### E. THE STOCHASTIC QUANTITIES AND THEIR DISTRIBUTIONS

*Energy imparted*  $\epsilon$  is the sum of all energy transfers within a specified site  $S$ . It is a random variable and its relative fluctuations are greatest for small sites, for densely ionizing radiations, and for small doses.

$$\epsilon = \sum \epsilon_i \quad (\epsilon_i \text{ in } S) \quad (10)$$

Energy imparted has a uniquely defined value in a specified region after an exposure has taken place. The values vary with repeated irradiations, and predictions can be made only on the basis of probability distributions.

A closely related quantity is the *specific energy*. The specific energy  $z$  is defined as the energy imparted divided by the mass  $m$  of the specified region:

$$z = \epsilon/m \quad (11)$$

Although  $z$  and  $\epsilon$  are closely related quantities, it is often more convenient to use  $z$  because it is the random analog of absorbed dose  $D$ . In many radiobiological applications one utilizes the energy unit keV and expresses the mass as the product of the volume  $V$  in cubic micrometers and the density  $\rho$  in grams per cubic centimeter. One has then the relation

$$z \text{ (Gy)} = 0.1602 \frac{\epsilon \text{ (keV)}}{V \text{ (\mu m}^3\text{)} \cdot \rho \text{ (g/cm}^3\text{)}} \quad (12)$$

or for a spherical site of diameter  $d$

$$z \text{ (Gy)} = 0.306 \frac{\epsilon \text{ (keV)}}{[d \text{ (\mu m)}]^3 \cdot \rho \text{ (g/cm}^3\text{)}} \quad (13)$$

The probability *distribution function* (or *sum distribution*) of  $z$  at an absorbed dose  $D$  is denoted by  $F(z; D)$ :

$$F(z; D) = P(\underline{z} \leq z \mid D) \quad (14)$$

i.e., the distribution function is equal to the probability that the random variable  $\underline{z}$  does not exceed  $z$  at an absorbed dose  $D$ .

The probability density (or differential distribution)  $f(z; D)$  of  $z$  is the derivative of  $F(z; D)$ :

$$f(z; D) = dF(z; D)/dz \quad (15)$$

The definitions of the distributions for energy imparted are entirely analogous and therefore need not be stated. The same applies to other subsequent considerations that are formulated in terms of specific energy but can equally be given for energy imparted.

Sum distribution and probability densities of specific energy are illustrated by a numerical example in Figs. 6 and 7. The distributions are computed from the

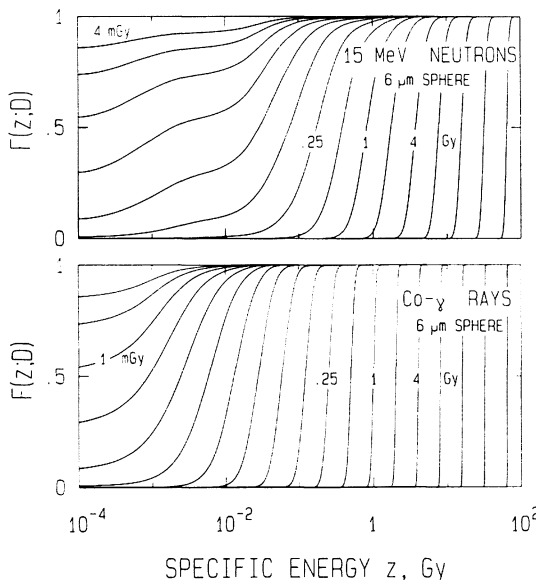


**Fig. 6.** Sum distributions  $F(z; D)$  of specific energy in a tissue sphere of 6- $\mu\text{m}$  diameter and unit density exposed to different doses of  $^{60}\text{Co}$   $\gamma$  rays and to 15-MeV neutrons. This and subsequent figures are based on data by Kliauga and Dvorak [66] for  $^{60}\text{Co}$   $\gamma$  rays and on data by Booz and Coppola [61] for neutrons. The distributions are calculated by the algorithm of successive convolutions that is explained in Section III and the Appendix.

single-event distributions that are introduced in the next subsection. The computational procedures and their theoretical basis are considered in Section III and the Appendix. One may note that dose-dependent distributions  $f(z; D)$  were obtained experimentally in the early microdosimetric studies [29] before the computational procedures were developed.

The function  $f(z; D)$  determines the probability for a specified value  $z$  of the specific energy at the absorbed dose  $D$ , i.e.,  $f(z; D) dz$  is the probability that the specific energy assumes a value between  $z$  and  $z + dz$ . At low doses the relative fluctuations are large, and it is then impractical to represent the distributions on a linear scale. Accordingly one uses, as in Figs. 6 and 7, a logarithmic scale. On a logarithmic scale the densities are transformed; one must plot the dimensionless quantity

$$dF(z; D)/d \ln z = z \cdot f(z; D) \quad (16)$$

This transformed density is properly normalized with respect to the natural logarithm of  $z$ . Normalization relative to the base-10 logarithm would require an additional numerical factor  $\ln(10) \sim 2.30$ .

There is always a finite probability  $F(0; D)$  for  $z = 0$ . Whenever this probability cannot be disregarded, a  $\delta$ -function  $F(0; D) \cdot \delta(z)$  has to be included in  $f(z; D)$ . When the densities are given on a logarithmic scale of  $z$ , this discrete com-

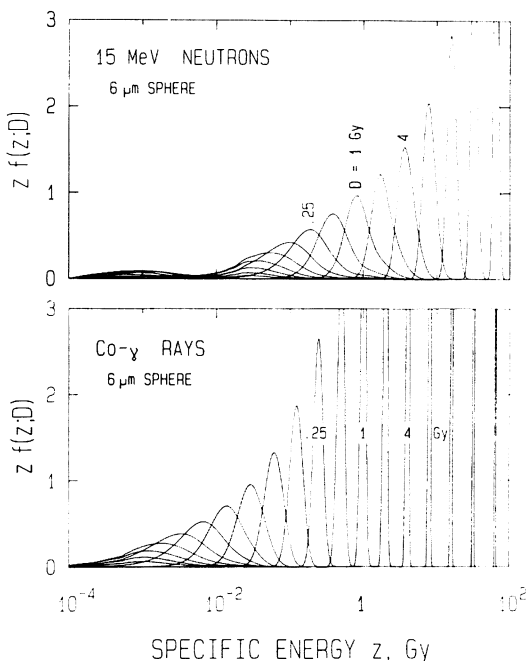


**Fig. 7.** Densities of specific energy that correspond to the sum distributions in Fig. 6.

ponent at  $z = 0$  cannot be represented. However, at low doses the area under the curves is less than unity, and, as in Fig. 7, the defect of the area indicates the magnitude of the  $\delta$  function.

The average (expectation value) specific energy in a site

$$\bar{z} = \int_0^\infty z f(z; D) dz = \int_0^\infty [1 - F(z; D)] dz \quad (17)$$

is equal to the absorbed dose  $D$  when the site is uniform and is exposed to a uniform radiation field. Otherwise  $\bar{z}$  equals the average absorbed dose in the site. Under nonuniform conditions a rigorous definition of absorbed dose must be given in terms of the limit value:

$$D = \lim_{m \rightarrow 0} \bar{z} \quad (18)$$

This relation illustrates the fact that the random variable  $z$  and its probability distribution are more fundamental than the absorbed dose.

For a specified reference site and a specified radiation one deals with functions,  $F(z; D)$  or  $f(z; D)$ , of two variables. In practice, it is rarely necessary to utilize the explicit functions; essential biophysical and radiobiological arguments can instead be based on a few parameters of these distributions (see Sec-

tion IV). In those cases where the explicit distributions are required, they can be derived from the probability distributions of specific energy produced in individual events of energy deposition. These distributions are considered next.

#### F. THE SINGLE-EVENT DISTRIBUTION

An *event* in a site is energy deposition due to particles that are statistically correlated [1]. If, for example, an  $\alpha$ -particle passes outside a reference region and injects a number of  $\delta$  rays, these  $\delta$  rays belong to the same event in the site. Similarly electrons of an Auger cascade contribute to the same event. Two recoils released by the same neutron, or two electrons liberated by one photon, are also correlated, but, as pointed out earlier, their spatial separation is usually so large that they are unlikely to appear in the same microscopic site.

The *single-event distribution* is denoted by  $F_1(z)$  and  $f_1(z)$ :

$$F_1(z) = P(z < z \mid \nu = 1) \quad \text{and} \quad f_1(z) = dF_1(z)/dz \quad (19)$$

The specification  $\nu = 1$  indicates that  $F_1(z)$  and  $f_1(z)$  are the distributions of specific energy under the condition that exactly one event has taken place in the site. It must be noted that the single-event distributions do not contain a discrete component at  $z = 0$ . By definition, an event requires energy deposition; the mere passage of a charged particle without energy transfer to the site is therefore not counted as an event.

The single-event distributions for energy imparted are defined in an analogous way. There is, furthermore, a related variable that has, originally in somewhat different form, been introduced by Rossi and colleagues as the random analog to LET. The *lineal energy*  $y$  is defined as the energy imparted in one event divided by the *mean chord length*  $\bar{l}$  that results from the random interception of the site by a straight line:<sup>\*</sup>

$$y = \epsilon/\bar{l} \quad (20)$$

The mean chord length is equal to  $4V/S$  for a convex site of volume  $V$  and surface  $S$  (see, e.g., [30–32])<sup>†</sup>

It is customary to give  $y$  in kilo-electron-volts per micrometer. For the density  $\rho = 1 \text{ g/cm}^3$ , as often assumed in radiobiological applications, one has the re-

\*The utilization of the mean chord length  $\bar{l}$  in the definition of  $y$  is somewhat arbitrary, because  $\bar{l}$  is the mean value for one special type of randomness, i.e., uniform isotropic randomness. Other types of randomness exist and are associated with other mean chord lengths (see Section VI).

<sup>†</sup>For a spherical site of diameter  $d$  one has  $\bar{l} = 2d/3$ ; for a circular cylinder of diameter  $d$  and height  $h$  the mean chord length is  $\bar{l} = 2dh/(d + 2h)$ ; for a spheroid with two axes  $d$  and one smaller axis  $(e \cdot d)$  one has, with  $\epsilon = \sqrt{1 - e^2}$ , the mean chord length  $\bar{l} = d/[1/2e + \ln(1/e + \epsilon^2)/2\epsilon]$  (see also Section V, B, Fig. 24).

lation between the specific energy and the lineal energy in a sphere of diameter  $d$ :

$$z \text{ (Gy)} = 0.204 \frac{y \text{ (keV}/\mu\text{m)}}{[d \text{ (\mu m)}]^2} \quad (21)$$

The definition of  $y$  is restricted to energy imparted in one event; this conventional restriction appears reasonable because  $y$  is the random analog of LET.

The single-event distributions of lineal energy are largely equivalent to the single-event distributions of specific energy. The values of the sum distributions are equal for corresponding values of  $z$  and  $y$ :‡

$$F(y) = F_1(z) \quad (22)$$

The relation is somewhat more complex for the corresponding densities. For a site of density  $\rho = 1 \text{ g}/\text{cm}^3$  with volume  $V$  and surface area  $S$  one has

$$f(y) = (V/\bar{l}) f_1(z) = (S/4) f_1(z) \quad (23)$$

where the last equality applies to convex sites.

In the convenient logarithmic representation, considered in the preceding subsection, the densities of specific energy and lineal energy are equal and can be represented in the same plot. Characteristic single-event spectra are represented in Fig. 8. They are given in terms of the weighted distributions that are introduced later in this section [see Eq. (27)]. One of the striking features of these distributions is the wide range of values assumed by the random variable. Narrow distributions result only if low-energy monoenergetic photons release photoelectrons in a site with linear dimensions substantially larger than the electron ranges. In the typical cases of very broad single-event distributions it is always appropriate to utilize a logarithmic scale of  $\epsilon$ ,  $z$ , or  $y$ , and the density must then be transformed, as explained in the preceding section.

The single-event distributions are of far greater pragmatic importance than the dose-dependent distributions. Because individual events are statistically independent it is sufficient to derive, experimentally or computationally, the single-event distributions. The dose-dependent distributions can then be computed, as will be explained in subsequent sections. These sections will also deal in some detail with the *moments* of the microdosimetric distributions. However, the most essential results will first be given without derivation, so that they are accessible without the need to penetrate the mathematical treatment.

The average specific energy produced by an event in the site is

$$\bar{z}_F = \int_0^\infty z f_1(z) dz = \int_0^\infty (1 - F_1(z)) dz \quad (24)$$

\*The index 1 is not required with the distribution of  $y$ , because  $y$  relates by definition only to a single event.

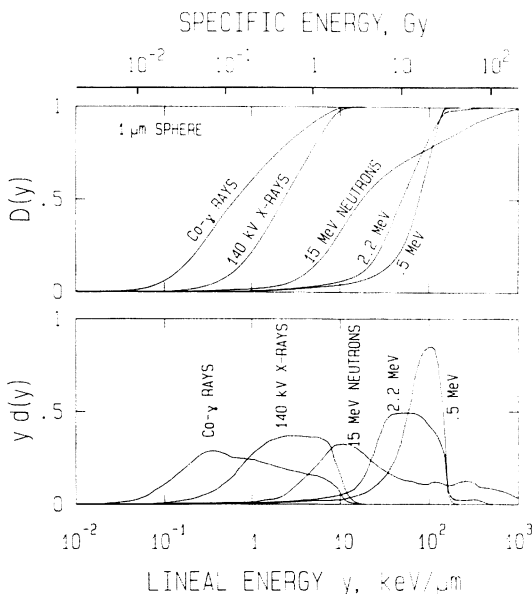


**Fig. 8.** Distributions of lineal energy in spherical tissue regional of 1- $\mu\text{m}$  diameter exposed to various radiations. In the lower panel the distributions are represented as dose-weighted densities  $y d(y)$  relative to a logarithmic scale of lineal energy  $y$ . These spectra determine the fraction of absorbed dose delivered per unit logarithmic interval of lineal energy. In the upper panel the corresponding sum distributions  $D(y)$  are given, and they specify the fraction of events up to a lineal energy  $y$ . On top of the upper panel an additional abscissa is given for the specific energy  $z$ . Relative to this scale the curves in the lower panel are the weighted densities  $z d_1(z)$  of specific energy in single events; the curves in the upper panel are the sum distributions  $D_1(z)$  of specific energy in single events.

The index F is used to distinguish this *frequency* average from the *weighted* average that plays a considerable role in many applications of microdosimetry and that will be considered later in this section.

The average specific energy at the absorbed dose  $D$  is the product of the mean event size  $\bar{z}_F$  and the mean number  $\bar{v}$  of events. But it is also equal to  $D$ :

$$\bar{z}_F \bar{v} = \bar{z}(D) = D \quad (25)$$

It follows that the average number  $\bar{v}$  of events is equal to  $D/\bar{z}_F$ . In particular, one concludes that the event frequency per unit absorbed dose is

$$\phi(0) = 1/\bar{z}_F \quad (26)$$

Knowledge of the event frequencies permits general and important conclusions in radiobiological applications (see Section IV, B). Table I gives a synopsis of event frequencies for several site diameters and different types of ionizing radiations.

TABLE I

EVENT FREQUENCIES ( $\phi$ ) PER GRAY IN SPHERICAL TISSUE REGIONS  
EXPOSED TO DIFFERENT RADIATIONS

Diameter of critical region $d$ ( $\mu\text{m}$ )	Type of radiation			
	$^{60}\text{Co}$ $\gamma$ rays	0.43 MeV	5.7 MeV	15 MeV
12	2000	55	51	61
5	360	4.2	8.6	11
2	58	0.39	1.2	1.6
1	12	0.08	0.32	0.38
0.5	1.7	0.02	0.073	0.09

In analogy to the frequency mean event size of specific energy one can define the frequency mean lineal energy  $\bar{y}_F$ . The quantity is related to  $\bar{z}_F$  according to Eq. (21).

The frequency mean lineal energy is largely analogous to the frequency mean LET introduced in Section II, B. When energy-loss straggling and the lateral escape of  $\delta$  rays out of the reference region play no role and when the range of the ionizing particle is sufficiently large, the two mean values  $\bar{L}_F$  and  $\bar{y}_F$  are approximately equal.

In analogy to the definitions of the LET distributions one can consider weighted distributions of lineal energy or of specific energy:

$$d(y) = y f(y)/\bar{y}_F \quad d_i(z) = z f_i(z)/\bar{z}_F \quad (27)$$

The weighted distributions are also termed *dose distributions*. They determine the fractions of absorbed dose or of energy imparted that are associated with certain values of  $y$  or  $z$ , and they are therefore relevant to all considerations of the effectiveness of radiation as a function of local energy concentration in microscopic sites.

The mean values of the weighted distributions are

$$\begin{aligned} \bar{y}_D &= \int y d(y) dy = \int y^2 f(y) dy / \bar{y}_F = \bar{y}_F^2 / \bar{y}_F \\ \bar{z}_D &= \int z d_i(z) dz = \int z^2 f_i(z) dz / \bar{z}_F = \bar{z}_F^2 / \bar{z}_F \end{aligned} \quad (28)$$

The variance of any distribution is equal to the second moment minus the square of the mean,

$$\sigma_F^2(y) = \bar{y}_F^2 - \bar{y}_F^2 \quad (29)$$

From this and the analogous relation for  $z$  one concludes that the dose averages  $\bar{y}_D$  and  $\bar{z}_D$  are always larger than the frequency averages  $\bar{y}_F$  and  $\bar{z}_F$ . Furthermore one has, again in analogy to the corresponding relation for LET (see Section II, B),

$$\sigma_F^2(y) = (\bar{y}_D - \bar{y}_F) \cdot \bar{y}_F, \quad \sigma_F^2(z) = (\bar{z}_D - \bar{z}_F) \cdot \bar{z}_F \quad (30)$$

The relative variance is equal for  $f(y)$  and  $f_1(z)$ :

$$V_1 = (\bar{y}_D/\bar{y}_F) - 1 = (\bar{z}_D/\bar{z}_F) - 1 \quad (31)$$

A less evident but equally fundamental relation links the second moment of the dose-dependent distributions  $f(z; D)$  of specific energy with the two first moments of the single-event distribution  $f_1(z)$ :

$$\bar{z}_F^2 = (\bar{z}_D + D)D \quad (32)$$

This relation will be derived in Section III, D; it is essential to the analysis of radiobiological mechanisms that depend on the square of specific energy. The relation is also important in dosimetry because it yields the relation for the variance of specific energy at a certain value of absorbed dose:

$$\sigma_z^2 = \bar{z}_F^2 - \bar{z}_F^2 = \bar{z}_D \cdot D \quad (33)$$

The relative standard deviation of  $z$  is therefore

$$\sigma_z/D = \sqrt{\bar{z}_D/D}, \quad \text{since } \bar{z}_F = D. \quad (34)$$

Applications of these relations are discussed in Section IV.

### III. The Compound Poisson Process in Microdosimetry

#### A. THE DOUBLE ROLE OF THE COMPOUND POISSON PROCESS

When a microscopic site is exposed to a radiation field, events of energy deposition occur in a random sequence. According to ICRU definition [1] the events are statistically independent: each individual event can be due to the appearance of one or several correlated charged particles in the site with consequent energy deposition. Frequently one deals with the simple case where independent charged particles traverse the site in straight random paths, and this situation is schematically represented in the left-hand panel of Fig. 9. During the time interval that corresponds to a specified absorbed dose  $D$  events occur randomly, and if the mean specific energy per event is  $\bar{z}_F$  the expected number of events is, as pointed out in the preceding subsection,  $\bar{v} = D/\bar{z}_F$ . The actual number  $v$  of events is subject to statistical fluctuations and, because the events are independent, it follows a Poisson distribution. Accordingly, if the event frequency per unit absorbed dose  $1/\bar{z}_F$  is known and if one is interested merely in

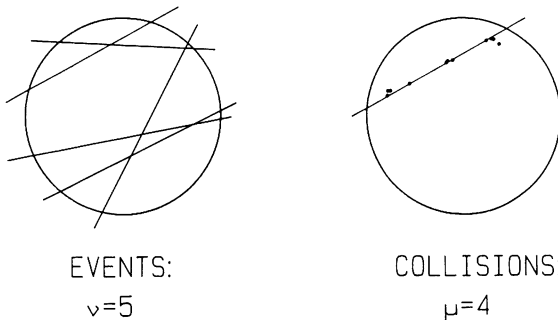


**Fig. 9.** Schematic diagram that indicates the double role of the compound Poisson process for the energy deposition in a site at specified dose. In the left panel  $\nu$  events are represented that correspond to statistically independent traversals of charged particles. In the right panel one of the events is selected and is represented as a sequence of  $\mu$  statistically independent collision processes along the particle track.

the number of events, one deals with a simple Poisson process. The probabilities for 0 events, for 1 event, or for any specified number of events can then be readily calculated.

The assessment of energy imparted is, however, far more complex because the energy imparted per event varies widely. As is apparent from the examples in Fig. 8, typical single-event distributions span several orders of magnitude of the random variable. The statistical fluctuations of energy imparted to a site are, in fact, predominantly determined by the varying amount of energy imparted per event. As will be shown in Section V, B, the fluctuations of the number of events, although they are always present, are far less consequential. It is therefore the essential feature of energy imparted that it results from a *mixed* (or *compound*) Poisson process, i.e., a process of independent events of varying magnitude. Formally this can be expressed by the relation

$$\epsilon = \sum_{i=1}^{\nu} \epsilon_i \quad (35)$$

The  $\epsilon_i$  are the energies imparted in individual events.  $\nu$  is the number of events, which follows the Poisson distribution. The subsequent section deals with the mathematical and numerical essentials of the compound Poisson process. Basic parameters of the dose-dependent distributions of energy imparted or specific energy in a site will be expressed in terms of the corresponding parameters of the single-event distributions. Furthermore, the explicit relation between the dose-dependent distributions and the single-event distributions will be treated, and the computational procedure will be described that can be utilized to derive the dose-dependent distributions from the single-event distributions.

The compound Poisson process is treated with emphasis on the mathematical relations rather than on the connection between single-event distributions and dose-dependent distributions. This is done because the compound Poisson

process plays a double role in microdosimetry. It applies equally to another step in the chain of random events, namely, the statistical sequence of energy losses of a charged particle traversing the site. This process, commonly termed *energy-loss straggling*, is treated in Section V, and it will be seen that the same mathematical relations and the same numerical procedures link, on the one hand,  $f(z; D)$  with  $f_i(z)$  and, on the other hand, the distribution of energy lost by a particle along a track segment with the distribution of energy losses in individual collisions.

The left panel of Fig. 9 indicates the events, i.e., the passages of charged particles, merely as line segments. On the right panel one such event is selected and is represented as a succession of *collision events*, i.e., energy losses by the charged particle. The collisions may result in excitations, individual ionizations, or  $\delta$  rays.

If the track segment within the site is much shorter than the range of the particle, any variations of LET of the particle within the site can be disregarded. As an important consequence the collisions along the track segment can be treated as independent. The number  $\mu$  of collisions is then again subject to the Poisson distribution. Its expectation value  $\bar{\mu}$  is proportional to the length of the segment and to the stopping power of the particle and is inversely proportional to the average energy imparted to the site in a collision. The Poisson fluctuations of the number  $\mu$  of collisions are always present. But, as in the analogous case of  $f_i(z)$  and  $f(z; D)$ , their influence is far smaller than the influence of the variations of energy lost by the particle, or energy imparted to the site, in individual collisions.

In summary, one can state that there is remarkable similarity on the two levels of the hierarchy of random events. The random variables  $\epsilon_i$  in Eq. (1) are themselves the result of a compound Poisson process:

$$\epsilon_i = \sum_{j=1}^{\mu_i} \epsilon_j \quad (36)$$

Accordingly the energy imparted to the site is

$$\epsilon = \sum_{i=1}^n \left( \sum_{j=1}^{\mu_i} \epsilon_j \right) \quad (37)$$

where the inner summation stands for the Poisson process on individual track segments (the energy-loss straggling) while the outer summation represents the Poisson process of charged particles traversing the site (the random sequence of events).

## B. THE BASIC EQUATION

At a specified absorbed dose, the energy imparted to the site and the related variable specific energy are, as stated in the preceding subsection, the result of

a *compound* (or *mixed*) *Poisson process*. The term *Poisson process* refers to the independence of events; the term *compound* refers to the fact that the size of the individual events is variable. The *spectrum* of the Poisson process is the single-event distribution  $f_i(z)$ . The *solutions* of the compound Poisson process are the dose-dependent distributions  $f(z; D)$ . For brevity the term *event fluctuation* is utilized to refer to this process and its mathematical treatment.

Although this and the following subsection refer to the distributions  $f_i(z)$  and  $f(z; D)$ , the mathematical treatment applies equally to the *energy-straggling* problem, i.e., to the random energy loss of a charged particle along a specified track segment. In all subsequent relations one can, accordingly, substitute  $f_i(z)$  by  $c_i(\epsilon)$ , the probability density of energy  $\epsilon$  lost by the charged particle in individual collisions. The solutions are then  $f(\epsilon; \Delta)$ , the probability densities of total energy lost along specified track segments, with expected energy loss  $\bar{\epsilon} = \Delta$ . These probability densities are termed *straggling distributions*.

The average specific energy produced by a single event is the mean value of  $f_i(z)$ . This mean value  $\bar{z}_F$ , which was introduced in Section II, F, is a fundamental parameter because it determines the event frequency  $\phi(0) = 1/\bar{z}_F$  per unit absorbed dose [see Eq. (26) and Table I in Section II, F]. Since events are by definition statistically independent, their number  $\nu$  in a specified site at a specified absorbed dose follows a Poisson distribution:

$$p(\nu) = \exp(-n)n^\nu/\nu!, \quad \text{with } n = \bar{\nu} = D/\bar{z}_F \quad (38)$$

Even if the number  $\nu$  of events is fixed, the specific energy in the site can vary widely. Its distribution is then the  $\nu$ -fold convolution of the single-event distribution. This convolution is denoted by  $f_\nu(z)$ , and it can be defined by the recurrence formula:

$$f_\nu(z) = \int_0^z f_1(x)f_{\nu-1}(z-x) dx \quad (\nu = 2, 3, \dots) \quad (39)$$

$f_\nu(z) dz$  is the probability that the specific energy has a value between  $z$  and  $z + dz$ , if exactly  $\nu$  events have taken place in the site.

Accordingly one obtains the relation for the dose-dependent distributions of specific energy:

$$f(z; D) = \sum_{\nu=0}^{\infty} e^{-n} \frac{n^\nu}{\nu!} f_\nu(z), \quad \text{with } n = \frac{D}{\bar{z}_F} \quad (40)$$

$f_0(z)$  equals  $\delta(z)$ , i.e., the delta function at  $z = 0$ . Accordingly  $f(z; D)$  contains always a discrete probability  $e^{-n}$  for no event, i.e., for  $z = 0$ .

The essence of the compound Poisson process is illustrated by the diagrams of Fig. 10. Individual Monte Carlo realizations of the process are represented for 15-MeV neutrons in the plane of the two variables  $D$  and  $z$ . Any combination of values  $D$  and  $z$  corresponds to a point;  $F(z; D)$  is the probability that the random path runs below the point. Those lines that run below the point pass it on

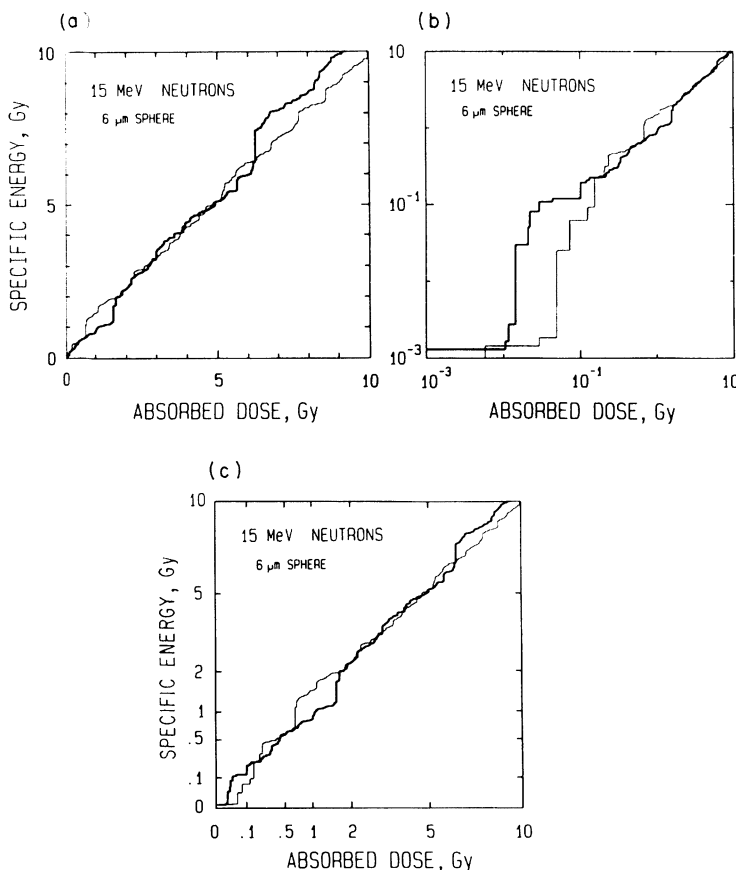


**Fig. 10.** Two random paths that represent the stochastic sequence of events of energy deposition in a 6- $\mu\text{m}$  tissue sphere exposed to 15-MeV neutrons. The two random sequences are represented (a) on a linear scale of dose and specific energy, (b) on a logarithmic scale, and (c) on a square-root scale. The absolute deviations of specific energy from absorbed dose increase with absorbed dose, while the relative deviations decrease. On the graph with the square-root scale the magnitude of the deviations remains on the average constant as the dose increases.

the right; i.e., they reach the value  $z$  at a dose exceeding  $D$ . The conclusion is that  $F(z; D)$  is a sum distribution both with reference to  $z$  as random variable and with reference to  $D$  as random variable:

$$F(z; D) = \text{Prob}\{z \leq z \mid D\} \quad (41)$$

$$G(D; z) = 1 - F(z; D) = \text{Prob}\{D \leq D \mid z\} \quad (42)$$

One must note that the densities of the two sum distributions are not closely linked. The function  $G(D; z)$  can be invoked whenever one considers a response with sharp threshold of energy imparted or specific energy. An instrument with

a response threshold at the specific energy  $z_c$  would have the dose dependence  $F(z_c; D)$  for no response. For a hypothetical cellular structure with a threshold of  $z_c$  the same dose dependence would have to apply. This condition and related matters are considered in Section IV, C.

It is informative to compare the linear and the logarithmic representations in Fig. 10. In the linear diagram the distances of the random paths to the line  $z = D$  tend to increase with increasing dose; this corresponds to the increasing standard deviation of  $z$  as  $D$  increases. As stated in Eq. (33) and derived in Section III, D, the standard deviations of  $z$  are proportional to  $\sqrt{D}$ . In the logarithmic representation the distances to the diagonal tend to decrease, as they correspond to the *relative* standard deviation, which is inversely proportional to  $\sqrt{D}$ . The dependence of the standard deviation of  $z$  on absorbed dose is further illustrated in the third panel, where  $\sqrt{z}$  is plotted versus  $\sqrt{D}$ . In this case the distances to the diagonal tend to be independent of  $D$ .

The individual random paths in Fig. 10 illustrate the stochastic nature of energy deposition in microscopic regions. However, to give the full information contained in dose-dependent microdosimetric distributions one would have to utilize suitable plots of the function  $F(z; D)$  or its complement, the function  $G(D; z)$ . Such plots have been produced [33] and Fig. 11 gives an example. Graphs of this type are suitable for considerations that require actual numerical values of the probabilities to reach or exceed certain specific energies at given values of absorbed dose; they also permit the construction of dose-effect relations for assumed threshold reactions. In the present context, however, it is helpful to visualize the character of the distributions in a less formalized way. To this purpose the analogs to Fig. 10 are given in Fig. 12 as scatter diagrams. For these diagrams a large number of simulated exposures of the spherical tissue region of 6  $\mu\text{m}$  by 15-MeV neutrons is used. Each dot represents the outcome of a simulated exposure. For a specified absorbed dose  $D$  a random value  $z$  of specific

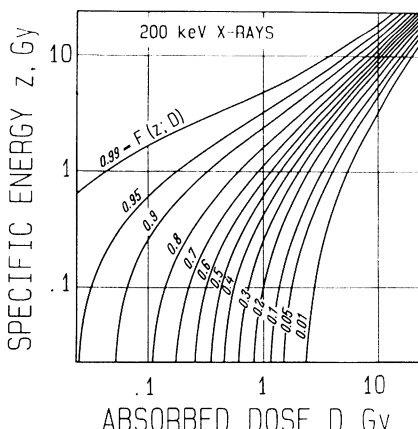


**Fig. 11.** A representation of the dose-dependent distributions of specific energy in terms of lines of equal values of the function,  $F(z; D)$ . The parameter on the curves gives the value  $F(z; D)$  or its complement  $1 - F(z; D)$ . (Redrawn from Kellerer [33].)

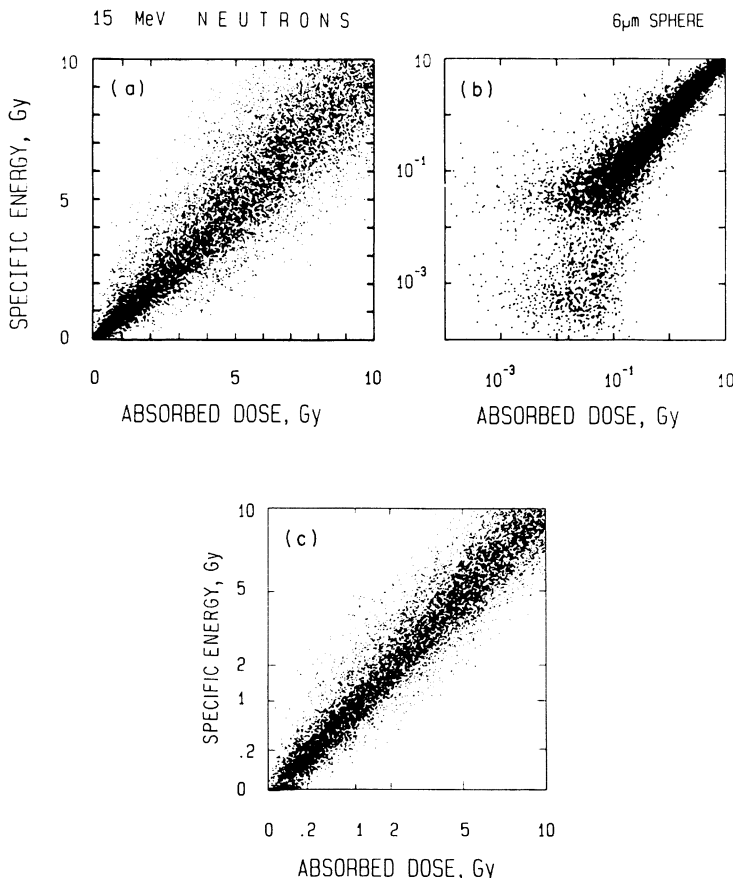


**Fig. 12.** Scatter diagram of the distribution of specific energy at specified absorbed doses in spherical tissue regions of 6- $\mu\text{m}$  diameter exposed to 15-MeV neutrons. In analogy to Fig. 10, (a) linear scales, (b) logarithmic scales, and (c) square-root scales of absorbed dose and specific energy are used. In each diagram a large number of dose values are uniformly distributed on the scale that is being used. Each dot represents the value of specific energy from a random simulation of the exposure with the specified absorbed dose. The reduction of the number of points at low doses reflects the increasing probability for zero events that are not visible in the graph. This and subsequent scatter diagrams are obtained by the algorithm described in the Appendix.

energy is computed and is represented by the corresponding point in the  $D-z$  plane. Dose values are randomly selected in such a way that they are uniformly distributed along the abscissa that is used in the representation. The scatter diagrams permit the visualization of the densities of specific energy as function of absorbed dose. Since the zero events are not represented, fewer points appear on the left-hand side of the graphs, where the event probabilities are substantially less than unity. The essential point comes out most clearly in the logarithmic

plot: at sufficiently low absorbed doses the event frequencies decrease but not the values of specific energy. At small doses they merely represent the distribution of values produced in individual energy deposition events.

The four panels of Fig. 13 permit the comparison of the distributions for two different site sizes and for  $^{60}\text{Co}$   $\gamma$  rays and 15-MeV neutrons. The site diameter of  $6\ \mu\text{m}$  is chosen to approximate the size of a cellular nucleus. The average volume of a mammalian cell nucleus exceeds somewhat the volume of a  $6\text{-}\mu\text{m}$  spherical site; however, if the nucleus is a spheroid rather than a sphere the slightly reduced diameter is more representative for the actual geometry.

A somewhat more complete synopsis for different radiation qualities is given in the various diagrams of Fig. 14 for a fixed site diameter of  $1\ \mu\text{m}$ . To recognize the fine differences in the microdosimetric distributions one has to consult Fig. 8. The scatter diagrams of  $z$ ,  $D$ -values are suitable for an appreciation of

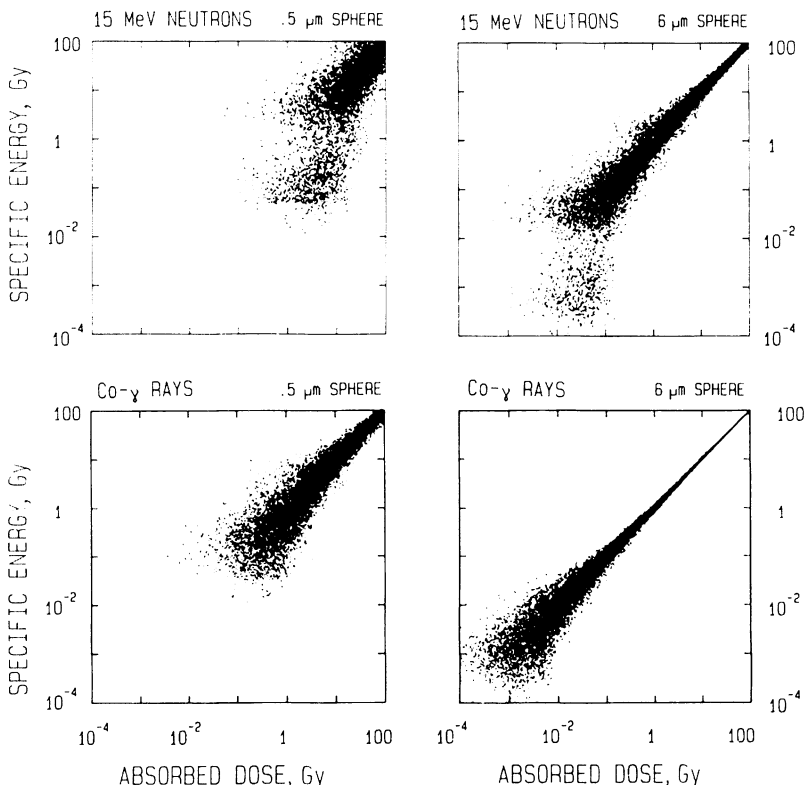


**Fig. 13.** Scatter diagrams for a comparison of  $z$  distributions in small sites and in sites that correspond roughly to the diameter of the nucleus of a cell ( $6\ \mu\text{m}$ ). Results are given for  $^{60}\text{Co}$   $\gamma$  rays and 15-MeV neutrons. Here and in Fig. 14 each panel contains 4000 values per decade of  $D$ , i.e., 24,000 simulations are utilized per graph. The actual number of points is considerably less at low doses because the events with  $z = 0$  are not visible.

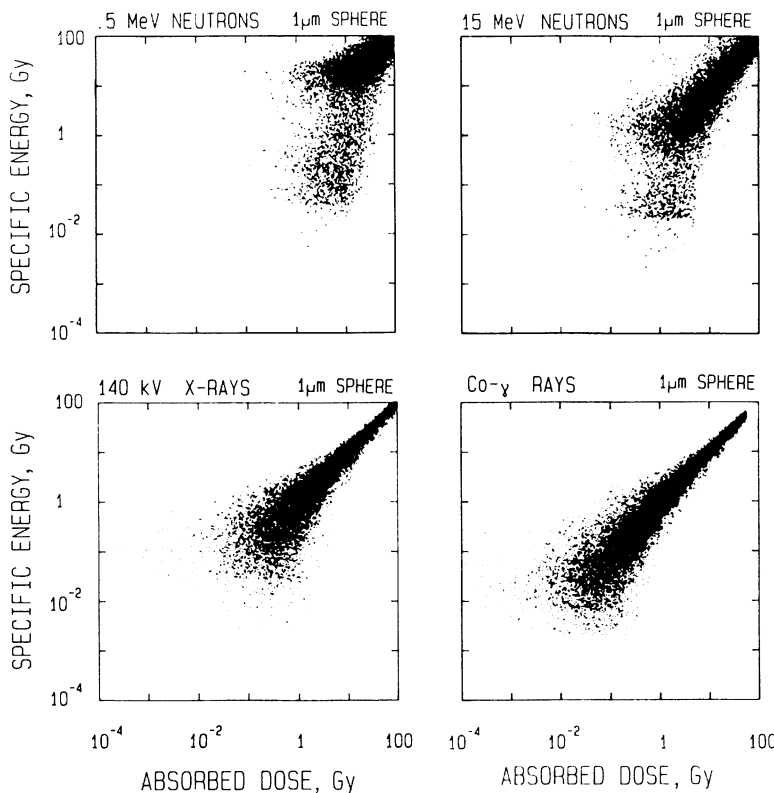


**Fig. 14.** Scatter diagrams as in Fig. 13 but for a comparison of 140-kV x rays,  ${}^{60}\text{Co} \gamma$  rays, 0.55-MeV neutrons, and 15-MeV neutrons for a spherical tissue site of 1-μm diameter.

the general features of the distributions and of their similarities for sparsely ionizing radiations on the one hand, and densely ionizing radiations on the other.

In the early microdosimetric studies Eq. (40) was utilized [29] to compute the dose-dependent distributions. However, this approach is inconvenient because a large number of convolutions  $f_\nu(z)$  is required. It is therefore more efficient to base numerical evaluations on another relation, fundamental to microdosimetry, which will be discussed in the next section.

### C. AN ADDITIVITY RELATION AND THE RESULTING SOLUTION

Because the convolution operation is fundamental in probability theory, and because it has all the characteristics of multiplication, it is convenient to abbreviate the integral. One writes

$$f_\nu(z) = \int_0^z f_1(x) \cdot f_{\nu-1}(z - x) dx = f_1(z) * f_{\nu-1}(z) \quad (43)$$

or generally

$$f_{\nu+\mu}(z) = \int_0^z f_\nu(x) \cdot f_\mu(z-x) dx = f_\nu(z) * f_\mu(z) \quad (44)$$

In a further step the repeated convolution of a distribution with itself is denoted by an exponent. For example,

$$f_1^{*2}(z) = f_2(z) = \int_0^\infty f_1(z-x) \cdot f_1(x) dx \quad (45)$$

or

$$f_1^{*\nu}(z) = f_\nu(z) \quad (46)$$

One can also utilize the multiplicative character of the convolution operation to obtain  $f_\nu(z)$  from  $f_1(z)$  by a sequence of convolutions that corresponds to the splitting of  $\nu$  into integer powers of 2. For example,

$$f_{84}(z) = f_4(z) * f_{16}(z) * f_{64}(z) = f_{|2|} * f_{|4|} * f_{|6|} \quad (47)$$

where the symbol  $|\nu|$  indicates  $2^\nu$  and thus the convolutions  $f_{|\nu|}(z)$  correspond to integer powers  $2^\nu$  of  $f_1(z)$ . They can be computed by the recurrence relation

$$f_{|0|} = f_1(z) \quad \text{and} \quad f_{|\nu|}(z) = f_{|\nu-1|}^{*2}(z) \quad (48)$$

This procedure is very efficient for Monte Carlo simulations of the compound Poisson process. It is the basis of the algorithm for the diagrams of Figs. 12 to 14. The numerical method is explained in the Appendix.

The computation of the distribution  $f(z; D)$  for a specified dose requires a somewhat modified algorithm. It can, however, be based on the same principle. The convolution relation applies not only to distributions of  $z$  for specified numbers  $\nu$  of events. It holds equally for the dose-dependent distributions. In the Poisson process the number and magnitude of events during two time periods, or due to two absorbed doses, are independent. The distribution of the sum of the two random variables equals the convolution of their probability distributions. Hence the specific energy at absorbed dose  $D_1 + D_2$  has the distribution

$$f(z; D_1 + D_2) = \int_0^z f(z-x; D_1) f(x; D_2) dx = f(z; D_1) * f(z; D_2) \quad (49)$$

and specifically

$$f(z; D) = f(z; D/2) * f(z; D/2) \quad (50)$$

Starting from an approximation of  $f(z; D)$  that is valid at low doses, and gaining a factor of 2 in  $D$  with each convolution, one can then derive the distributions for arbitrary doses. The approximation of the  $z$  distribution is simple at doses

that correspond to very small event frequencies. At the small dose  $\eta = \epsilon \bar{z}_F$  the event frequency (i.e., the expected number of events) is  $\epsilon$ , and with  $\epsilon \ll 1$  one has

$$f(z; \eta) = (1 - \epsilon)\delta(z) + \epsilon f_j(z) \quad (51)$$

if the terms with higher powers of  $\epsilon$  are omitted. In the next subsection it will be seen that the resulting error of the standard deviation of the computed distribution of  $z$  is less than the factor  $(1 - \epsilon)$ . In practice a value  $\epsilon < 10^{-2}$  is adequate to provide a precision of the numerical results that is considerably better than the accuracy of any input data  $f_i(z)$ . One can set

$$\eta = D/2^N \quad (52)$$

and can choose  $N$  so that  $\epsilon < 10^{-2}$ . With  $N$  successive convolutions one reaches the desired distribution for the absorbed dose  $D$ :

$$f(z; 2\eta) = f(z; \eta) * f(z; \eta) \\ f(z; 4\eta) = f(z; 2\eta) * f(z; 2\eta) \quad (53)$$

$$f(z; D) = f(z; D/2) * f(z; D/2)$$

Formally this procedure of  $N$  successive convolutions can also be expressed as

$$f(z; D) = f(z; h)^{*2^N} \quad (54)$$

The process requires relatively few convolutions. For example, a total of 14 convolutions are required to reach distributions that correspond to average event numbers around  $n = 100$ . The distributions in Figs. 6 and 7 exemplify the procedure.

The Appendix contains the computer algorithm for the solution of the Poisson process in terms of successive convolutions. Because the spectrum of the process [i.e., the distribution  $f_i(z)$ ] can span several orders of magnitude of the random variable, the convolution has to be executed on a suitable scale; a logarithmic scale of  $z$  is chosen for the purpose.

## D. RELATIONS FOR THE MOMENTS

Frequently the explicit dose-dependent distributions of specific energy are not required. The moments of the distributions or related parameters are of far greater pragmatic importance. They can be expressed in terms of the moments of the single-event distribution. The second moment and the variance of  $z$  play

the greatest role in various applications; they are therefore derived first. The more complicated relations for the higher moments are given subsequently. They are less relevant to radiobiological applications of microdosimetry, but they can be useful tools in any quantitative assessment of experimental or computed microdosimetric data and of their interrelations.

### 1. Second Moment and Variance

The expectation of specific energy is, as pointed out in Sections II, E and II, F, equal to absorbed dose:<sup>\*</sup>

$$\bar{z} = n\bar{z}_1 = D \quad (55)$$

The variance  $\sigma_z^2(D)$  of the specific energy  $z$  at absorbed dose  $D$  is readily obtained. One utilizes the fact that the variance of the sum of two independent random variables is equal to the sum of their variances, i.e., that the variances are additive in the convolution of two distributions. It follows that the variance of  $z$  at dose  $D_1 + D_2$  is equal to the sum of the variances at dose  $D_1$  and at dose  $D_2$ . The variance must, accordingly, be proportional to absorbed dose:

$$\sigma_z^2 = cD \quad (56)$$

As a next step one can derive the constant  $c$ . The variance of a random variable is equal to the second moment minus the square of the expectation value:

$$\sigma_z^2 = \overline{(z - \bar{z})^2} = \overline{z^2} - \bar{z}^2 = \overline{z^2} - D^2 \quad (57)$$

The second moment can be expressed in terms of Eq. (40):

$$\overline{z^2} = \sum_{\nu=0}^{\infty} e^{-n} \frac{n^\nu}{\nu!} \int_0^\infty z^2 f_\nu(z) dz = e^{-n} \sum_{\nu=1}^{\infty} \frac{n^\nu}{\nu!} \overline{z_\nu^2} \quad (58)$$

where  $\overline{z_\nu^2}$  is the second moment of the  $\nu$ -event distribution  $f_\nu(z)$ ; in contrast to  $\overline{z^2}$ , the values  $\overline{z_\nu^2}$  are not dependent of dose.

The power expansion of Eq. (58) is

$$\begin{aligned} \overline{z^2} &= (1 - n + \frac{1}{2}n^2 - \dots) \cdot (n\overline{z_1^2} + \frac{1}{2}n^2\overline{z_2^2} + \dots) \\ &= \overline{z_1^2}n + (\overline{z_2^2} - \overline{z_1^2})n^2 + \dots \\ &= (\overline{z_1^2}/z_1)D + [(\overline{z_2^2} - \overline{z_1^2})/\overline{z_1^2}] \cdot D^2 + \dots \end{aligned} \quad (59)$$

<sup>\*</sup>In the context of this and the following subsection it is practical to utilize the notation  $\overline{z_1}$  and  $\overline{z_1^2}$ , rather than the notation  $\overline{z_F}$  and  $\overline{z_F^2}$ , which is employed whenever the discrimination of the frequency distributions (index F) from the dose-weighted distributions (index D) is essential. For the expectation values at a specified absorbed dose no index is used and the argument  $D$  is omitted whenever the meaning is clear from the context. Thus  $\bar{z}$ ,  $\overline{z^2}$ , and  $\sigma_z$  stand for  $\bar{z}(D)$ ,  $\overline{z^2}(D)$ , and  $\sigma_z(D)$ , respectively.

Accordingly, one has

$$c = \sigma_z^2/D = \bar{z}_1^2/\bar{z}_1 + [(\bar{z}_1^2 - \bar{z}_1^2)/\bar{z}_1^2] \cdot D + \dots \quad (60)$$

Since  $c$  is a constant, one can obtain its value from the limit  $D \rightarrow 0$ :

$$c = \lim_{D \rightarrow 0} c = \frac{\bar{z}_1^2}{\bar{z}_1} \quad (61)$$

Thus one obtains the essential relations

$$\sigma_z^2 = (\bar{z}_1^2/\bar{z}_1) \cdot D \quad \text{and} \quad \bar{z}^2 = (\bar{z}_1^2/\bar{z}_1) \cdot D + D^2 \quad (62)$$

that were cited without derivation in Section II. F.

In view of important radiobiological applications (see Section IV. C), the term  $\bar{z}_1^2/\bar{z}_1$  has been given a special symbol:

$$\xi = \bar{z}_1^2/\bar{z}_1 \quad (63)$$

As pointed out in Section II. F, this is the mean value of the dose-weighted single-event distribution  $d_1(z)$ .

## 2. Utilization of the Relation for the Variance

Section IV deals with various applications of microdosimetry and Eq. (62) plays a prominent role in these applications. Two specific applications are of interest already in the immediate context of the present section.

Equation (62) can be utilized to assess the error that is caused by the omission of the multiple-event terms in the low-dose approximation in Eq. (51). The mean value of this approximation is correct:

$$\bar{z} = \epsilon \int z f_1(z) dz = \epsilon \bar{z}_1 = \eta \quad (64)$$

However, the second moment is somewhat smaller than the exact value  $\xi\eta + \eta^2$ . It is instead

$$\bar{z}^2 = \epsilon \int z^2 f_1(z) dz = \xi\eta \quad (65)$$

For  $\sigma_z^2$  one has therefore  $\xi\eta - \eta^2$  instead of the correct value  $\xi\eta$ . The standard deviation of the approximation used in Eq. (51) is, accordingly, too small by the factor

$$f = (1 + \epsilon \bar{z}_1 / \xi)^{1/2} \quad (66)$$

The dose average  $\xi$  of the single-event distribution is always larger than the frequency average  $\bar{z}_1$ , and the error factor is therefore substantially closer to unity than  $(1 - \epsilon/2)$ . Hence the condition  $\epsilon < 10^{-2}$  ensures adequate precision of the iterative convolution algorithm described in the preceding subsection.

The second consideration relates to the relative role of the fluctuations of the event number and the event size in the compound Poisson process. In Section III, A the statement has been made that the variations of event size are the dominant factor. To quantify this statement it is practical to consider the *relative* variance  $V_z = \sigma_z^2(D)/D^2$  of the distribution  $f(z; D)$  and express it in terms of the relative variance  $V_1 = \sigma_z^2/\bar{z}_1^2$  of the single-event spectrum:

$$V_z = (V_1 + 1)/n \quad (67)$$

Let  $n = D/\bar{z}_1$  be the mean event number at dose  $D$ ; for simplicity  $D$  may be assumed to be an integer multiple of  $\bar{z}_1$ . Without fluctuations of the event number one would obtain the distribution  $f^{**}(z)$  instead of  $f(z; D)$ . The variance of this distribution is

$$\sigma_z^2(n) = n\sigma_1^2 \quad (68)$$

The relative variance is

$$V'_z = \sigma_z^2(n)/D^2 = V_1/n \quad (69)$$

where  $1/n$  is the relative variance  $V_1$  of the number of events. Therefore,  $V_z$  is the sum of the term  $V_1/n$ , due to the fluctuations of event size, and the term  $1/n$ , due to the variations of event number. For the single-event spectra  $V_1$  is commonly considerably larger than one; the fluctuations of event size are, therefore, more important than the variations of event number. The same statement applies to the energy-loss straggling problem that is treated in Section V.

### 3. General Relations for the Moments

The remainder of this subsection has a somewhat more mathematical character. It deals with the higher moments for the compound Poisson process. The results—although applicable to a variety of problems—are not required in the subsequent sections.

The higher moments could be obtained by a method largely analogous to the considerations in the preceding section. The subsequent, less elementary treatment has, however, the advantage that it uses concepts and relations that are also of interest and utility in themselves. There is particular relevance to the energy-loss straggling problem that is considered in Section V.

The first step in the derivation is the introduction of certain combinations of the moments that are termed *semi-invariants* and that are additive in convolutions. Let  $\phi(t)$  be the characteristic function, i.e., the Fourier transform, of the probability density  $f(z)$ :

$$\phi(t) = \int_0^\infty e^{itz} f(z) dz \quad (70)$$

The power expansion of  $\phi(t)$  is

$$\begin{aligned}\phi(t) &= \sum_{\lambda=0}^{\infty} \int_0^{\infty} \frac{(it)^{\lambda}}{\lambda!} z^{\lambda} f(z) dz \\ &= \sum_{\lambda=0}^{\infty} m_{\lambda} \frac{(it)^{\lambda}}{\lambda!}\end{aligned}\quad (71)$$

where  $m_{\lambda}$  are the moments of the distribution  $f(z)$ .

A different representation of  $\phi(t)$  can be obtained by expanding the logarithm of  $\phi(t)$  into a power series:

$$\ln \phi(t) = \sum_{\lambda=1}^{\infty} k_{\lambda} \frac{(it)^{\lambda}}{\lambda!} \quad (72)$$

The resulting coefficients  $k_{\lambda}$  are termed semi-invariants. In the convolution of two distributions the logarithms of the characteristic functions are additive, and so are the semi-invariants.

To express the semi-invariants in terms of the moments  $m_{\lambda}$  one can juxtapose the expressions from Eqs. (71) and (72):

$$\begin{aligned}\sum_{\lambda=0}^{\infty} m_{\lambda} \frac{(it)^{\lambda}}{\lambda!} &= \exp \sum_{j=1}^{\infty} k_j \frac{(it)^j}{j!} \\ &= \sum_{\mu=0}^{\infty} \left( \sum_{j=1}^{\infty} k_j \frac{(it)^j}{j!} \right)^{\mu} \Bigg| \mu! \\ &= 1 + k_1(it) + (k_2 + k_1^2) \frac{(it)^2}{2!} \\ &\quad + (k_3 + 3k_1k_2 + k_1^3) \frac{(it)^3}{3!} + \dots\end{aligned}\quad (73)$$

The comparison of the coefficients and resolution for the  $k_i$  yields

$$\begin{aligned}k_1 &= m_1 \\ k_2 &= m_2 - m_1^2 = \sigma_2 \\ k_3 &= m_3 - 3m_2m_1 + 2m_1^3 = \sigma_3 \\ k_4 &= m_4 - 4m_3m_1 - 3m_2^2 + 12m_2m_1^2 - 6m_1^4 = \sigma_4 - 3\sigma_2^2\end{aligned}\quad (74)$$

where  $\sigma_{\lambda}$  are the central moments:

$$\sigma_{\lambda} = \int_0^{\infty} (x - \bar{x})^{\lambda} f(z) dz \quad (75)$$

The relations between the central moments  $\sigma_\lambda$  and the noncentral moments  $m_\lambda$  that are used in Eq. (74) are readily verified. Equation (74) shows that, next to the mean and the variance, the third central moment is additive in a convolution and generally in a Poisson process.

It remains to express the semi-invariants in terms of the moments of the single-event spectrum. The relations for  $k_1$  and  $k_2$  have already been obtained in the preceding subsection:

$$\begin{aligned} k_1 &= n\bar{z}_1 = D \\ k_2 &= n\bar{z}_1^2 = (\bar{z}_1^2/\bar{z}_1)D \end{aligned} \quad (76)$$

The general relation is of the same form:

$$k_\lambda = n\bar{z}_1^\lambda = (\bar{z}_1^\lambda/\bar{z}_1)D \quad (77)$$

This result could be derived in analogy to Eqs. (58)–(61); i.e., one could utilize the limit of  $f(z; D)$  as  $D$  goes to zero. Instead, a derivation will be used that is instructive because it demonstrates also the solution of the compound Poisson process in terms of the Fourier transform.

For the Fourier transforms the convolution reduces to a multiplication. Accordingly one can write the equation for the compound Poisson process in terms of the transforms:

$$\phi(t; D) = \sum_{\nu=0}^{\infty} e^{-n} \frac{n^\nu}{\nu!} \phi_1^\nu(t) = e^{n[\phi_1(t) - 1]} \quad (78)$$

or

$$\ln \phi(t; D) = n[\phi_1(t) - 1] \quad (79)$$

where  $\phi(t; D)$  and  $\phi_1(t)$  are the Fourier transforms of  $f(z; D)$  and  $f_1(z)$ .

Inserting the relation from Eq. (71)

$$\phi_1(t) = \sum_{\lambda=0}^{\infty} \bar{z}_1^\lambda \frac{(it)^\lambda}{\lambda!} = 1 + \sum_{\lambda=1}^{\infty} \bar{z}_1^\lambda \frac{(it)^\lambda}{\lambda} \quad (80)$$

into Eq. (79) one has

$$\ln \phi(t; D) = \sum_{\lambda=1}^{\infty} n\bar{z}_1^\lambda \frac{(it)^\lambda}{\lambda!} \quad (81)$$

From the identity of the coefficients one obtains the result of Eq. (77). The semi-invariants of the compound Poisson process are proportional to the noncentral moments of the spectrum  $f_1(z)$ , of the Poisson process.

Equation (78) is of interest in itself, since it gives the solution of the Poisson process in terms of the Fourier transforms. The use of this solution and the fast

Fourier-transform algorithm might appear to be the most efficient method of computing the solutions of the compound Poisson process. However, the microdosimetric distributions  $f_i(z)$ —and the same applies to the collision spectra  $f_c(\epsilon)$ , which will be considered in Section V—cover such a broad range of the random variable that the Fourier transform requires impractically large arrays or, alternatively, necessitates a splitting of the spectrum into sections that are separately processed. The method of the Fourier transform is therefore not superior to the direct convolution that can be executed on a suitable logarithmic scale with arrays of moderate size (see Appendix).

#### IV. Determination and Utilization of the Microdosimetric Parameters

Most microdosimetric measurements are performed with proportional counters filled with tissue-equivalent gas. The instruments are either wall-less or have tissue-equivalent walls. These *Rossi counters* can be utilized under a wide variety of experimental conditions and for a multiplicity of purposes. It is not the objective of this chapter to deal with the experimental methods and with the scientific or practical applications of the microdosimetric data. A brief consideration of certain aspects of the measurements and of some principles of utilization of the results will, however, facilitate the comprehension of the fundamentals of microdosimetry.

The microdosimetric spectra, and particularly the important single-event spectra, cover broad ranges of values of lineal energy or specific energy. It is evident that such spectra cannot, without loss of information, be characterized by their first two moments only. Nevertheless, the majority of the applications of microdosimetry utilize merely these first moments, or the equivalent parameters *frequency average* and *dose average* of event size. There are, of course, radiations—and the most important and interesting case is that of heavy ions, which are not treated in this chapter—where the pairs of values  $\bar{y}_F$  and  $\bar{y}_D$  or  $\bar{z}_F$  and  $\bar{z}_D$  ( $= \xi$ ) are grossly inadequate. But these are exceptions and if one does not deal with particles of extremely high LET, such as heavy ions, or with particles of very short ranges, such as the low-energy electrons released by ultrasoft x rays, the two mean values of the single-event spectra are of fundamental importance. This is the justification for the detailed treatment given to the moments of the microdosimetric spectra in the preceding section. For the same reason these parameters will be considered further from a more practical point of view.

##### A. ASPECTS OF DOSIMETRIC AND MICRODOSIMETRIC MEASUREMENTS

###### 1. *Inherent Imprecision of Dose Determinations*

The statistical fluctuations of energy deposition set an absolute limit to the precision of dose determinations. The physical size of the sensitive volume of

an instrument determines the expected number of events and its standard deviation. It also determines the expectation value of the energy imparted or specific energy and the standard deviation of these quantities. Even an ideal instrument cannot attain a precision beyond that determined by these standard deviations.

Consider a spherical, gas-filled proportional counter. For simplicity it is assumed that it is tissue equivalent. Let  $\rho$  be the density of the counting gas in grams per cubic centimeter. The value  $\rho$  then is also the ratio of the density of the counting gas to the density of tissue, which is assumed to be  $1 \text{ g/cm}^3$ . If the counter has the diameter  $d^*$ , the diameter of the equivalent tissue region is  $d = \rho d^*$ . Neglecting density effects and possible wall effects in the measurement, the single-event spectrum in the counter equals the spectrum in the corresponding tissue site. The mass of the counting gas exceeds the mass of the corresponding tissue site by the factor  $1/\rho^2$ . The event frequency is higher, by the same factor, in the gas cavity than in the tissue site. The expected number of events in the gas is

$$n = \phi \cdot D/\rho^2 \quad (82)$$

where  $\phi$  is the event frequency per unit absorbed dose in the tissue region of diameter  $d$ .

The actual number of events follows the Poisson distribution. The relative standard deviation of the number of events is therefore

$$\sigma_n/n = 1/\sqrt{n} = \rho/\sqrt{\phi D} \quad (83)$$

A numerical example can illustrate the relation. Consider a spherical detector with a diameter of 1 cm that is filled with tissue-equivalent gas at atmospheric pressure ( $\rho \approx 10^{-3} \text{ g/cm}^3$ ) and is exposed to a field of 15-MeV neutrons. The corresponding tissue site has a diameter of  $10 \mu\text{m}$  and the event frequency for 15-MeV neutrons is roughly 50/Gy (see Table I, Section II). The relative standard deviation in the determination of 1 mGy is then

$$\sigma_n/n = 10^{-3}/\sqrt{50} \cdot 10^{-3} = 0.0045 \quad (84)$$

This means that even an ideal instrument with the specified size and gas pressure cannot reach a precision of better than 0.5% in determining a dose of 1 mGy of 15-MeV neutrons. Utilization of the detector in the counting mode is, of course, a procedure that requires previous knowledge of the event frequency for the radiation in question. Event frequencies are sensitive to minor modifications of radiation quality. To measure energy imparted is therefore, in general, more appropriate than counting pulses. The relation for the inherent imprecision of a measurement of energy imparted, or of specific energy, is accordingly of main pragmatic interest. It will be considered next.

According to the relation obtained in the preceding section [see Eqs. (62) or the earlier statement in Eq. (33)], the standard deviation of specific energy in

the tissue region is

$$\sigma_z^2 = \xi D \quad (85)$$

where  $\xi$  is the dose-weighted average [see Eq. (28)] of the single-event spectrum. In the gas cavity the number of events is increased by the factor  $1/\rho^2$ . The variance of the specific energies is proportional to the number of events and is therefore equal to

$$\sigma_z^2 = \xi D / (1/\rho^2) \quad (86)$$

Hence one obtains the relative standard deviation of the specific energy:

$$\sigma_z/D = \sqrt{\xi/D}(\rho) \quad (87)$$

In the above example  $\xi = 0.15$  Gy (see Fig. 15). Accordingly, at an absorbed dose of 1 mGy the inherent relative standard error is

$$\sigma_z/D = \sqrt{0.15/10^{-3}}(10^{-3}) = 0.012 \quad (88)$$

The specified instrument can therefore, ideally, attain a precision of 1.2% in a measurement of specific energy or energy imparted at an absorbed dose of 1 mGy of 15-MeV neutrons. This inherent imprecision may appear to be insignificantly low. However, in radiation protection applications, specifically in area monitoring, one commonly deals with very low dose rates. The dose determinations are then associated with correspondingly larger relative errors that may necessitate the utilization of considerably larger detectors.

## 2. The Variance Method

The weighted mean values  $\bar{y}_D$  and  $\xi$  of single events are fundamental parameters of radiation quality. It is therefore of particular interest that they can

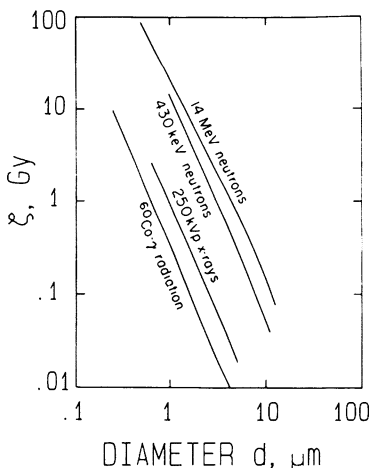


Fig. 15. Weighted mean  $\xi$  of the specific energy produced in individual events by different radiations in spherical tissue sites of diameter  $d$ . (From Kellerer and Rossi [41].)

be obtained directly without determination of the explicit spectra. The direct measurement is important also because it is applicable to site sizes that are smaller than those for which the spectra themselves can be measured with present experimental techniques.

A Rossi counter measures the values  $\epsilon_k$  of energies imparted due to successive single events. The average of a sufficient number of the squares of observed values is the second moment  $\bar{\epsilon}_F^2$ ; the average of the observed values is the mean  $\bar{\epsilon}_F$ . Accordingly one can determine both mean values  $\bar{\epsilon}_D$  and  $\bar{\epsilon}_F$  from averages over a sufficient number of measured pulses:

$$\bar{\epsilon}_D = \sum_1^K \epsilon_k^2 / \sum_1^K \epsilon_k \quad \text{and} \quad \bar{\epsilon}_F = \frac{1}{K} \sum_1^K \epsilon_k \quad (89)$$

Related quantities are  $\bar{z}_D = \bar{\epsilon}_D/m$  and  $\bar{y}_D = \bar{\epsilon}_D/\bar{l}$ .

Proportional counters cannot simulate sites with diameters less than approximately 0.3  $\mu\text{m}$ . If the gas pressure in the instruments is too low, one cannot achieve sufficient multiplication with adequate uniformity of response throughout the sensitive region. In view of this limitation, Bengtsson [35] and Forsberg and Lindborg [36] have introduced an alternative method that is linked to the fundamental relation for the variance of specific energy. They utilize the fact that one can perform measurements with little or no multiplication, if the detector is set to integrate the response over finite dose increments,  $D$ . Let the observed values of energy imparted in repeated measurements with absorbed dose  $D$  be denoted by the symbol  $e_k$  ( $k = 1, \dots, K$ ). With a sufficient number of measurements the moments of the distribution  $f(z; D)$  are obtained as

$$\bar{z}^2 = \frac{1}{K} \sum_1^K \left( \frac{e_k}{m} \right)^2, \quad \bar{z} = D = \frac{1}{K} \sum_1^K \frac{e_k}{m} \quad (90)$$

From the relation [see Eq. (62)]

$$\bar{z}^2 = \sigma_z^2(D) + \bar{z}^2 = \xi D + D^2 \quad (91)$$

one obtains

$$\begin{aligned} \xi &= \frac{\sigma_z^2}{D} = \frac{\bar{z}^2}{D} - D \\ &= \frac{\sigma_c^2/\bar{e}}{m} = \frac{\sum_1^K e_k^2 / \sum_1^K e_k - (1/K) \sum_1^K e_k}{m} \end{aligned} \quad (92)$$

This determination of  $\xi$ , the *variance method*, depends critically on the absence of experimental fluctuations that contribute to  $\sigma_z^2$  and can, therefore, lead to erroneously large values of  $\xi$ . With variable or pulsed sources, such as accelerators, a modified method is accordingly required. A suitable approach is the utilization of two detectors that work independently, but in phase, in the radia-

tion field. With the twin detectors the parameter  $\xi$  is obtained from the variance of specific energy in one of the detectors minus the covariance of specific energy in the two detectors [37]. The *variance-covariance method* exemplifies the fundamental role of the relations between the moments of the microdosimetric distributions. It makes it possible to perform microdosimetric measurements in accelerator-produced radiation fields that are often too intense during pulses to permit the resolution of individual events in microdosimetric detectors.

### B. APPLICATION OF MICRODOSIMETRIC DATA IN RADIATION PROTECTION

There are a variety of uses for microdosimetric data. A brief survey exemplifies first some applications to radiation protection. Biophysical implications will be considered subsequently.

Perhaps the most important application of microdosimetric techniques and data is the exploration of unknown or inadequately known radiation fields, or the monitoring for changes in radiation quality. The need for such procedures arises in radiation protection but also in applications of ionizing radiation, such as radiation therapy. For most fields of high-energy photons or neutrons, conventional, walled counters can be utilized to obtain the microdosimetric spectra or their mean values. Only in exceptional situations, for example, with high-energy charged particles, must wall-less counters be used.

For purposes of radiation protection one can derive adequately precise values of the quality factor by substituting spectra of lineal energy for the unknown and often unmeasurable LET spectra, which enter the strict definition of the quality factor. Instead of the relation ([38]; see Section II. B for the notation)

$$\bar{Q} = \int Q(L) d(L) dL = \int Q(L) L t(L) dL / \bar{L}_F \quad (93)$$

one utilizes the equation

$$\bar{Q} = \int Q(y) d(y) dy = \int Q(y) y f(y) dy / \bar{y}_F \quad (94)$$

where the dependence of the quality factor on LET and on lineal energy is taken to be the same, i.e.,  $Q(y) = Q(L)$  for  $y = L$ . The numerical differences caused by the use of  $y$  spectra instead of LET spectra are of little concern in radiation protection applications. It is therefore feasible to couple a Rossi counter to suitable electronics and to a microprocessor, and to use the device as a dose-equivalent-rate meter.

The deficiencies of the LET concept have been considered in Section II, and it has been noted that LET is less relevant to the biological effectiveness of radiations than the actual energy concentrations that determine the  $y$  spectra or  $z$  spectra. If one thinks merely in terms of LET, it remains unclear why the quality

factor, according to its present definition [1, 38], should be constant up to 3.5 keV/ $\mu\text{m}$  before it increases with LET. In terms of lineal energy, however, this feature of the definition is readily understood. For densely ionizing radiations the values of lineal energy tend to be proportional to LET. For very sparsely ionizing radiations the values of lineal energy do not decrease proportionally, but tend to be larger than LET. The reason is the energy-loss straggling, i.e., the clustered deposition of energy in the volume by  $\delta$  rays or groups of  $\delta$  rays. In the same context one may note that a definition in terms of lineal energy could adequately take into account any increase of biological effectiveness due to Auger cascades or other correlated ionizing particles. The increase cannot be accounted for in terms of the LET concept.

If the quality factor were defined in terms of lineal energy in sites of diameter 0.3  $\mu\text{m}$  [39], the quality factor could be set to be proportional to lineal energy for sparsely ionizing and moderately densely ionizing radiations, and almost the same numerical values would be obtained as with the present definition of  $Q$  in terms of LET (see also [10]). Proportionality between the quality factor and  $y$  would have the practical advantage that the mean quality factor  $\bar{Q}$  for a radiation could be obtained directly from  $\bar{y}_D$  without knowledge of the explicit  $y$  spectrum. With  $Q(y) = qy$  one obtains [see Eq. (94)]

$$Q = \int qy^2 f(y) dy / \bar{y}^F = q\bar{y}_D = Q(\bar{y}_D) \quad (95)$$

With the definition in terms of LET one cannot, strictly, set  $\bar{Q} = Q(\bar{L}_D)$ , although this is often done. The preceding considerations apply, of course, only to sparsely ionizing radiations. For very densely ionizing radiations ( $L > 100$  keV/ $\mu\text{m}$  or  $y > 100$  keV/ $\mu\text{m}$ ) nonlinearities enter because of the saturation effect.

Rossi has reexamined the definition of the quality factor [40] and has proposed a change that goes beyond a mere substitution of LET by lineal energy. His modified definition of the quality factors in terms of lineal energy would be in better agreement with radiobiological data than the present quality factors, which do not sufficiently account for the different effectiveness of densely ionizing and sparsely ionizing radiations at low doses.

Beyond its practical uses, microdosimetry has fundamental implications for radiation protection. In radiation protection one discriminates between *stochastic* effects, such as hereditary damage and radiation carcinogenesis, and *nonstochastic* effects, such as skin damage, impairment of fertility, lens opacification, and prenatal malformations. It is an objective of radiation protection to avoid nonstochastic effects entirely. One assumes that this objective can be reached because nonstochastic effects depend on damage to a multiplicity of cells in a tissue, with resultant curvilinear, or even thresholdlike, dose dependence. Stochastic effects, on the other hand, cannot be avoided entirely. One assumes that they result from damage to individual cells and that they exhibit linear

dose dependences at small doses. The aim of radiation protection can therefore be merely to minimize radiation exposures and to reduce thereby the risk of stochastic effects to a level comparable to or substantially below other risks associated with human activities.

The assumption of linear dependences for the stochastic effects of low doses is crucial and specific to the risk considerations for ionizing radiations. Similar assumptions are not common in the consideration of chemical carcinogens. Microdosimetric principles clarify this fundamental difference. The effects of ionizing radiations and their dose dependences reflect the stochastic distribution of energy in individual cells. Chemicals, on the other hand, affect individual cells according to their concentration without substantial random fluctuations.

Knowledge of event frequencies in the nuclei of mammalian cells permits statements where dose dependences for effects on individual cells must be linear. If the dose is smaller than  $\bar{z}_F$  the event frequency  $D/\bar{z}_F$  is less than 1. Only a few cell nuclei then receive multiple events of energy deposition, and the specific energy is predominantly determined by the single-event spectrum; i.e., it depends on radiation quality and not on absorbed dose. At sufficiently low doses most cells receive no energy deposition; the number of affected cells is proportional to absorbed dose. Rossi has introduced the notion of radiation effects on *autonomous* cells [40], and implies by this term that cells are not influenced by radiation effects on neighboring cells or by radiation effects on the tissue level. For effects on autonomous cells—and the mutations that cause hereditary effects are the main example—linear dose-effect relations must be assumed at sufficiently low doses. Figure 16 indicates for different types of ionizing radiations those combinations of doses and site diameters that correspond to event frequencies less than 1.

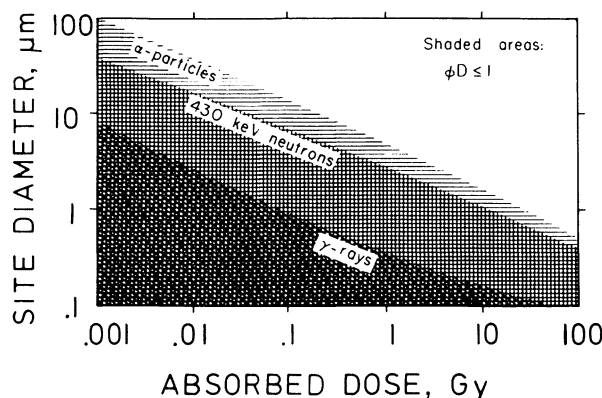


**Fig. 16.** Diagram of site diameters and of absorbed doses that correspond to mean event frequencies  $\phi D$  less than one. The regions with  $\phi D \leq 1$  are indicated for three different radiations.

However, it must be noted that linear dose–effect relations cannot be postulated for radiation carcinogenesis, which may be codetermined by radiation-induced alterations on the tissue level. Nonlinear dose–effect relations have been found for tumors induced by 400 keV neutrons. Remarkably, these dependences correspond to dose exponents less than 1 at neutron doses where only a minor fraction of all cells receive any energy deposition. One must conclude that the effect is not one on autonomous cells; other, more complex factors must codetermine the dose–effect relation [41–43, 20]. The nature of these factors is still unknown; microdosimetry can serve only to exclude certain mechanisms of radiation action.

### C. BIOPHYSICAL IMPLICATIONS OF MICRODOSIMETRIC DATA

The subsequent remarks deal with the somewhat more complex problem of the dose–effect relations at higher doses, where multiple events occur in the nucleus of the cell. The classical multihit or multitarget theory had no actual validity. Nevertheless, its equations were, and are still, widely used for the description of observed dose–effect relations. The simple target-theory models can also illustrate valid arguments that can be recast in the conceptual and quantitative framework of microdosimetry.

#### 1. *The Equations of the Multihit and Multitarget Theory*

The target theory had considerable success in explaining the single-hit inactivation of microorganisms. It was, therefore, natural that an attempt was made [2–4] to explain also curvilinear dose–effect relations in terms of random hits in hypothetical targets. An evident weakness of the approach has been the unrealistic assumption of equal, statistically independent hit events and of hypothetical, equal targets. If these unrealistic assumptions were to be dropped, the number of free parameters would be far too large for a meaningful use of the models. Only two highly simplified models have therefore been retained.

In the *multihit model* it is assumed that the cell contains one hypothetical critical target. The target can tolerate ( $n - 1$ ) hits. If  $n$  or more hits occur the cell is inactivated. This is a pure Poisson process. The probability for survival of the cell is

$$S(D) = e^{-\alpha D} \sum_{\nu=0}^{n-1} \frac{(\alpha D)^\nu}{\nu!} \quad (96)$$

For  $n > 1$  this equation yields dose–effect relations with a shoulder in an initial region where  $S(D)$  decreases with dose at a less than an exponential rate. The slope of the shoulder increases with increasing hit number  $n$ . To reconcile the equation with the common observation of an initial slope of the cellular survival curves an additional factor  $e^{-\gamma D}$  is multiplied into the survival probability; it is

interpreted as single-hit inactivation by the densely ionizing component of the radiation:

$$S(D) = e^{-(\alpha + \gamma)D} \sum_{\nu=0}^{n-1} \frac{(\alpha D)^\nu}{\nu!} \quad (97)$$

The multi-hit curves have the asymptotic slope  $-\alpha$  or  $-(\alpha + \gamma)$  in the common representation of the logarithm of survival versus dose. The curves do not (for  $n > 1$ ) have an asymptotic tangent; in the terminology of radiation biology they are said to have an infinite extrapolation number.

The *multitarget model* postulates  $m$  hypothetical, equal targets, each of which can be inactivated by a single hit. Equal hit probabilities are assumed and also statistical independence of the hits on individual targets. The resulting equation for the survival of the cell is

$$S(D) = 1 - (1 - e^{-\alpha D})^m \quad (98)$$

Again one introduces, somewhat artificially, an additional exponential term to account for the observed initial slope of most survival curves:

$$S(D) = e^{-\gamma D} [1 - (1 - e^{-\alpha D})^m] \quad (99)$$

The multitarget curves have similar characteristics as the multihit curves. Their asymptotic slope is also  $-\alpha$  or  $-(\alpha + \gamma)$ , but this slope is attained sufficiently fast that the curves have an asymptotic tangent that intersects the ordinate at the finite value  $m$ . The term *extrapolation number* is currently used rather than the term *target number* for this value  $m$ .

The target-theory equations are obviously crude approximations that can have only heuristic value. A multiplicity of assumptions could readily be modified, and a far more general description in terms of Markov processes contains the conventional equations as simple special cases [34]. The more general stochastic treatment presents no mathematical difficulties, but any realistic analysis requires an adequate consideration of the microscopic patterns of energy deposition for different radiations. The micropatterns determine the striking differences of the biological effectiveness of ionizing radiations, and it is evident that a biophysical analysis without microdosimetric data can have little value. It is, therefore, of interest to examine how the basic ideas of target theory can be translated into the language of microdosimetry.

## 2. The Threshold Model in Terms of Microdosimetry

A dose-effect relation is the expression of several stochastic processes. The energy deposition in the cell varies randomly, but the response of the cell itself, too, must be described in probabilistic terms. The multihit or multitarget models

disregard the inherent stochastic response of the cell; the dose-effect relation is interpreted merely in terms of the statistics of energy deposition. Such an interpretation is obviously incomplete and even unrealistic, and the same objection applies to any threshold model that is formulated in terms of microdosimetry. Nonetheless, one can draw certain valid conclusions from the consideration of the threshold model that can then lead to a more realistic treatment.

One could imagine a microscopic dosimeter that registers specific energy in a spherical tissue region of diameter  $d$  and responds precisely when a critical value  $z_c$  is reached. As explained in Section III, B, the probability for no response  $S(D)$  is then

$$S(D) = \int_0^{\infty} f(z; D) dz = F(z_c; D) \quad (100)$$

Figure 17 represents such dependences for x rays, a spherical site of  $1 \mu\text{m}$ , and for various critical values  $z_c$ . In spite of the assumed threshold reaction, the resulting dose dependence is, of course, not a step function. If  $z_c$  is comparable to, or smaller than, the average event size  $\bar{z}_F$  for the radiation, the dependence is nearly exponential; one deals then with a *single-hit reaction*. For larger values  $z_c$  the dose-response relations have a shoulder; i.e., they are the result of cumulative damage. For a specified  $z_c$  the curves come closer to the step function as larger site diameters  $d$  are assumed. For any observed dose-effect relation  $S(D)$  one can determine the values  $z_c$  and  $d$  that make the function  $F(z; D)$  agree most closely with  $S(D)$ . The functions  $F(z; D)$  and  $S(D)$  can be formally regarded as sum distributions of the dose required to produce the effect. As with any distribution, one can compute for the functions a mean  $\bar{D}$  and a standard deviation (see Hug and Kellerer [34]). Since there are only two free parameters  $z_c$  and  $d$  it is sufficient to fit the two curves in terms of these two parameters. The diameter  $d$  obtained in this way is not the actual size of any critical target

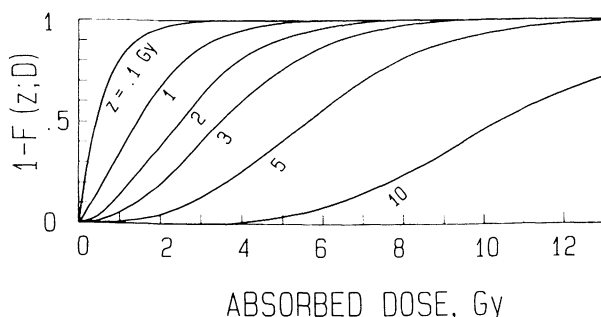


**Fig. 17.** The probabilities  $1 - F(z; D)$  not to exceed a critical value  $z$  of the specific energy versus absorbed dose in a spherical tissue site of  $1-\mu\text{m}$  diameter exposed to x rays. (Redrawn from Hug and Kellerer [34].)

or gross sensitive volume in the cell, it is merely a lower bound. The sensitive volume may be larger, or a multiplicity of small targets may be dispersed through a larger volume. Only part of the observed deviation from the step function need then be due to the stochastics of energy deposition; the other part could reflect the stochastic response of the cell, even to a fixed specific energy. On the other hand, one can exclude any model that invokes one smaller critical target or a multiplicity of critical targets contained in a region of diameter less than  $d$ ; even under the hypothetical assumption of a threshold reaction, the deviations from the step function would have to be larger than those observed. By this argumentation gross sensitive volumes not smaller than 1  $\mu\text{m}$  have been inferred [34] from survival curves of mammalian cells exposed to x rays. For cellular inactivation studies this result is in agreement with the accepted belief that DNA, dispersed through the whole nucleus, is the target of radiation action. For more specific radiation effects, such as chromosome aberrations or cellular transformations, this argument by exclusion can be more informative.

### 3. Dependence of the Effect on Dose and on Specific Energy

In principle it is easy to generalize the formulation. Let  $S(D)$  be the probability for no effect versus dose and let  $S(z)$  be the same probability versus specific energy in the nucleus. The function  $S(z)$  must be somewhat steeper than the function  $S(D)$ . The relation between the  $S(D)$  and  $S(z)$  is

$$S(D) = \int_0^\infty S(z)f(z; D) dz \quad (101)$$

If the dose-effect relation were known with sufficient precision, one could utilize  $f(z; D)$  to invert the equation and determine the dependence on specific energy. In practice this is impossible because dose-effect relations are not known well enough to permit the inversion of the equation. Even if the numerical procedure were possible, the dependence of the effect on specific energy in the nucleus may provide not much more information than the dependence of the effect on absorbed dose. Thus, for sparsely ionizing radiations the fluctuations of  $z$  relative to the entire nucleus of a mammalian cell are insignificant at doses of a few grays (see Fig. 13). The effects of ionizing radiations on the cell are influenced by energy fluctuations on a smaller scale.

The attempt has therefore been made, in various early applications of microdosimetry, but also in recent studies, to search for combinations of smaller site sizes and of functions  $S(z)$  that would fit observed dose-effect relations. However, it is evident that this approach, in addition to various other limitations, contains too many free parameters. An infinite number of fits is possible, which provides no real information. A simpler and less formalistic approach is, therefore, required. Such an approach can be illustrated in terms of the model of *dual radiation action*.

#### 4. Treatment of a Second-Order Process

Lea (see [5]) and later Neary *et al.* [44] have examined the condition that cellular lesions result from the interaction of pairs of chromosomal lesions within the nucleus of the cell. They inferred a dependence of the yield of lesions on the square of the specific energy in certain sites, and they deduced from curvilinear dose dependences for sparsely ionizing radiations site sizes of a fraction of a micrometer or more. The microdosimetric analysis of dose dependences for a large variety of radiation effects and the study of RBE dose dependences for neutrons later led to largely similar conclusions [45]. In particular, high RBE values for neutrons were predicted that were subsequently verified in experiments on radiation carcinogenesis, life shortening, and chromosome aberrations. Details of these studies are not the subject matter of this chapter, but the basic microdosimetric relations for the treatment of dual radiation action can be given.

If the yield of a particular cellular damage is proportional to the square  $z^2$  of the specific energy within a certain site, the average yield will be proportional to the mean of the square  $\bar{z}^2$  of the specific energy, i.e., to the second moment of  $f(z; D)$ :

$$E(D) = k\bar{z}^2 \quad (102)$$

With the fundamental relation [see Eq. (62) or Eq. (33)]

$$\bar{z}^2 = \sigma_z^2 + \bar{z}^2 = \xi D + D^2 \quad (103)$$

one obtains

$$E(D) = k(\xi D + D^2) \quad (104)$$

Under the assumed dependence on the square of specific energy, the effect is, therefore, a linear-quadratic function of absorbed dose. The magnitude of the linear component is proportional to the weighted average  $\xi$  of the specific energy produced in individual events.  $\xi$  is largest for small sites and for densely ionizing radiations (see Fig. 15).

The existence of the linear component can be understood in terms of the intratrack interaction of sublesions; i.e., it can be due to the fact that a substantial amount of energy is deposited in the site even in single events. Accordingly, the energy concentration, and therefore  $z^2$ , can be large in those sites that are affected by an event, even if the absorbed dose is small. The number of sites affected by an event is proportional to absorbed dose.

The treatment in terms of the site concept has the advantage that the specific energy and its distribution can be measured for any radiation. However, it is obviously a simplification. Radiation products will not react with equal probability with all potential reaction partners within an imagined site. The probability for the reaction will, instead, depend on the separation of the partners. In those ex-

ceptional cases where short-range electrons or heavy recoils produce the same  $z$  in a site as long-range particles, the cellular effects may be markedly different. It has also become clear from recent radiobiological investigations that short-distance interactions predominate in the intratrack effect while larger distances are involved in the cumulative cellular damage from independent charged particles (see Section VI, E).

## V. The Straggling Problem and the Single-Event Spectrum

The present section deals with essential features of the single-event spectrum and with the different factors that determine it. Particular attention is given to energy-loss straggling, a problem that is of interest not only in microdosimetry but also in high-energy physics.

For sites of diameter less than roughly 300 nm no reliable methods exist for measuring the microdosimetric spectra. However, computations are possible. To refer to the case of very small sites the term *nanodosimetry* has sometimes been used. In this small region of interest, charged particles undergo few collisions. The fluctuations of *energy loss* can be computed. They are the result of a compound Poisson process, and the convolution algorithm of Section III can be utilized instead of the approximate solutions of the energy-loss straggling problem given by Landau [46], and later by Vavilov [47]. This is the topic of Section V, A.

The computation of the *energy imparted* to submicroscopic sites is more complicated. When the ranges of the  $\delta$  rays are comparable to the site size, a substantial part of the energy lost by the charged particle is transported out of the site. Due to the complex configurations of  $\delta$  rays, i.e., secondary electrons, exact computations are nearly impossible. One can either apply approximate corrections to the solution of the straggling problem, or one can utilize Monte Carlo simulations. The modified solution of the straggling problem is dealt with in Section V, A. Technical details of Monte Carlo simulations are outside the scope of the present chapter, and are therefore not considered. Essentials of the sampling procedures and fundamental relations for the mean values of the spectra will, however, be treated in Section VI; some of the relations hold regardless of the complexities of the particle tracks.

For larger regions with diameters exceeding several hundred nanometers the single-event spectra can be measured. Their calculation is also simpler, and certain complicating factors that are essential for small regions can be disregarded. One condition of particular interest is treated in detail in Section V, B. This condition of *short track segments* requires that the ranges of the charged primaries\*

\*The term *charged primaries* denotes—if one disregards certain special cases—all ionizing charged particles except the  $\delta$  rays. Electrons liberated by photons, or recoil nuclei set into motion by neutrons, are regarded as charged primaries.

are much larger than the site diameter. The change of LET of the particle while traversing the site can then be neglected, and one deals with a set of random factors that can largely be separated. These factors are the LET of the particle, the chord length of the trajectory in the site, and, last but often predominantly, the energy-loss straggling. The case of short track segments applies to moderate- or high-energy electrons, to fast heavy ions, and to the proton recoils of fast neutrons, for regions of fractions of a micrometer to several micrometers.

Another case of considerable pragmatic interest is the condition of *large track segments*. In this case the ranges of the charged primaries are comparable to or smaller than the dimensions of the site. The particles then lose substantial fractions of their energy while traversing the site, and the change of LET during the traversal must be taken into account. Incomplete traversals can also occur. For heavy particles—but usually not for electrons—it is then possible to disregard energy-loss straggling and the transport of energy by  $\delta$  rays. The reason is that the maximum ranges of  $\delta$  rays are small compared to the particle ranges and site diameters (see Fig. 3). Numerous computations of this type have been performed for neutrons (see, e.g., [50–52]), and a detailed discussion is therefore not required in the present context.

Energy-loss straggling is so commonly a dominant factor in microdosimetry that one can term the microdistribution of energy the result of LET plus straggling. The treatment of LET is relatively straightforward. The straggling problem demands a separate treatment that pertains also to work with particle detectors in nuclear physics.

#### A. ENERGY-LOSS STRAGGLING

The straggling problem will be treated for the case of short segments of particle tracks. The change in the kinetic energy and LET of the particles can then be disregarded. In microdosimetry one is interested in the *energy imparted* to a specified region, rather than the *energy lost* by the charged particle. The difference can be substantial whenever  $\delta$  rays have ranges comparable to the region of interest. The straggling problem will first be treated in terms of energy lost by the particle. Subsequently the modifications will be considered that are required when one considers energy imparted to the site.

##### 1. *The Collision Spectrum and Its Convolutions*

The distribution  $f_s(\epsilon, \Delta)$  of energy  $\epsilon$  lost by charged particles along a short track segment with average energy loss  $\Delta$  is the result of a compound Poisson process. The characteristic spectrum of the process is the distribution  $f_c(\epsilon)$  of energy losses in individual electronic collisions. As pointed out in Section III, the mathematical relation is entirely analogous to that between  $f(z; D)$  and  $f_1(z)$ . The same formulae and the same computer program apply to both

problems. The subsequent remarks are therefore partly a repeat of considerations in Section III.

If an ionizing charged particle with stopping power  $L$  traverses a short length  $l$  in matter it loses on the average the energy  $\Delta = lL$ . The energy  $\epsilon$  actually lost is a random variable. There are two random factors. The number of collisions follows a Poisson distribution; the amount of energy lost in individual collisions varies widely and is the more important stochastic factor.

Let  $f_c(\epsilon)$  be the probability density of energy losses in individual collisions. In the free electron model, which is used in the solutions of Landau [46] and Vavilov [47], one has

$$f_c(\epsilon) = k/\epsilon^2, \quad \text{for } I^2/\epsilon_{\max} < \epsilon < \epsilon_{\max} \quad (105)$$

where  $I$  ( $= 70$  eV for water) is the mean excitation potential of the medium, and  $\epsilon_{\max}$  is the maximum energy loss in a collision. For the case of electrons—where a somewhat different spectrum applies— $\epsilon_{\max}$  is conventionally set equal to half the kinetic energy of the particle. For heavy charged particles  $\epsilon_{\max}$  is roughly the kinetic energy of the particle multiplied by four times the ratio of masses of the electron and the heavy particle.

To obtain a properly normalized spectrum one must set

$$k = \epsilon_{\max} I^2 / (\epsilon_{\max}^2 - I^2) \sim I^2 / \epsilon_{\max} \quad (106)$$

With Eq. (105) the average loss  $\delta_1$  per collision is

$$\begin{aligned} \delta_1 &= \int \epsilon f_c(\epsilon) d\epsilon = 2 \ln(\epsilon_{\max}/I) \cdot \epsilon_{\max} I^2 / (\epsilon_{\max}^2 - I^2) \\ &\approx 2 \ln(\epsilon_{\max}/I) \cdot I^2 / \epsilon_{\max} \end{aligned} \quad (107)$$

This is, as will be seen, a purely formal value, which is far smaller than the actual mean energy loss per collision.

The second moment is

$$\epsilon_1^2 = \int \epsilon^2 f_c(\epsilon) d\epsilon = (\epsilon_{\max} - I^2/\epsilon_{\max}) \cdot I^2 / \epsilon_{\max} \quad (108)$$

and the weighted average, i.e., the average of the energy-weighted spectrum,  $d_c(\epsilon) = \epsilon f_c(\epsilon)/\bar{\epsilon}_F$  is\*

$$\begin{aligned} \delta_2 &= \overline{\epsilon^2}/\delta_1 = (\epsilon_{\max} - I^2/\epsilon_{\max})/2 \ln(\epsilon_{\max}/I) \\ &\sim \epsilon_{\max}/2 \ln(\epsilon_{\max}/I) \end{aligned} \quad (109)$$

\*The notation  $d_c(\epsilon)$  for the weighted spectrum is chosen to emphasize the analogy to the dose-weighted spectra  $d(L)$ ,  $d(y)$ , and  $d_1(z)$  of LET, lineal energy  $y$ , and specific energy  $z$ , respectively. However, the simpler notation  $\delta_1$  and  $\delta_2$  is used for the frequency average and the weighted average of the collision spectrum.

This quantity is meaningful because it is not strongly influenced by the unrealistic low-energy part of the free electron collision spectrum.

According to the fundamental relation for the compound Poisson process [see Eq. (62)] the weighted average  $\delta_2$  determines the standard deviation of the straggling distribution  $f(\epsilon; \Delta)$ :

$$\sigma(\Delta) = \sqrt{\delta_2 \Delta} = \sqrt{\delta_2 l L} \quad (110)$$

and with Eq. (105), i.e., the free electron model, one obtains

$$\sigma(\Delta) \sim \sqrt{\epsilon_{\max} \cdot Ll/2 \ln(\epsilon_{\max}/I)} \quad (111)$$

where  $L$  is the collision stopping power and  $l$  is the length of the track segment. For simplicity bremsstrahlung and nuclear interactions are here disregarded.

The free electron model applies to knock-on collisions, i.e., to collisions with  $\epsilon$  large compared to the binding energies of the electrons. For glancing collisions, i.e., energy losses  $\epsilon$  comparable to  $I$  or less than  $I$ , Eq. (105) is unrealistic. The extension of the  $1/\epsilon^2$  spectrum down to the energy  $\epsilon_{\min} = I^2/\epsilon_{\max}$  serves merely to make the spectrum agree with the actual stopping power.

It is evident that the  $1/\epsilon^2$  spectrum cannot lead to valid results for very short track segments where only few collisions occur. In microdosimetry, however—and not only in microdosimetry—this is a case of considerable interest, and it is therefore useful to deal with the exact solution by the method of Section III, which can replace the familiar approximate solutions of the straggling problem.

For a realistic treatment of the glancing collisions various quantum-mechanical approximations can be used, or measured data can be employed. A discussion of these approaches and an examination of the actual shape of the collision spectra are beyond the scope of this chapter. For the present discussion it is sufficient to consider the principles of the straggling problem. Figure 18 indicates the general nature of the difference between the  $1/\epsilon^2$  spectra and the ac-

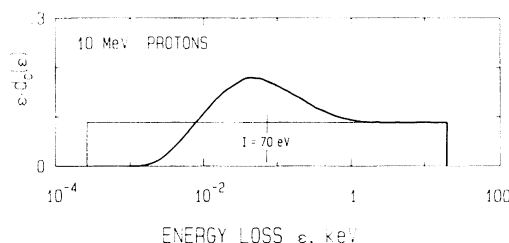


**Fig. 18.** Energy-weighted density of energy loss per collision relative to a logarithmic scale for a 10-MeV proton in water. The box-shaped distribution corresponds to the  $1/\epsilon^2$  spectrum. The heavier line indicates a possible dependence that accounts for glancing collisions. The curves represent the fraction of energy lost by the particle per unit logarithmic interval of  $\epsilon$ .

tual distributions for heavy ions of 10 MeV/nucleon. As earlier in Fig. 8 the weighted spectra relative to a logarithmic scale in  $\epsilon$  are plotted as

$$\epsilon d_c(\epsilon) = \epsilon^2 f_c(\epsilon)/\delta_1 \quad (112)$$

These spectra represent the fraction of energy loss, i.e., stopping power, in specified logarithmic intervals of  $\epsilon$ . For the free electron model one has a constant density on the logarithmic scale:

$$\epsilon d_c(\epsilon) = 1/\ln(\epsilon_{\max}/\epsilon_{\min}) = 1/2 \ln(\epsilon_{\max}/I) \quad (113)$$

i.e., equal logarithmic intervals of  $\epsilon$  contribute equally to the stopping power. For large values of  $\epsilon$  this simple rule is reasonably accurate even for realistic spectra. In many microdosimetric considerations, particularly with high-energy charged particles, it permits adequate estimates of basic features of track structure.

The parts of the spectra corresponding to glancing collisions are not well known and, as stated, they will not be considered quantitatively. The heavy curve Fig. 18 merely illustrates a possible dependence at small values of  $\epsilon$ . The subsequent considerations and the resulting solution of the straggling problem apply regardless of the form of the collision spectrum.

Analytical solutions of the energy-loss straggling problem have been derived by Landau [46] and Vavilov [47] (see also [48]) on the basis of the  $1/\epsilon^2$  spectrum. Landau's solution disregards both the upper and lower limits of the spectrum. It is applicable to those cases where the number of collisions is large, but it requires also that the number is sufficiently small that the probability for collisions near  $\epsilon_{\max}$  can be disregarded. Vavilov has given an improved solution that accounts for the upper limit of energy loss in individual collisions. However, his solution, too, is restricted to the case of many collisions and is linked to the  $1/\epsilon^2$  spectrum and certain other analytical expressions.

The solution of the compound Poisson process in Section III is equally applicable to the straggling problem. One can use the method of successive convolutions to obtain from any specified collision spectrum the straggling distribution  $f_s(\epsilon; \Delta)$  for a specified mean energy loss  $\Delta$ . In analogy to the procedure in Section III, a very short track segment with a mean collision number  $\tau < 10^{-3}$  is considered first. The number  $\tau$  is taken to be smaller by an integer power of 2 than the actual mean collision number  $\Delta/\delta_1$ . The approximation of the solution for the very short segment is, in analogy to Eq. (51),

$$f_s(\epsilon; \eta) = (1 - \tau)\delta(\epsilon) + \tau f_s(\epsilon) \quad (114)$$

with  $\eta = 2^{-N}\Delta$  and  $\tau = 2^{-N}\Delta/\delta_1$ .

The solution  $f(\epsilon; \Delta)$  is then, in the same way as in Section III, obtained by

$N$  successive convolutions:

$$\begin{aligned}
 f_s(\epsilon; 2\eta) &= f_s(\epsilon; \eta) * f_s(\epsilon; \eta) \\
 f_s(\epsilon; 4\eta) &= f_s(\epsilon; 2\eta) * f_s(\epsilon; 2\eta) \\
 &\quad \cdot \quad \cdot \quad \cdot \\
 &\quad \cdot \quad \cdot \quad \cdot \\
 &\quad \cdot \quad \cdot \quad \cdot \\
 f_s(\epsilon; \Delta) &= f_s(\epsilon; \Delta/2) * f_s(\epsilon; \Delta/2)
 \end{aligned} \tag{115}$$

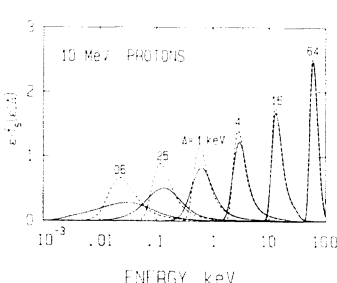
As in the application to  $f_1(z)$  and  $f(z; D)$ , it is essential to execute the convolutions on a logarithmic scale of  $\epsilon$ . The algorithm described in the Appendix can therefore be used. A linear scale would require awkwardly big arrays for the representations of  $f_c(\epsilon)$  and the straggling distributions, and the inconvenient lengths of the arrays make it equally impractical to use the solution in terms of Fourier transforms.

Figure 19 gives solutions for the 10 MeV/nucleon heavy ion obtained with the spectra in Fig. 18. The inadequacy of the simple  $1/\epsilon^2$  spectrum at small mean energy losses  $\Delta$  is evident. At larger values the shape of the solutions is mainly determined by the weighted mean  $\delta_2$  of the collision spectrum. The value 1.81 keV for the realistic spectrum is not substantially larger than the value  $\epsilon_{\max}/2 \ln(\epsilon_{\max}/I) = 1.77$  keV for the simple spectrum. Accordingly, the solutions for the two spectra are similar at larger energy losses.

To further illustrate the identity of the problem of Section III and the energy-loss straggling problem, scatter diagrams are given in Fig. 20 that correspond to the curves in Fig. 19. These diagrams are entirely analogous to the  $D-z$  diagrams in Section III (see Figs. 13 and 14).

## 2. Correction for the Difference between Energy Lost and Energy Imparted

In microdosimetry, as in work with particle detectors, the relevant quantity is the *energy imparted* to a reference region, rather than the *energy lost* by the



**Fig. 19.** Distributions of energy lost by a 10-MeV proton in a foil of thickness corresponding to the specified mean energy loss  $\Delta$ . Densities  $\epsilon \cdot f_s(\epsilon; \Delta)$  relative to the logarithmic scale of  $\epsilon$  are plotted. The solid lines correspond to the heavier lines in Fig. 18. The dashed lines correspond to the free electron spectrum, i.e., the box-shaped distribution in Fig. 18. At sufficiently large mean energy losses both sets of distributions are in agreement; the classical solutions are then adequate.

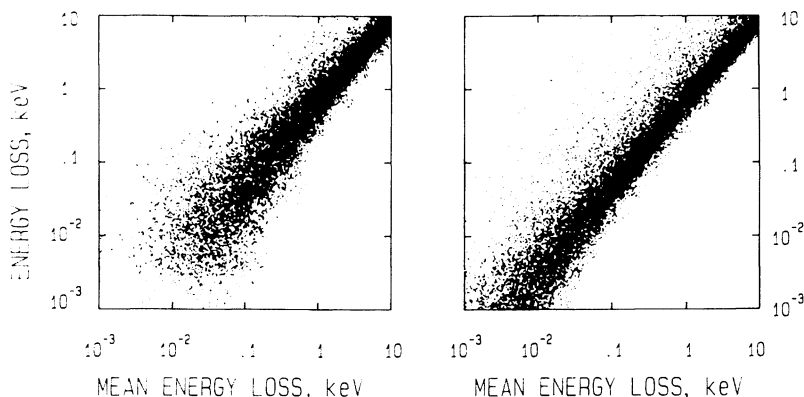


**Fig. 20.** Scatter diagrams corresponding to the solutions in Fig. 19. The right panel corresponds to the free electron model.

particle. The mean energy lost by a particle in a thin foil is equal to the mean energy imparted. However, even with this special geometry, the two straggling distributions differ. The reason is that high-energy  $\delta$  rays transport energy out of the site and into it. The net effect is a reduction of the frequency of high values of energy lost due to individual collisions. This can significantly cut the tail, and therefore the second moment, of the collision spectrum. The width of the straggling distribution is correspondingly reduced.

A quantitative treatment would have to account for the complexities of the energy transport by  $\delta$  rays. However, an approximation can at least illustrate the method to account for the difference between the two straggling distributions.

Figure 21 exemplifies the problem for heavy ions of 10 MeV/nucleon, i.e., for the same case that has been treated in the preceding subsection. In Fig. 18 an approximate modification of the  $1/\epsilon^2$  spectrum at low values of  $\epsilon$  has been included. This same modification is also given in Fig. 21. As stated earlier, this correction has little influence on  $\delta_2$  and on the variance of the straggling distributions. In contrast, the variance of the distributions is substantially affected by any modification of the high-energy part of the collision spectrum  $f_c(\epsilon)$ . A

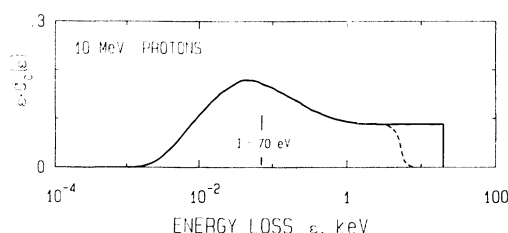


**Fig. 21.** The spectrum shown in Fig. 18 with a modification (dashed line) that accounts for  $\delta$  ray efflux from a 1- $\mu\text{m}$ -diameter site.

modification of the spectrum that may, for a 1- $\mu\text{m}$  site, account very roughly for the efflux of some of the energy of  $\delta$  rays is indicated by the broken line. The distributions of energy lost by a proton of 10 MeV and the energy transferred to the site, according to the modified spectrum, are compared in Fig. 22. The difference is considerable; the weighted average of energy per collision is  $\delta_2 = 550 \text{ eV}$  for the modified spectrum instead of the value of  $\delta_2 = 1.8 \text{ keV}$  for the energy-loss spectrum. The straggling distributions for energy imparted have a substantially smaller tail than the distributions of energy lost.

It is evident that complex calculations are required to obtain the modifications of the collision spectrum with adequate precision. If rough approximations are not sufficient, Monte Carlo simulations are more appropriate. An example for such computations is the work by Berger [18] for electrons and for spherical sites with diameters of 1  $\mu\text{m}$  or more.

## B. COMPARISON OF THE VARIOUS RANDOM FACTORS

The complexity of microdosimetric distributions makes it difficult to establish general rules for the experimental determination or the computation of these distributions. Different site sizes and different radiations require different treatment. It is nevertheless possible to derive certain guidelines to identify those random factors that are most essential in a given situation, and to discriminate them from other factors that play a minor role and may be disregarded under some conditions. The subsequent considerations are aimed at such a comparative assessment.

### 1. The Chain of Random Factors

If the medium is exposed to an absorbed dose  $D$  the energy imparted to a specified region is determined by a chain of random factors, as indicated in the diagram of Fig. 23. This diagram refers to the condition of small sites, i.e., of particle ranges considerably larger than the site diameter.

The first arrow indicates the random variable  $v$ , i.e., the *number of events* or, in a simplified statement, the number of independent charged particles

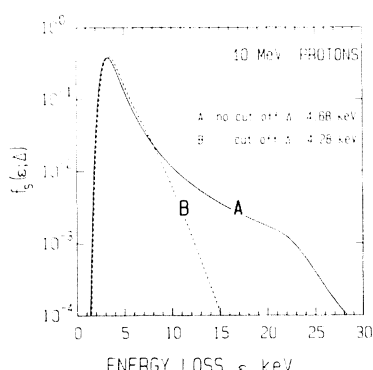


**Fig. 22.** Comparison of the distributions of energy lost and energy imparted for a 10-MeV proton traversing the 1- $\mu\text{m}$  diameter of a spherical tissue site. The distributions are based on the spectra in Fig. 21.

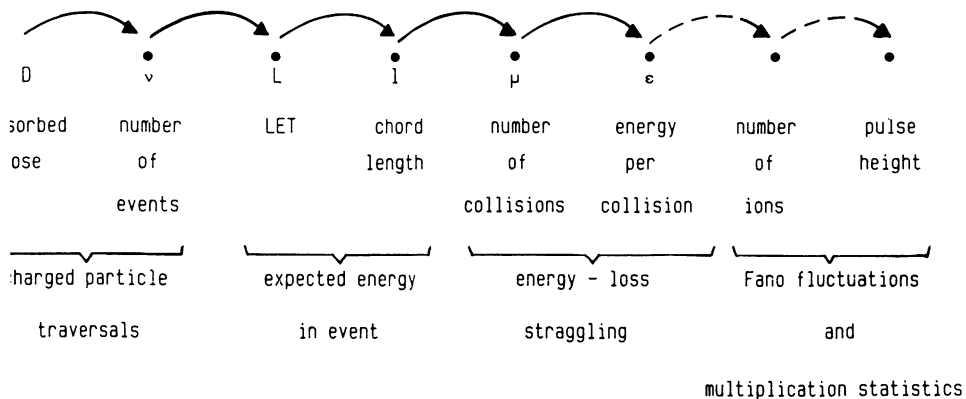


Fig. 23. Diagram of the chain of random factors that determine energy deposition in a site.

traversing the region. As stated earlier, this random variable follows a Poisson distribution.

The second random variable is the *stopping power*  $L$  of the ionizing particle. The LET distribution is designated by  $f(L)$  (see Section II, B), i.e.,  $f(L) dL$  is the probability that a particle traversing the site has an LET between  $L$  and  $L + dL$ . Whenever the range of the most energetic  $\delta$  rays is comparable to the size of the region, the LET is, in effect, reduced.

The expected energy imparted by an event is the product of the LET of the particle and the *chord length* in the site. The third arrow in the diagram refers to this random factor. The distribution  $f(l)$  of the chord length  $l$  depends on the geometry of the exposed region. Spheres of diameter  $d$  have the triangular distribution  $f(l) = 2l/d^2$ , with  $0 < l \leq d$ . For other regions, such as cylinders or spheroids, the chord-length distributions are more complex [31, 68].

Due to the energy-loss straggling the energy actually imparted to the region of interest may deviate considerably from the product of chord length and (restricted) stopping power,  $l \cdot L$ . A fourth random factor is therefore the number  $\mu$  of collisions along the chord, and the fifth, and more important, factor is the energy lost in each collision.

The last two arrows refer to factors that enter only into measured spectra. They are the *Fano fluctuations* of the number of ions produced for specified energy transfer, and the *multiplication statistics*, i.e., the stochastic fluctuation of pulse heights produced by a specified number of ions. The influence of these factors is, as will be seen, small.

## 2. The Formula for the Relative Variance

The influence of the different random factors on the single-event distribution can be assessed in terms of the relative variance, i.e., the variance divided by

the square of the mean. Utilization of a relative, i.e., dimensionless, quantity has the advantage that the resulting quantity is largely independent of particularities in the definitions of the quantities. Thus,  $V_1$ , the relative variance of the single-event spectrum, has the same value for the distributions  $f_1(z)$ ,  $f_1(\epsilon)$ , or  $f(y)$  [see Eq. (31)].

Under the condition of small sites and considerably longer particle ranges the relative variance of the single-event spectra can be expressed in terms of the relative variance of the LET distribution  $V_L$ , the chord-length distribution  $V_l$ , and the straggling distributions  $V_s$ . The additional terms added in brackets represent Fano fluctuations  $V_F$  and the multiplication statistics  $V_m$  and apply only to the measured spectra:

$$V_1 = V_L + V_l + V_L V_l + V_s + (V_F + V_m) \quad (116)$$

The formula is here cited without derivation [see Kellerer (33, 49)]. Its simplicity makes it a practical tool for assessing the role of the different random factors. The relative variances are additive, apart from the additional term  $V_L V_l$  that enhances the joint effect of the LET and chord-length variations. In effect, one need merely compare the relative variances for the individual random factors to establish their respective importance. The magnitudes of the relative variances are, therefore, examined next.

### 3. Magnitudes of the Relative Variances

*a. Linear Energy Transfer.*  $V_L$  is the relative variance of the LET distribution  $t(L)$  (see Section II,B):

$$V_L = (\bar{L}_D / \bar{L}_F) - 1 \quad (117)$$

where  $\bar{L}_D$  is the dose average LET, and  $\bar{L}_F$  is the track average LET. Both quantities require a suitable cutoff, if the maximum  $\delta$  ray range exceeds the dimensions of the reference region. Whenever one deals with sites of the order of fractions of  $1 \mu\text{m}$  or more, the cutoff has little effect on the numerical values of  $\bar{L}_D$  and  $\bar{L}_F$ . For the mixed radiation fields produced by uncharged primaries  $V_L$  is usually larger than 1. Small values of  $V_L$  apply only in the track-segment experiments where microorganisms are exposed to monoenergetic heavy ions.

*b. Chord-Length Distributions.* The relative variance  $V_l$  of the chord-length distribution  $f(l)$  is given by

$$V_l = (\bar{l}_D / \bar{l}_F) - 1 \quad (\text{for the sphere: } V_l = \frac{1}{8}) \quad (118)$$

where  $\bar{l}_D$  is the weighted average of the chord length ( $3d/4$  for the sphere of diameter  $d$ ), and  $\bar{l}_F$  the unweighted average ( $2d/3$  for the sphere). The mean chord length  $\bar{l}_F$  is for isotropic radiation fields, or for isotropic orientation of the sites, equal to  $4V/S$ , where  $V$  is the volume and  $S$  the surface of the (convex)

site. Figure 24 gives the values  $V_l$  for spheroids, which are often good approximations for a cell or a cell nucleus.

From the data for spheroids one concludes that  $V_l$  can be comparable to  $V_L$  only for the case of the track-segment irradiations or for sites that deviate very substantially from the spherical shape. Except in these cases the chord-length variations are of minor importance.

c. *Straggling.* The quantity  $V_s$  is the relative variance of the straggling distribution

$$V_s = \delta_2/\Delta \quad (119)$$

and comprises, as shown in Section III.D, the term  $(\delta_2 - \delta_1)/\Delta$  due to the fluctuations of energy loss per collision and the considerably smaller term  $\delta_1/\Delta$  due to the fluctuations of the number of collisions.

As shown in the preceding section,  $\delta_2$ , the weighted average of the energy imparted per collision, depends not only on the velocity of the particle but, due to the  $\delta$ -ray efflux, also on the geometry of the site. This influence of the geometry is, on the one hand, a complication but, on the other hand, a simplification. For sufficiently fast particles, i.e., particles with ranges substantially exceeding the site diameter, the maximum  $\delta$  ray ranges tend to be larger than the site diameter. The geometric cutoff determines the weighted energy imparted per collision  $\delta_2$  and it is (to a first approximation) merely a function of the site diameter. Thus for the example of the preceding section a value of  $\sim 550$  eV was deduced for a 1- $\mu\text{m}$  spherical site. As a rough approximation one may assume the value  $E_d/2 \ln(E_d/I)$ , where  $E_d$  is the energy of the electron with range somewhat smaller than the diameter of the site.

The comparison of the relations for  $V_L$  and  $V_s$  shows that LET is the dominant random factor for mixed fields of heavy particles, such as neutron recoils, and site sizes of fractions of 1  $\mu\text{m}$  or more. Straggling can nevertheless have a substantial influence on the shape of the spectra for sufficiently fast heavy ions. For slower heavy recoils with ranges comparable to the site diameter, straggling becomes insignificant. It is, therefore, justified that Caswell and

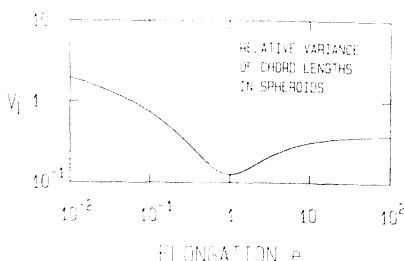


Fig. 24. Relative variance of chord length in prolate and oblate spheroids.

Coyne have disregarded straggling in computations of microdosimetric spectra for neutrons [50–52]. For much smaller sites straggling is, of course, the dominant factor.

*d. Fano Fluctuations and Multiplication Statistics.* For a given energy imparted,  $V_F$  is the relative variance of the number of ions produced. The relative variance of the pulse heights generated by the proportional counter for a given number of ions is denoted by  $V_m$ .

The Fano factor is smaller than the term  $w/\Delta$  that would result if Poisson statistics were applicable. The symbol  $\Delta$  is the energy imparted, and  $w$  is the mean energy per ionization. An approximation is

$$V_F = w/2\Delta \quad (120)$$

The influence of the multiplication statistics is somewhat larger. Under near optimal conditions a proportional counter responds with an exponential distribution of pulse heights to single electrons. One obtains then

$$V_m = w/\Delta \quad (121)$$

Since  $w$  is always much smaller than  $\delta_2$ , the two terms  $V_F$  and  $V_m$  are insignificant in microdosimetry. It follows that microdosimetric spectra are not greatly affected if one measures ionizations only, instead of all energy transfers. Computations with simulated tracks have shown [53] that, at least for electrons up to 10 keV, the differences between the exact spectra and spectra based on ionization counts are indiscernible. With adequate performance of microdosimetric instruments, measured spectra should be nearly identical to correctly computed spectra.

To summarize the comparison of the various random factors, one can give the entire formula for the relative variance of the single-event spectrum  $f(y)$  or  $f_l(z)$ . The case of a spherical site is assumed; the modification for a different geometry with  $V_l > \frac{1}{8}$  is straightforward. The value 34 eV is inserted for  $w$ :

$$\begin{aligned} V_l &= \frac{1}{8} + \frac{9}{8} V_L + \frac{\delta_2}{\Delta} + \left( -\frac{50 \text{ eV}}{\Delta} \right) \\ &= \frac{9 \bar{L}_D}{8 \bar{L}_T} - 1 + \frac{\delta_2}{\Delta} + \left( -\frac{50 \text{ eV}}{\Delta} \right) \end{aligned} \quad (122)$$

This is equivalent to a relation for the weighted mean of the single-event spectrum. Substituting  $V_l = (\bar{y}_D/\bar{y}_F) - 1$  and  $\bar{y}_F = \Delta/l_F$  one obtains for the spherical site of diameter  $d$

$$\bar{y}_D = \frac{9}{8} \bar{L}_D + \frac{3\delta_2}{2d} + \left( -\frac{3 \cdot 50 \text{ eV}}{2d} \right) \quad (123)$$

with analogous expressions for  $\bar{\epsilon}_D$  and  $\zeta$ . The term in parentheses applies as stated, only to experimental determinations.

Finally, one has, according to Eq. (65), the relation for the dose-dependent distributions  $f(z; D)$ :

$$V_z = (\bar{z}_r/D)(1 + V_1) = (1/n)(1 + V_1) \quad (124)$$

where  $n$  is the mean event number. The first term represents the (usually insignificant) influence of the Poisson fluctuations of the event numbers; the second term represents the fluctuations of event size.

## VI. Geometric Aspects of the Inchoate Distribution

The computational simulation of charged particle tracks—initiated by the electron transport studies of Berger [18, 54] and first realized in full detail in the computer code of Paretzke [17, 55]—has become an important and common tool of microdosimetry (see also [19, 56–60]) and has stimulated its recent development. The method permits the assessment of the microdistribution of energy in small regions that are not, at present, accessible to experimental investigations.

The simulation of charged particle tracks is more than a substitute for deficiencies in the experimental techniques. Its theoretical implications have been equally important and have led to various new concepts and quantities in microdosimetry. These developments would require a separate treatment. Even a summary is, at present, difficult, because the mathematical foundations for some of the essential results are still inadequate; few rigorous derivations have yet been given. However, in spite of their insufficiently developed foundations, the new concepts are extensively used, and any survey of the fundamentals of microdosimetry without their consideration would remain incomplete. A brief synopsis of essentials is therefore given in this final section. Some of the new ideas have arisen from problems of sampling of simulated tracks [62]. A consideration of sampling procedures is therefore a suitable starting point.

### A. UNIFORM AND WEIGHTED RANDOM SAMPLING

Simulated charged particle tracks can be utilized to derive the distributions  $f(y)$  or  $f_i(z)$  and the corresponding mean values. In analogy to microdosimetric measurements one may envisage a fixed site surrounded by randomly positioned tracks. Each interception of the site by a track determines then the size of an energy-deposition event. In the computations a reversed point of view is far more suitable. One can envision a fixed particle track surrounded by randomly positioned equal sites (probes), which are usually spheres. Each interception

of the track by a site determines then the size of an energy-deposition event. The resulting distributions and parameters are the same, provided correct sampling procedures are applied. There are several different sampling procedures that are equally correct but not equally efficient or convenient.

It is assumed that simulated charged particle tracks are specified by the spatial coordinates of the transfer points  $T_i$  and by their associated energy transfers  $\epsilon_i$ . The sampling procedure will be explained with reference to individual tracks. Actual computations require a set of tracks, i.e., repeated random realizations. Energies and types of the particles will vary for mixed radiation fields. If one considers track-segment experiments, one deals with partial tracks. For simplicity the subsequent explanations will refer to entire tracks.

### 1. Associated Volume and Event Frequency

One can begin the discussion with the seemingly simple problem of determining from a simulated track the mean specific energy  $\bar{z}_F$  per event in a spherical region of radius  $r$ .

To deal with the problem one needs first the notion of the associated volume  $A$  of the track.\* This is the union of all spheres of radius  $r$  that are centered at transfer points. The specific energy  $z$  in a sphere of radius  $r$  differs from zero if and only if the sphere is centered within the associated volume. It is convenient to assign the value  $z$  for a sphere to the center  $C$  of the sphere; i.e., to treat  $z$  as a *point* function although its value depends, of course, on the energy transfers within the spherical neighborhood of  $C$ . With this formal convention one can say that the associated volume is that region where the specific energy is larger than zero.

The notion of the associated volume was introduced by Lea [5] for the specific purpose of computing event frequencies. It is, however, merely a special case of one of the basic concepts of geometric probability, namely, the *Minkowsky product* (or *direct product*) of two geometrical configurations [63, 64]. In the general definition the two geometric configurations can be arbitrary. In Lea's definition they are the spherical site  $S$  and the set  $T$  of transfer points forming the track, i.e., the inchoate distribution of energy transfers. A spherical site will be assumed in the subsequent considerations, too, but it will be evident how the results can be generalized.

A site incurs an event if it is centered within the associated volume of a track. Accordingly the event frequency equals the associated volume per unit volume of the exposed medium. Let  $E$  be the fixed initial energy of charged particles and  $A$  the mean associated volume per particle. The number of particles per unit volume and unit dose is then  $\rho/E$ , and the associated volume per unit volume

\*To avoid complicated terminology the expression *associated volume* and the symbol  $A$  are used both for the domain itself and for its measure, the volume.

and unit dose is  $\rho A/E$ . As stated, this equals the event frequency  $\phi(0)$  per unit dose:

$$\phi(0) = \rho A/E \quad \text{and} \quad \bar{z}_F = E/\rho A \quad (\rho = \text{density of the medium}) \quad (125)$$

To determine  $\phi(0)$  or  $\bar{z}_F$  one need therefore merely compute the associated volume of simulated tracks of specified energy. This may seem a simple procedure, but even the two-dimensional analog in Figure 25 demonstrates that an exact computation is nearly impossible. There is no practical algorithm to obtain the volumes of multiple intersections.

To derive the distribution of specific energy, or even the volume of the associated region, one must therefore use random sampling. The naive approach would be to define a box or a cylindrical region of volume  $B$  that contains the associated volume and then to choose uniformly distributed random points within this region. With a sufficiently large number of trials the associated volume is then

$$A = f \cdot B \quad (126)$$

where  $f$  is the fraction of sampling points that are contained in the associated volume.

By the same sampling procedure one can, in principle, also determine the parameter  $\bar{z}_D$  or the distribution  $f_1(z)$  or  $F_1(z)$ . For this purpose one must merely disregard those trials that lie outside the associated volume; for the sample points that are inside one must determine the specific energy. Then  $F_1(z)$  is the fraction of points with specific energy up to  $z$ :

$$\text{Prob}\{z_i \leq z\} = \int_0^z f_1(z) dz = F_1(z) \quad (127)$$

The parameter  $\bar{z}_D$  is obtained in terms of the mean values over all sample results in the associated volume:

$$\bar{z}^2/\bar{z} = \bar{z}_D \quad (128)$$

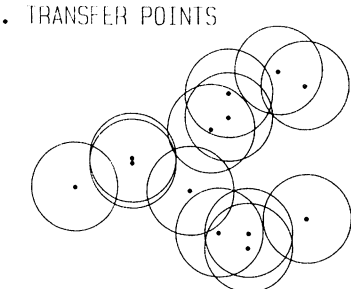


**Fig. 25.** Diagram to indicate the problem of the computation of the associated volume for a given inchoate distribution.

The frequency mean need not be determined by Eq. (125). It could also be derived as the mean of all observed  $z$ -values for the sample points in the associated volume:

$$\bar{z} = \bar{z}_F \quad (129)$$

The naive *uniform* sampling is correct, but it is too inconvenient and wasteful to be practicable. In actual computations a different method is therefore required.

## 2. Formulas for Weighted Sampling

With *uniform* sampling any volume element  $dB$  of the sample space has equal probability to be selected. An alternative method is *weighted* sampling, i.e., sampling where the probability of  $dB$  to be selected is proportional to the specific energy at  $dB$ . The specific energy at  $dB$  is, as has been stated, the specific energy in a sphere centered at  $dB$ .

Weighted sampling can be achieved as follows. In a first step one selects randomly an energy transfer point  $T_i$ , the selection probability being proportional to the corresponding energy transfer  $\epsilon_i$ . In a second step one chooses a random point in the sphere of radius  $r$  centered at the selected random point. In this way any point in the associated volume is reached with probability proportional to the specific energy at the point.

While uniform sampling provides the density  $f_1(z)$ , weighted sampling provides the weighted distribution  $d_1(z)$  (see Section II,F). Accordingly one derives, from the average of values  $z_k$  obtained with weighted sampling, the parameter  $\bar{z}_D$ :

$$\langle z \rangle = \int z d_1(z) dz = \bar{z}_D \quad (130)$$

The symbol  $\langle \rangle$  denotes the average obtained with weighted sampling, and discriminates it from the averages obtained by uniform sampling.

To determine the frequency average with weighted sampling one must average the reciprocals of the observed values [see Eq. (27)]:

$$\langle z^{-1} \rangle = \int z^{-1} d_1(z) dz = \int f_1(z) dz / \bar{z}_F \quad (131)$$

and therefore

$$\bar{z}_F = 1 / \langle z^{-1} \rangle \quad (132)$$

The procedures for uniform and for weighted sampling can be formulated in a modified but equivalent form that applies also to nonspherical regions  $S$  of reference:

For uniform sampling one selects a random point  $P$  in a sufficiently large region containing the track, and then positions the center, i.e., a fixed reference point, of  $S$  at  $P$ . The direction of  $S$  is distributed randomly for isotropic sampling.

For weighted sampling one selects a random point on the track, i.e., a transfer point, and a random point in  $S$ , and one then superimposes the two selected points. The direction of  $S$  is distributed randomly for isotropic sampling.

It is readily seen that this more general formulation defines a procedure that is equivalent to the one specified for spherical sites.

The procedure for weighted sampling is required in numerical evaluations of simulated particle tracks [62, 65]. It is also essential in considerations that lead to the proximity function and its applications, and it will be discussed in this context in Section VI,C. However, before these matters are treated, certain simplified formulas for the event frequencies and the mean event sizes can be derived.

With uniform sampling one obtains the distribution  $f_1(z)$  directly; however, as stated, uniform sampling is highly inefficient. With weighted sampling one obtains the distribution  $d_1(z)$ , but the distribution  $f_1(z)$  can be obtained from  $d_1(z)$ :

$$f_1(z) = z^{-1}d_1(z) \Big/ \int z^{-1}d_1(z) dz \quad (133)$$

## B. FORMULAS FOR THE ASSOCIATED VOLUME AND FOR THE UNWEIGHTED AVERAGES

For a complex inchoate distribution it is, as has been stated, difficult to compute the associated volume, and random sampling is therefore required. However, for the special case of linear tracks there are simple solutions and it has been found [66] that the solutions apply surprisingly well even to electrons.

### 1. Spherical Sites

Consider for a particle of range  $R$  and initial energy  $E$  a track that is depicted as a straight line segment with the continuous slowing-down approximation. This will be termed a *linear track*. The associated volume of this track is

$$A = r^2\pi R + 4r^3/3 \quad (134)$$

Accordingly the event frequency per unit absorbed dose is [see Eq. (125)]

$$\phi(0) = 1/\bar{z}_F = \rho(r^2\pi R + 4r^3\pi/3)/E \quad (135)$$

Evidently this relation applies also for the mean range  $\bar{R}$  of the particles in a mixed field and for the mean initial energy  $\bar{E}$  and in this more general form it permits a convenient check for internal consistencies of experimental microdosimetric data.

The frequency mean lineal energy  $\bar{y}_F$  is linked to  $\phi(0)$  by the equation

$$\bar{y}_F^{-1} = \phi(0)/r^2\pi\rho \quad (136)$$

Utilizing the relation  $\bar{L}_F = \bar{E}/\bar{R}$  one obtains with Eq. (135)

$$1/\bar{y}_F = \bar{R}/\bar{E} + 4r/3\bar{E} = 1/\bar{L}_F + \bar{l}/\bar{E} \quad (137)$$

Accordingly one obtains a straight line if  $1/\bar{z}_F$  is plotted versus the mean chord length  $\bar{l} = 4r/3$  of the site. The event frequency or the unweighted mean event sizes  $\bar{y}_F$ ,  $\bar{z}_F$ , or  $\bar{\epsilon}_F$  are therefore determined for all site sizes if they are known for two sizes. The knowledge of merely two values permits also the determination of the track average LET  $\bar{L}_F$ , the mean range  $\bar{R}$ , and the mean initial energy  $\bar{E}$  of the particles.

Figure 26 indicates the application of the result to photons.

## 2. Generalization of the Result to Nonspherical Sites

The average chord length  $\bar{l}$  is, for all convex bodies, equal to four times the volume  $V$  divided by the surface area  $S$ . For example, one has for circular cylinders of radius  $r$  and height  $h$ :

$$\bar{l} = 4V/S = 2rh/(r + h) \quad (138)$$

The mean intercept  $\bar{s}$  of tracks with a convex site depends only on the mean chord length  $\bar{l} = 4V/S$  of the site and the mean range  $\bar{R}$  of the tracks (31):

$$1/\bar{s} = 1/\bar{l} + 1/\bar{R} \quad (139)$$

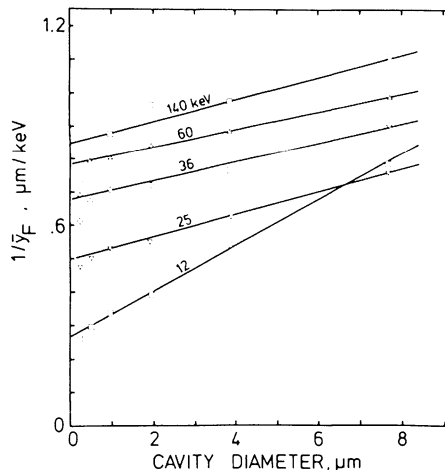


**Fig. 26.** Diagram of frequency average event sizes  $\bar{y}_F$  for x rays according to Kliauga and Dvorak [66].

With the relation for the mean energy imparted:

$$\bar{\epsilon}_F = \bar{E}(\bar{s}/\bar{R}) \quad (140)$$

one obtains

$$1/\bar{y}_F = \bar{l}/\bar{\epsilon}_F = \bar{l} \cdot \bar{R}/\bar{E} \cdot \bar{s} = 1/\bar{L}_F + \bar{l}/\bar{E} \quad (141)$$

The result of this subsection applies, therefore, generally to all convex sites.

### C. THE RANDOM INTERCEPT OF TWO GEOMETRIC OBJECTS

This subsection deals with a formula of considerable generality that permits—applied to microdosimetry—the computation of the weighted averages of the single-event spectra in sites of specified shape. The formula also demonstrates the important role of the proximity functions, or point-pair distance distributions. All considerations in this subsection are given in purely geometric terms, but without mathematical rigor. The application to microdosimetry is treated in Section VI.D.

#### 1. Uniform and Weighted Randomness of Straight Random Lines

Uniform isotropic sampling corresponds to *uniform isotropic randomness* for the intercept of two geometric objects  $S$  and  $T$ . Weighted isotropic sampling corresponds to *weighted randomness*. The concepts are familiar, and a satisfactory mathematical theory exists in the special case where  $S$  is a convex body (in a space of arbitrary dimensions) and  $T$  is a straight random line (see, e.g., [67, 68]).

For uniform randomness one selects a random point in the space that contains  $S$  and then chooses a straight line  $T$  with random direction that passes through the point. Only those lines are considered that intersect  $S$ , and the resulting distribution of intercepts  $l$  is termed the chord-length distribution  $f(l)$  for uniform randomness.

For weighted randomness one selects a random point within  $S$  and then chooses a straight line  $T$  with random direction that passes through the point. The resulting distribution of intercepts  $l$  is termed the chord-length distribution  $d(l)$  for weighted randomness.\*

Kingman [69] has obtained the important relation that links the densities for uniform and for weighted randomness:

$$d(l) = l f(l)/\bar{l}_F \quad (142)$$

\*Uniform randomness and weighted randomness have also been termed  $\nu$ -randomness and  $\mu$ -randomness, and the notation  $f_\mu(l)$  and  $f_\nu(l)$  has been used for the densities. The notation  $f(l)$  and  $d(l)$  is here used to emphasize the correspondence to the frequency distributions and weighted distributions  $f_i(z)$  and  $d_i(z)$ .

where  $\bar{l}_F$  is the mean chord length for uniform randomness.  $\bar{l}_F$  equals, as has been pointed out in earlier sections,  $4V/S$  for convex bodies of volume  $V$  and surface  $S$ .

Equation (142) is analogous to the relations that link other densities and weighted densities, such as  $f_i(z)$  and  $d_i(z)$  [see Eq. (27)], and as with the other densities one obtains the relation between the weighted mean and the first two moments of the unweighted distribution

$$\bar{l}_D = \int l d(l) dl = \frac{\bar{l}_F^2}{\bar{l}_F} \quad (143)$$

The variance for uniform randomness is

$$\sigma_F^2 = (\bar{l}_D - \bar{l}_F) \cdot \bar{l}_F \quad (144)$$

## 2. Uniform and Weighted Randomness of Pairs of General Geometric Objects

The notion of uniform and weighted randomness can be extended to apply to arbitrary geometric objects, provided these objects meet certain minimum requirements of regularity that need not be considered in the present nonmathematical context.

*Uniform isotropic randomness* of the intersection of two objects  $S$  and  $T$  results if  $S$  is kept in fixed position and if a reference point, called center, of  $T$  is superimposed with a random point in a sufficiently large region containing  $S$ . Random orientation of  $T$  is assumed. If  $T$  misses  $S$ , i.e., if  $T \cap S = 0$ , the trial is disregarded.

The resulting density of the volumes\*  $u$  of the intersection  $T \cap S$  is termed the frequency distribution  $f(u)$ .

*Weighted isotropic randomness* of the intersection of two objects  $S$  and  $T$  results if a random point is chosen in  $S$  and in  $T$ , if  $S$  is kept in fixed position, and if  $T$  is shifted so that the two random points coincide. Again  $T$  is randomly oriented. The resulting density of the volumes  $u$  of intersection is termed the weighted distribution  $d(u)$ .

One can show [70] that the familiar relation between densities and weighted densities applies also in this general case:

$$d(u) = u f(u)/\bar{u}_F \quad (145)$$

where  $\bar{u}_F$  is the mean overlap under uniform randomness. Relations for  $\bar{u}_F$  are obtained from the *fundamental formula* of Blaschke and Santalò (71, 72); for a simplified, nonmathematical explanation see Kellerer [73].

\*The term volume is used in the general sense of measure, i.e., the region of overlap need not be three-dimensional.

As in the familiar case of straight random lines one obtains the relation between the weighted mean intercept and the first moments of the unweighted distribution:

$$\bar{u}_D = \int u d(u) du = \frac{\bar{u}_F^2}{\bar{u}_F} \quad (146)$$

For uniform randomness the variance of the overlap  $u$  is

$$\sigma_F^2 = (\bar{u}_D - \bar{u}_F) \cdot \bar{u}_F \quad (147)$$

The importance of Eqs. (145) to (147) lies in the fact that a general and fairly simple formula exists for the weighted averages, and therefore that the variance of  $f(u)$  can be obtained also.

The formula will be considered next. It contains the *proximity functions*, or *point-pair distance distributions*, of the geometric objects  $T$  and  $S$ .

### 3. The Formula for the Weighted Mean Intersection and Definition of the Proximity Functions

One may choose pairs of independently and uniformly distributed random points in a geometric object and determine the density  $p(x)$ , of distances  $x$  between the points. The function  $p(x)$  is termed the *point-pair distance distribution*, and  $p(x) dx$  is the probability that a pair of random points has a distance between  $x$  and  $x + dx$ .

For some geometries it is convenient to utilize the nonnormalized densities that result when  $p(x)$  is multiplied by the measure of the geometric object. This nonnormalized distribution is called the *proximity function*. For convenience the proximity functions for the geometric objects  $S$  and  $T$  will be denoted by  $s(x)$  and  $t(x)$ ,

$$s(x) = V_S \cdot p_S(x) \quad \text{and} \quad t(x) = V_T \cdot p_T(x) \quad (148)$$

where  $V_S$  is the measure, i.e., volume, of  $S$ , and  $V_T$  is the measure of  $T$ , and  $p_S(x)$  and  $p_T(x)$  are the distance distributions for  $S$  and  $T$ .

A fundamental relation [70] expresses the weighted mean of the intercept in terms of the proximity functions

$$\bar{u}_D = \int_0^{x_{\max}} \frac{s(x)t(x)}{4\pi x^2} dx \quad (\text{in three-dimensional space}) \quad (149)$$

and

$$\bar{u}_D = \int_0^{x_{\max}} \frac{s(x)t(x)}{2\pi x} dx \quad (\text{in two-dimensional space}) \quad (150)$$

where  $x_{\max}$  is the maximum point-pair distance in  $S$  or  $T$ , whichever value is smaller.

The somewhat lengthy proof of this remarkably general result is omitted; it has certain connections to a theorem derived by Robbins [74]. The fundamental formula of Blaschke and Santalò determines the unweighted average  $\bar{u}_F$  of the random intersection, for uniform isotropic randomness. Equation (149) together with Eq. (147) determine the second moment of the intercept for uniform randomness or the variance

$$\sigma_u^2 = (\bar{u}_D - \bar{u}_F) \cdot \bar{u}_F \quad (151)$$

Proximity functions are known for regular geometric objects such as cubes [75], cylinders [76], or spheroids [68]. As an example one can give the familiar relation for a sphere of radius  $r$ ,

$$s(x) = 4\pi x^2 \left[ 1 - \frac{3x}{4r} + \frac{1}{16} \left( \frac{x}{r} \right)^3 \right], \quad 0 \leq x \leq 2r \quad (152)$$

Instead of the proximity function one often uses, when one deals with compact geometric objects, the *geometric reduction factor*:

$$\begin{aligned} U(x) &= s(x)/4\pi x^2 && \text{(in three-dimensional space)} \\ U(x) &= s(x)/2\pi x && \text{(in two-dimensional space)} \end{aligned} \quad (153)$$

For complicated structures the computation of the proximity function may require complex numerical integrations or even Monte Carlo simulations, but the functions can always be obtained. It is striking that the variance of the overlap of two objects or their weighted mean overlap can be expressed by a simple integration over two functions each of which depends on only one of the structures.

An application of the result to microdosimetry is straightforward and will be considered next.

#### D. APPLICATION TO MICRODOSIMETRY

In the preceding subsection the random intercept of two configurations has been treated purely as a geometric problem. This has made the essential result more transparent.

However, the considerations are intimately linked to the problems of energy deposition by ionizing radiations. The point-pair distance distributions and the geometric reduction factor have been introduced into dosimetric computations by Berger [77]; his treatment also contains the essence of later results. The equation for the weighted mean intercept, too, has been derived in microdosimetric studies; Eq. (149) is merely a generalization of this result.

##### 1. Proximity Function for Charged Particle Tracks

To apply Eq. (149) to microdosimetry one must first introduce the concept of the proximity function of a particle track. This concept is entirely analogous

to that of the geometric proximity function, with the only modification being that energy replaces volume. The function  $t(x)$  is the proximity function of the particle track. Analogously to the (volume) proximity function, the (energy) proximity function  $t(x)$  can be understood as the distance distribution of energy transfers (weighted by their values  $\epsilon_i$ ) multiplied by the total energy of the track. The proximity function includes a  $\delta$  function at  $x = 0$  that is proportional to the weighted mean of individual energy transfers  $\bar{\epsilon}_i$ .

The actual computation is best explained in terms of the integral proximity function

$$T(x) = \int_0^x t(x') dx' \quad (154)$$

From a simulated track,  $T(x)$  is obtained by considering all pairs of transfer points that are separated by a distance less than  $x$ :

$$T(x) = \sum_{i, k} \epsilon_i \epsilon_k / \sum_i \epsilon_i \quad (155)$$

where the summation runs over all  $i$  and over all transfer points  $k$  separated by distance up to  $x$  from the transfer point  $i$ . The value  $T(0)$  determines the  $\delta$  function  $T(0) \cdot \delta(x)$  in  $t(x)$ . It results from the pairs with  $i = k$ :

$$T(0) = \sum_i \epsilon_i^2 / \sum_i \epsilon_i \quad (156)$$

From Eq. (155) one recognizes that  $T(x)$  equals the expected energy (on the same track) in a sphere centered randomly on an energy transfer. Accordingly  $t(x) dx$  is the expected energy within the distance interval  $x$  to  $x + dx$  from a randomly selected energy transfer.

In actual computations the proximity function is derived by sampling all pairs of energy transfers in a sufficiently large number of simulated particle tracks. If the particle tracks have different initial energies, the proximity function is the energy-weighted average for the different tracks. Proximity functions have been computed for electrons and for track segments of heavy ions (see, e.g., [53, 62, 78–81]). Figure 27 gives the functions for electrons up to 10 keV.

## 2. The Formula for the Dose Average Event Size

The theorem from Section (VI,C) can be applied to the overlap of a site  $S$  with a charged particle track  $T$ . Thus one obtains the weighted average of the energy imparted per event:

$$\bar{\epsilon}_D = \int_0^{x_{\max}} \frac{t(x)s(x)}{4\pi x^2} dx = \int_0^{x_{\max}} t(x)U(x) dx \quad (157)$$

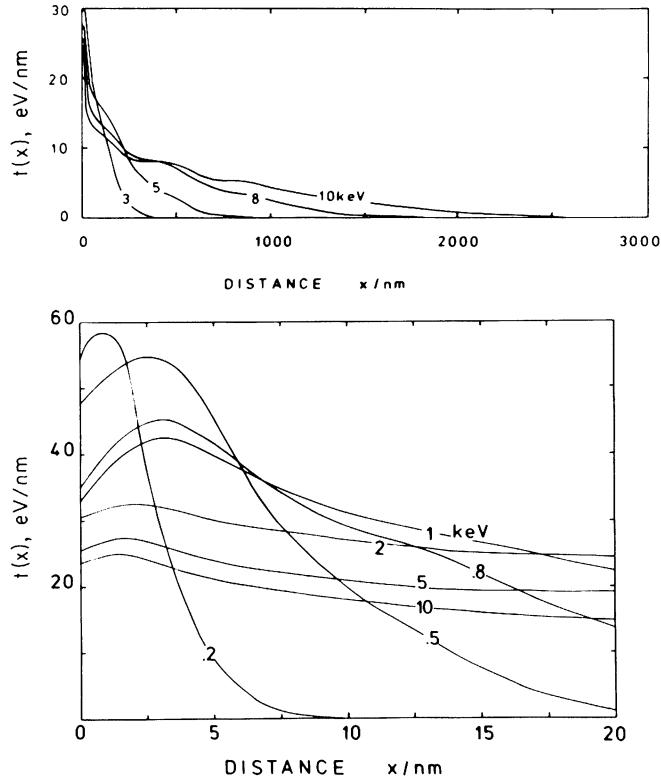
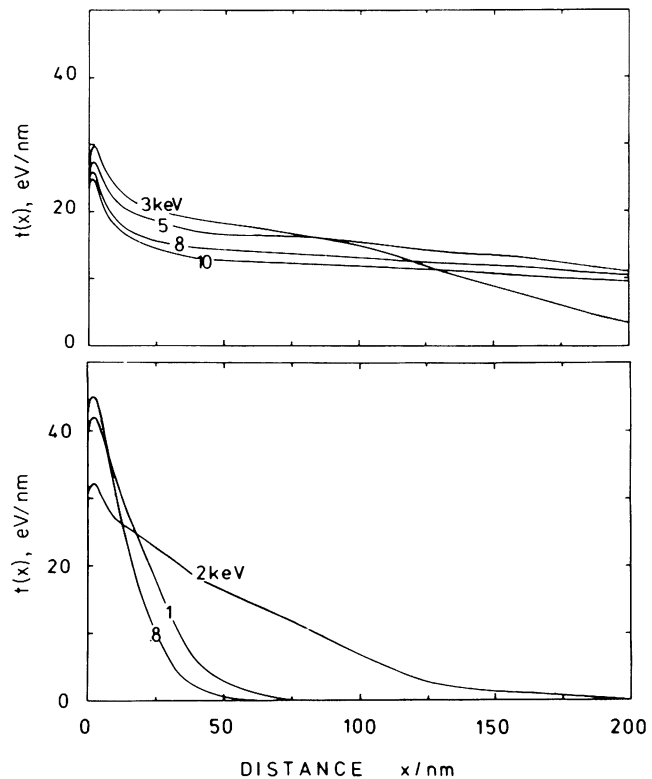


**Fig. 27.** Proximity functions  $t(x)$  for low-energy electrons. (From Chmelevsky *et al.* [53].)

The right-hand expression utilizes the geometric reduction factor  $U(x)$  of the site rather than the proximity function  $s(x)$  of the site.

The upper bound of integration is the maximal diameter of the site, in the case of the sphere its diameter. With  $\bar{\epsilon}_D$  one also obtains the averages  $\bar{z}_D$  and  $\bar{y}_D$  of specific energy or lineal energy in single events.

The result is valid regardless of the complexity of the tracks and the structure of the sites. The site need be neither spherical nor convex, nor even simply connected. The generality of the theorem permits a great variety of applications and extensions.

### 3. Further Considerations of the Proximity Function

If a particle of initial energy  $E$  were represented by a straight line segment of length  $R$  and constant energy transfer  $E/R$ , the proximity function would have the simple form

$$t(x) = 2E/R(1 - x/R), \quad 0 \leq x \leq R \quad (158)$$

A somewhat better approximation postulates straight line segments with energy transfer varying as a function of remaining range (continuous slowing-down approximation). One obtains then [24]

$$t(x) = 2 \int_x^R L(s)L(s-x) ds/E \quad (159)$$

where  $L(s)$  is the LET at remaining range  $s$ . At sufficiently large values  $x$  the approximation in terms of Eq. (159) is good for heavy ions. For electrons the approximation fails as shown in Fig. 28.

From Eq. (159) one obtains  $t(x) = 2\bar{L}_D$  for sufficiently small  $x$ . The proximity function can therefore be considered as an extension of the LET concept that takes into account additional factors, such as the ranges of the particles.

Equation (159) is appropriate for heavy particles for all values of  $x$  that exceed the maximum range of the  $\delta$  rays. At smaller distances  $t(x)$  is codetermined by energy-loss straggling and the radial distribution of energy around the center of the track.

For track segments the influence of straggling and radial energy distribution can be separated [24, 62]. The proximity function is the sum of a term,  $t_\delta(x)$ , that is the weighted average of the proximity functions for all  $\delta$  rays, and a term that is equal to the proximity function of a continuous track with the same radial energy distribution as the actual track:

$$t(x) = t_\delta(x) + t_a(x) \cdot L \quad (160)$$

The index of the second term indicates the fact that it refers to an *amorphous* track that averages out  $\delta$  rays. This term contains the stopping power as a factor,

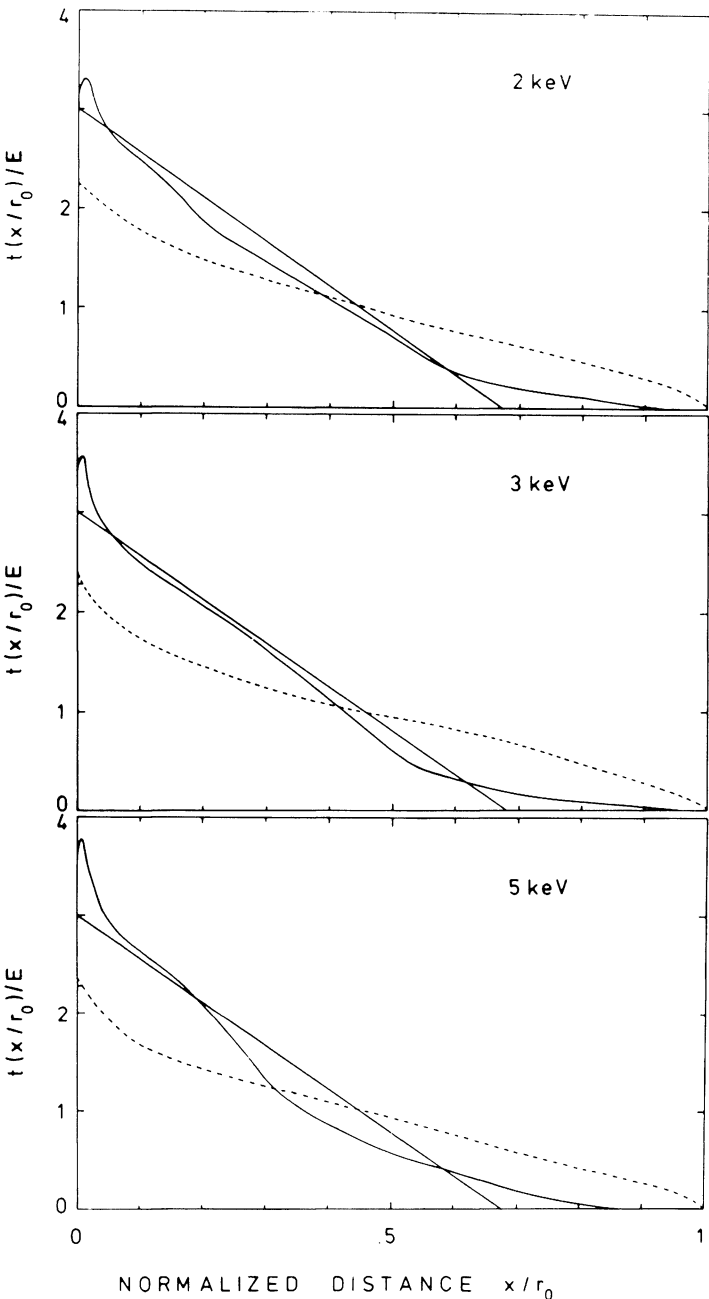


**Fig. 28.** Comparison of proximity functions for electrons (solid curves) with functions that result from simplified models of Chmelevsky *et al.* [53]. The dashed curves are obtained when the electron tracks are treated as straight lines with continuous energy loss according to the LET. The solid straight lines result if the tracks are pictured as straight lines with constant energy loss rate and ranges equal to  $\frac{2}{3}$  of the continuous slowing-down range. The ranges and LET values are for water. The curves show that the LET approximation is unsuitable for electrons because of straggling and angular scattering.

and the other factor,  $t_a(x)$ , depends only on the radial dose distribution and can be calculated from it.

Examples of the proximity functions for track segments of heavy ions of 20 MeV/nucleon and their separation into the  $\delta$  term and the term for the continuous track are given in Fig. 29 for short track segments of fast heavy ions.

Equation (160) can be utilized for an alternative derivation of the weighted average and the variance of the single-event distribution. One obtains with the theorem of Eq. (157).

$$\begin{aligned}\bar{y}_D &= \frac{1}{l} \int U(x)(t_\delta(x) + t_a(x) \cdot L) dx \\ &= \frac{1}{l} \int U(x)t_\delta(x) dx + L \cdot \int U(x)t_a(x) dx = \frac{\delta_2}{l} + \frac{Lx'}{l} \quad (161)\end{aligned}$$

The first term contains the weighted mean energy imparted per collision. It represents, as stated earlier with reference to Eq. (123), the influence of straggling. The second term contains the parameter  $x'$ , which equals the weighted mean chord length whenever  $t_a(x)$  is sufficiently close to 2.

The comparison with Eq. (123) shows that the proximity functions make it possible to account exactly for track structure and site geometry where the earlier considerations had to be based on relatively crude approximations (see also Kellerer [82]).

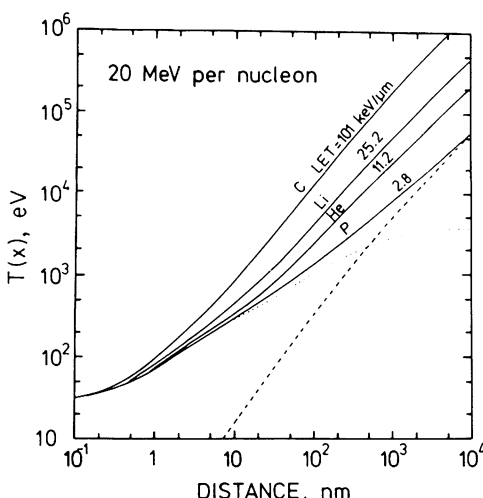


**Fig. 29.** Integral proximity functions  $T(x)$  for different heavy ions of kinetic energy of 20 MeV per nucleon from Chmelevsky [62]. The dotted line represents the contribution  $T_\delta(x)$  due to  $\delta$  rays and the dashed line corresponds to the LET-dependent term for protons. For the other ions this term is shifted by a factor corresponding to the increased LET.

### E. A BIOPHYSICAL MODEL

As in Section IV, a concluding section is added here that indicates, without actual assessment of radiobiological findings, the applicability of some of the microdosimetric concepts and data. The treatment is a generalization of the considerations that have been given, with reference to the site concept, in Section IV,C.

Assume that energy transfers produce a proportional number  $k\epsilon_i$  of *sublesions*. Such sublesions can be molecular alterations, for example, in DNA. They can also be more complex changes, such as chromosome instabilities (breaks). Assume further that the sublesions can interact pairwise. The formation of *lesions* is then a *second-order process*.

A second-order process leads, under certain conditions, to a quadratic dependence of the yield on the concentration of reactants (sublesions). One implied condition is the absence of saturation, i.e., the absence of concentrations that are so high that there is no further proportional increase of reactants. Another condition is lack of competition between sublesions (depletion); this amounts to the postulate that the pairwise interactions of sublesions are independent processes. Lack of saturation is a realistic concept for sparsely ionizing and medium-densely ionizing particles. However, with densely ionizing particles saturation plays a role on various levels toward the observable cellular damage. Lack of competition may well be a realistic postulate for DNA single strand breaks that have relatively small probabilities of combining into double strand breaks. It may also be realistic for chromosome instabilities that are far more numerous than observable chromosome aberrations.

In a second-order process the probability of a reactant interacting is proportional to the concentration of neighboring reaction partners. With chemical reactions this is a simple situation. The reactants are uniformly distributed throughout the medium, and the yield depends then simply on the square of the concentration. With ionizing radiations the situation is characteristically different. The concentrations of energy transfers or of subsequent radiation products vary greatly, and with a nonlinear dependence of the yield on concentration a complex relation exists between microscopic patterns of energy deposition and the resultant yield of cellular damage. This makes microdosimetry necessary. However, the difficulty goes beyond the problem of variations of concentration in the medium. Instead, the very concept *concentration* of energy transfers or radiation products is, in a strict sense, inapplicable. Any derived value depends on the size of the reference volume, as demonstrated by the strong dependence of the microdosimetric distributions on site size. The notion of a concentration is therefore meaningless. However, one can invoke an *effective concentration* if one has knowledge of the scale of potential interactions between reaction partners.

The microdosimetric variables  $\epsilon$ ,  $z$ , and  $y$  are defined in terms of a test region, the site. Its dimensions determine the scale of possible interaction. According to this concept, an energy transfer, or the resulting reactant, has as potential reaction partners all transfers that happen to be located in the same region. This treatment has the advantage that the distributions of microdosimetric variables can be measured. On the other hand, it is, as stated in Section IV, an obvious simplification; the reactants within the site cannot, regardless of their mutual distances, be equally likely to interact. In many biophysical applications the resulting inaccuracy of the treatment may be of little concern. The principal aim is the derivation of a rough effective interaction distance, and this can be achieved in terms of the site concept. The concept is, however, grossly inadequate if long-range particles are compared with very short range particles. The long-range particles dissipate energy throughout the site; the short-range particles concentrate the energy in small clusters. For an adequate comparison of such disparate configurations and for any investigation of distance-dependent interaction probabilities, one needs a modified analysis.

The concept of the proximity function permits such an analysis. Although this chapter does not deal with radiobiophysical applications, the essential formulas can be given. An abbreviated terminology will be used in speaking of the *interaction of pairs of energy transfers*. This refers to the probability that sublesions are formed by the two energy transfers and that they interact to form a lesion.

It is assumed that the probability that a transfer will interact is proportional to the number of its neighbors multiplied by a distance-dependent interaction probability  $\gamma(x)$ . Evidently each transfer has to be weighted by the corresponding amount of energy. Accordingly the probability of interaction of an energy transfer  $\epsilon_i$  is

$$p_i \sim \epsilon_i \int_0^\infty t_D(x)\gamma(x) dx \quad (162)$$

where  $t_D(x)$  is a proximity function that includes the trivial dose-dependent term that is due to independent particle tracks:

$$t_D(x) = t(x) + 4\pi x^2 \rho D \quad (163)$$

It is practical to normalize  $\gamma(x)$  so that its integral over the whole space is unity:

$$\int_0^\infty \gamma(x)4\pi x^2 \rho dx = 1 \quad (164)$$

One then obtains

$$p_i = k\epsilon_i \left[ \int_0^\infty t_D(x)\gamma(x) dx + D \right] \quad (165)$$

The yield  $E(D)$  of lesions, arbitrarily normalized to unit mass, is then

$$E(D) = kD \left( \int_0^\infty t(x)\gamma(x) dx + D \right) = k(\xi D + D^2) \quad (166)$$

The essential result is that, with the proximity concept in the same way as with the site concept, one obtains a linear-quadratic dose dependence. The coefficient  $\xi$  of the linear term is, as with the site concept, a measure of an *effective local concentration* of energy transfers in the individual charged particle tracks of the radiation.

One can consider the earlier result for the site concept as a special case of the present formula. Assume that an energy transfer has constant interaction probability with all transfers within the same site, and zero interaction probability with transfers outside the site. The geometric reduction factor  $U(x)$  is the probability that a neighboring transfer at distance  $x$  is within the site. The interaction probability  $\gamma(x)$  is therefore proportional to  $U(x)$ . Inserting  $\gamma(x) = U(x)/\int 4\pi x^2 \rho U(x) dx = U(x)/m$  into Eq. (166) one obtains

$$\begin{aligned} E(D) &= kD \left( \int_0^\infty t(x)U(x) dx/m + D \right) \quad (m = \text{mass of the site}) \\ &= k(\xi D + D^2) \end{aligned} \quad (167)$$

This is the earlier result for the site concept.

In reality both the site and the proximity aspect may jointly play a role. The function  $\gamma(x)$  is then the product of two terms representing the inherent dependence on distance and the influence of the geometry of the site,  $\gamma(x) = g(x) \cdot U(x)$ . In an experiment it may be difficult to separate the two factors and the aim of a biophysical investigation is therefore to determine the compound function  $\gamma(x)$ .

The above considerations can serve as a frame of reference, but it is evident that additional factors play a role. There can, for example, be an inherently linear component in the dependence of the effect on  $z$ , and it is certain that the quadratic term in absorbed dose is, unlike the linear intratrack term, dependent on dose rate. In spite of such added complexities the formulation in terms of the proximity function leads to definite conclusions when applied to experiments with correlated heavy particles [83, 84]. It is found that  $\gamma(x)$  decreases sharply at small distances, but reaches out to distances of the order of several micrometers. The result is in line with the relatively high efficiency of low-energy photons [85–89], and it illustrates the need for the analysis in terms of the proximity concept.

## APPENDIX: Algorithm for the Compound Poisson Process

### A. SOLUTION BY SUCCESSIVE CONVOLUTIONS

The function  $f_i(x)$  is the density of the spectrum of the Poisson process. In the application of this section  $f_i(x)$  equals the function  $f_i(z)$ . In the application to the energy-loss-straggling problem

$f_1(x)$  stands for the collision spectrum  $f_c(\epsilon)$ . The symbol  $x$  is used for the variable of the Poisson process to avoid the impression that the algorithm is linked to a particular application.

The spectrum  $f_1(x)$  can extend over several orders of magnitude of the variable  $x$ . It is therefore essential that the convolution is executed on a logarithmic scale.

The solutions  $f(x)$  correspond to the dose-dependent distributions  $f(z; D)$  or to the straggling distributions  $f(\epsilon; \Delta)$ . The solutions have a finite component at  $x = 0$ :

$$f_0 = \exp(-n) \quad (n = \text{mean event number}) \quad (\text{A.1})$$

The remaining density  $f(x)$  contains no zero component and its norm is  $(1 - f_0)$ .

For the initial approximation a suitable, small mean event number  $\epsilon$  is chosen and the solution is approximated by

$$f_0 = (1 - \epsilon), \quad f(x) = \epsilon \cdot f_1(x) \quad (\text{A.2})$$

Each of the successive convolutions then replaces

$$f_0 \quad \text{by} \quad f_0^2 \quad (\text{A.3a})$$

and

$$f(x) \quad \text{by} \quad 2f_0 \cdot f(x) + f(x) * f(x) \quad (\text{A.3b})$$

This is continued until the desired mean event number and, accordingly, the desired mean value  $\bar{x}$  are reached.

In the computer code  $f_0$  is a scalar and  $f(x)$  is represented by an array:

$$F(L) = f(x), \quad L = 1 \text{ to } N \quad (\text{A.4})$$

where

$$x = x_0 \cdot X(L) \quad \text{with} \quad X(L) = 2^{L/N} = \exp(L \cdot U), \quad U = \ln(2)/N_2 \quad (\text{A.5})$$

and  $N_2$  is the integer number of grid points in an interval that corresponds to a factor of two of the random variable. One needs then  $N_2 \ln(10)/\ln(2) = 3.3N_2$  points per decade of the random variable. A typical value for the start of the procedure is  $N_2 = 8$ ; common microdosimetric spectra can then be represented by arrays with a length  $N$  of 100 to 150.

As the convolutions proceed insignificant tails of the array  $F(L)$  are cut and the parameters  $N$  and  $x_0$  are adjusted. When the arrays become too short, for example if their length falls below 60,  $N_2$  is doubled and  $F(L)$ ,  $X(L)$ , and certain auxiliary arrays that are required in the convolution are recalculated.

The convolution is the only nontrivial step in the algorithm. It is therefore considered in detail, and a BASIC version of the subroutine is included.\* The formula for the convolution is

$$h(x) = \int_{x_0}^x f(x - s)f(s) ds = 2 \int_{x_0}^{x/2} f(x - s)f(s) ds \quad (\text{A.6})$$

Changing to the new variable

$$L = \ln(x/x_0)/U, \quad x = x_0 \exp(L \cdot U) \quad (\text{A.7})$$

\*A FORTRAN listing was given in an earlier report [33] with the first description of the algorithm.

and using the functions

$$\left. \begin{aligned} H(L) &= h(x) \\ F(L) &= f(x) \\ X(L) &= \exp(L \cdot U) = x/x_0 \end{aligned} \right\} \quad \text{for } 0 \leq L \leq N \quad (\text{A.8})$$

one obtains from Eq. (A.6) with  $ds = x_0 \cdot U \cdot X(K) dK$

$$H(L) = 2x_0U \int_0^{L-N_2} F(W)F(K)X(K) dK \quad (\text{A.9})$$

with

$$\begin{aligned} W &= \ln[(x - s)/x_0]/U \\ &= \ln[\exp(L \cdot U) - \exp(K \cdot U)]/U \\ &= L + \ln[1 - \exp((K - L) \cdot U)]/U \\ &= L - A(K - L) \end{aligned} \quad (\text{A.10})$$

where

$$A(J) = -\ln[1 - \exp(J \cdot U)]/U \quad (\text{A.11})$$

is an auxiliary function. To reduce computing time in the necessary interpolation  $A(J)$  is split into its integer part  $\text{IN}(J)$  and its fractional part  $\text{FR}(J)$ .

With the additional convention  $FX(K) = F(K) \cdot X(K)$  one has the integral

$$\begin{aligned} H(L) &= 2x_0U \int_{K_0}^{L-N_2} F(L - \text{IN}(L - K) - \text{FR}(L - K)) FX(K) dK \\ &\quad \text{for } N_2 \leq L \leq N + N_2 \end{aligned} \quad (\text{A.12})$$

with

$$K_0 = \begin{cases} 0 & \text{for } L \leq N \\ \max[0, L - A(L - N)] & \text{for } L \leq N \end{cases} \quad (\text{A.13})$$

In the actual computation this is substituted by the sum

$$H(L) = 2x_0U \sum_{K_0}^{L-N_2} [P \cdot F(J-1) + (1-P) \cdot F(J)] \cdot FE(K) \quad (\text{A.14})$$

with

$$P = \text{FR}(L - K) \quad J = L - \text{IN}(L - K) \quad (\text{A.15})$$

Only half of the last term ( $K = L - K_2$ ) is included in the sum.

The following BASIC subroutine returns the array  $H(L)$  with  $L \times 1$  to  $N$ . The parameter  $x_0$  is, accordingly, replaced by  $2x_0$ .

```

REM SUBROUTINE *** CONVOLUTION ***
FOR L = 1 TO N: FX(L) = F(L) * X(L): NEXTL:
    C = X0 * U * 2: F(N + 1) = 0
FOR LL = 1 TO N L = LL + N2: H = 0 K0 = 1
IF L > N THEN K0 = L - IN%(L - N) - 1
IF K0 < 1 THEN K0 = 1
FOR K = K0 TO LL: LK = L - K: P = FR(LK):
    I = L - IN%(LK)
    S = (P * F(I - 1) + (1 - P) * F(I)) * FX(K):
    H = H + S: NEXT K
H(LL) = C * (H - S/2):   NEXTLL:   RETURN

```

```

REM SUBROUTINE *** AUXILIARY FUNCTIONS ***
LM = 2 * N: FOR L = 1 TO LM: X(L) = EXP(L * U):
A = LOG(1 - EXP(-U * L))/U: IN%(L) = INT(A):
    FR(L) = A - IN%(L)
NEXTL: X(0) = 1:      RETURN

```

## B. SIMULATION OF SPECIFIC ENERGY DISTRIBUTIONS

The method of successive convolutions permits the computation of the distribution of specific energy for a given dose. If, as in the computations for Figs. 12 to 14, values of specific energy are required for many different values of absorbed dose, simulations can be more efficient. A fast method to perform such simulations is therefore described.

As explained in the first part of this Appendix, the single-event distribution  $f_i(z)$  is represented by an array on a logarithmic scale of  $z$ . The integral distribution is then computed on the same scale, but in contrast to the usual convention it is summed from the tail:

$$S_i(z) = \text{Prob}\{z \geq z\} = 1 - F_i(z) \quad (\text{A.16})$$

Taking the example of 15-MeV neutrons and a 6- $\mu\text{m}$  spherical site and plotting  $\ln(S_i)$  versus  $\ln(z)$  one obtains the lowest curve in Fig. 30.

When a random variable  $z$ , with sum distribution  $S_i(z)$ , is to be generated, the familiar procedure is to choose a random value  $S_i$ , uniformly distributed between 0 and 1, and to select the corresponding  $z$ . The simulation requires, therefore, the reciprocal of the sum distribution. For this purpose values of  $z$  corresponding to a logarithmic grid of the probabilities are stored in an array:

$$z(L) \quad (L = 0 \text{ to } LL), \quad \text{with corresponding probabilities } S_i = \exp(-L/M) \quad (\text{A.17})$$

With  $LL = 200$  and  $M = 16$  one covers, in this way, the range of probabilities 1 to  $3.7 \times 10^{-6}$ .

To obtain a value of specific energy for one event, one generates a random number  $S$ , uniformly distributed between 0 and 1, and sets  $L = -\ln(S) \cdot M$ .\* With proper interpolation one obtains then from the array  $z(L)$  the random value  $z$ .

\*Computing times can be reduced by utilizing fast algorithms to generate exponentially distributed random variables without computation of a logarithm.

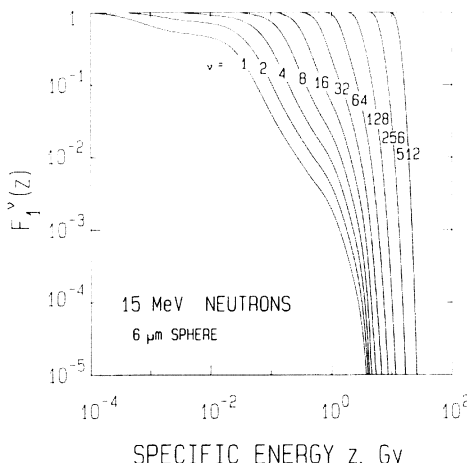


**Fig. 30.** Sum distributions  $1 - F(z)$  for a spherical tissue region of 6- $\mu\text{m}$  diameter exposed to 15-MeV neutrons. Such curves are used for the fast simulation of specific energy. The event numbers are indicated as parameters.

Simulation of random paths, such as in Fig. 10, is the naive method to obtain random values of  $z$  at specified absorbed dose  $D$ . A random path is a succession of random steps of  $D$  and  $z$ . The random steps of dose are generated by choosing a random number  $S$  and setting  $\Delta D = -\ln(S) \cdot \bar{a}_F$ ; this corresponds to the sum distribution,  $S = \exp(-\Delta D/\bar{z}_F)$ , of doses  $\Delta D$  to the next event. The random steps of  $z$  are obtained as described above. The process is continued until the specified dose  $D$  is reached.

The simulation of a large number of events is, however, too uneconomical. Instead one utilizes sum distributions of  $z$  obtained by successive convolutions. These distributions that correspond to the event numbers  $2^N$  are also shown in Fig. 30. They are stored in the same way as the single-event distribution.

For a given absorbed dose one computes first the expected event number  $D/\bar{z}_F$ . Using the inverse of the Poisson distribution one selects then a random event number that belongs to this mean value. (For large values one uses the Gauss distribution.) The resulting event number is split into integer powers of 2. For each of the powers a random value of specific energy is selected and the values are added. The result is a random value of specific energy belonging to the dose  $D$ .

#### REFERENCES

1. International Commission on Radiation Units and Measurements. "Radiation Quantities and Units," ICRU Rep. 33. ICRU, Washington, D.C., 1980.
2. Crowther, J. A. Some considerations relative to the action of X-rays on tissue cells. *Proc. R. Soc. London, Ser. B* **96**, 207 (1924).
3. Dessauer, F. Quantenphysik der biologischen Röntgenstrahlen-Wirkungen. *Z. Phys.* **84**, 218 (1933).
4. Timofeeff-Ressowsky, N. V., and Zimmer, K. G. "Das Trefferprinzip in der Biologie." Hirzel, Leipzig, 1947.
5. Lea, D. E. "Actions of Radiations on Living Cells," Cambridge Univ. Press, London and Macmillan, New York, 1946.
6. Rossi, H. H. Specification of radiation quality. *Radiat. Res.* **10**, 522-531 (1959).
7. Rossi, H. H. Spatial distribution of energy deposition by ionizing radiation. *Radiat. Res., Suppl.* No. 2, 290-299 (1960).

8. Rossi, H. H. Energy distribution in the absorption of radiation. *Adv. Biol. Med. Phys.* **11**, 27-85 (1967).
9. Rossi, H. H. Microscopic energy distribution in irradiated matter. In "Radiation Dosimetry" (F. H. Attix and W. C. Roesch, eds.), 2nd Ed., Vol. 1, pp. 43-92. Academic Press, New York, 1968.
10. International Commission on Radiation Units and Measurements. "Microdosimetry," ICRU Rep. 36. ICRU, Bethesda, Maryland, 1983.
11. Charlton, D. E., Booz, J., and Pomplun, E. X-Ray-induction of the Auger effect: Quantification of the different energy-transfer mechanisms and dosimetric implications. *Proc. Symp. Microdosim.*, 8th, Jülich, pp. 611-624. *Comm. Eur. Communities [Rep.] EUR EUR-8395* (1983).
12. Charlton, D. E., and Booz, J. A Monte Carlo treatment of the decay of  $^{125}\text{I}$ . *Radiat. Res.* **87**, 10-23 (1981).
13. Roesch, W. C. Microdosimetry of internal sources. *Radiat. Res.* **70**, 494-510 (1977).
14. Katz, R., and Kobeticich, E. J. Particle tracks in condensed matter. In "Charged Particle Tracks in Solids and Liquids" (G. E. Adams, D. K. Bewley, and J. W. Boag, eds.), Conf. Ser. Inst. Phys. No. 8, pp. 109-119. Inst. Phys. Phys. Soc., London, 1970.
15. Wittendorf-Rechenmann, E., Senger, B., and Rechenmann, R. V. Strong ionizing events produced by medium energy  $\alpha$  particles crossing nuclear emulsion. *Proc. Symp. Microdosim.*, 8th, Jülich, pp. 121-133. *Comm. Eur. Communities [Rep.] EUR EUR-8395* (1983).
16. Budd, T., Marshall, M., and Kwok, C. S. Microdosimetric properties of particle tracks measured in a low-pressure cloud chamber. *Proc. Symp. Microdosim.*, 8th, Jülich, pp. 89-99. *Comm. Eur. Communities [Rep.] EUR EUR-8395* (1983).
17. Paretzke, H. G. Comparison of track structure calculations with experimental results. *Symp. Microdosim. Proc.*, 4th, Verbania-Pallanza, Italy, 1973 **1**, 141-165. *Comm. Eur. Communities [Rep.] EUR EUR-5122 d-e-f* (1974).
18. Berger, M. J. Some new transport calculations of the deposition of energy in biological materials by low-energy electrons. *Symp. Microdosim. Proc.*, 4th, Verbania-Pallanza, Italy, 1973 **2**, 695-711. *Comm. Eur. Communities [Rep.] EUR EUR-5122 d-e-f* (1974).
19. Terrissol, M., Patau, J. P., and Eudaldo, T. Application à la microdosimétrie et à la radiobiologie de la simulation du transport des électrons de basse énergie dans l'eau à l'état liquide. *Symp. Microdosim.*, 6th, Brussels, **1**, 169-178. *Comm. Eur. Communities [Rep.] EUR EUR-6064 d-e-f* (1978).
20. Han, A., and Elkind, M. M. Transformation of mouse C3H/10T 1/2 cells by single and fractionated doses of X rays and fission spectrum neutrons. *Cancer Res.* **39**, 123-130 (1979).
21. International Commission on Radiation Units and Measurements. "Linear Energy Transfer," ICRU Rep. 16. ICRU, Washington, D.C., 1970.
22. Kellerer, A. M., and Chmelevsky, D. Criteria for the applicability of LET. *Radiat. Res.* **63**, 226-234 (1975).
23. Glass, W. A., and Gross, W. A. Wall-less detectors in microdosimetry. In "Radiation Dosimetry, Suppl. 1, Topics in Radiation Dosimetry" (F. H. Attix, ed.), pp. 221-260. Academic Press, New York, 1972.
24. Kellerer, A. M., and Chmelevsky, D. Concepts of microdosimetry. I. Quantities. *Radiat. Environ. Biophys.* **12**, 61-69 (1975); Kellerer, A. M., and Chmelevsky, D. Concepts of microdosimetry. II. Probability distributions of the microdosimetric variables. *Radiat. Environ. Biophys.* **12**, 205-216 (1975); Kellerer, A. M., and Chmelevsky, D. Concepts of Microdosimetry. III. Mean values of the microdosimetric distributions. *Radiat. Environ. Biophys.* **12**, 321-335 (1975).
25. Zaider, M., and Brenner, D. J. Microdosimetry and radiation chemistry. *Proc. Int. Congr. Radiat. Res.*, 7th, Amsterdam, E1-22 (1983). M. Nijhoff Publ.
26. Kellerer, A. M., and Rossi, H. H. a generalized formulation of dual radiation action. *Radiat. Res.* **75**, 471-488 (1978).

27. Brenner, D. J., and Zaider, M. The soft X-ray Experiment revisited—A theoretical approach. *Proc. Symp. Microdosim., 8th, Jülich*, pp. 639–649. *Comm. Eur. Communities [Rep.] EUR EUR-8395* (1983).
28. Alm Carlsson, G. This volume.
29. Rossi, H. H., Biavati, M. H., and Gross, W. Local energy density in irradiated tissues. I. Radiobiological significance. *Radiat. Res.* **15**, 431–439 (1961).
30. Kendall, M. G., and Moran, P. A. P. "Geometrical Probability." Griffin, London, 1963.
31. Kellerer, A. M. Considerations on the random traversal of convex bodies and solutions for general cylinders. *Radiat. Res.* **47**, 359–376 (1971).
32. Crofton, M. W. Probability, In "Encyclopaedia Britannica," 9th Ed., 1885; partly contained also in Probability. In "Encyclopaedia Britannica," 11th Ed., 1913).
33. Kellerer, A. M. "Mikrodosimetrie, Grundlagen einer Theorie der Strahlenqualität," Gesellschaft für Strahlenforschung, GSF Ser. Monogr. B1. Munich, 1968.
34. Hug, O., and Kellerer, A. M. "Stochastik der Strahlenwirkung." Springer-Verlag, Berlin and New York, 1966.
35. Bengtsson, L. G. Assessment of dose equivalent from fluctuations of energy deposition. *Symp. Microdosim., 2nd, Stresa, Italy, 1969* pp. 375–395. *Comm. Eur. Communities [Rep.] EUR EUR-4452 d-f-e* (1970).
36. Forsberg, B., and Lindborg, L. Experimental limitations in microdosimetry measurements using the variance technique. *Radiat. Environ. Biophys.* **19**, 125–135 (1981).
37. Kellerer, A. M., and Rossi, H. H. On the determination of microdosimetric parameters in variable radiation fields. The variance-covariance method. *Radiat. Res.* **97**, 237–245 (1984).
38. International Commission on Radiological Protection. "Recommendations of the International Commission on Radiological Protection," ICRP Publ. 26. Vol. I, No. 3, Pergamon, Oxford, 1977.
39. Kellerer, A. M. Parameters of track structure. In "Charged Particle Tracks in Solids and Liquids" (G. E. Adams, D. K. Bewley, and J. W. Boag, eds.), pp. 77–85. Inst. Phys., London, 1970.
40. Rossi, H. H. A proposal for revision of the quality factor. *Radiat. Environ. Biophys.* **14**, 275–283 (1977).
41. Kellerer, A. M., and Rossi, H. H. Biophysical aspects of radiation carcinogenesis. In "Cancer," (F. F. Becker, ed.), 1st ed., Vol. I, pp. 405–439. 1975; 2nd Ed., pp. 569–616. Plenum, New York, 1982.
42. Shellabarger, C. J., Chmelevsky, D., and Kellerer, A. M. Induction of mammary neoplasms in the Sprague-Dawley rat by 430 keV neutrons and X-rays. *J. Natl. Cancer Inst.* **64**, 821–833 (1980).
43. Shellabarger, C. J., Chmelevsky, D., Kellerer, A. M., Stone, J. P., and Holtzman, S. Induction of mammary neoplasms in the ACI rat by 430 keV neutrons, X-rays, and diethylstilbestrol. *Natl. Cancer Inst.* **69**, 1135–1146 (1982).
44. Nearn, G. J., Preston, R. Y., and Savage, J. R. K. Chromosome aberrations and the theory of RBE. III. Evidence from experiments with soft X-rays and a consideration of the effects of hard X-rays. *Int. J. Radiat. Biol.* **12**, 317–345 (1967).
45. Kellerer, A. M., and Rossi, H. H. The theory of dual radiation action. *Curr. Top. Radiat. Res. Q.* **8**, 85–158 (1972).
46. Landau, L. J. *Phys. (Moscow)* **8**, 201 (1944).
47. Vavilov, P. V. *Zh. Exp. Teor. Fiz.* **32**, 920 (1957). [*Sov. Phys.—JETP (Engl. Transl.)* **5**, 749 (1957)].
48. Maccabee, H. D. Fluctuations of energy loss by heavy charged particles in thin absorbers. *Phys. Rev.* **165**, 469–474 (1968).

49. Kellerer, A. M. Analysis of patterns of energy deposition. A survey of theoretical relations in microdosimetry. *Symp. Microdosim. 2nd, Stresa, Italy, 1969* pp. 107–134. *Comm. Eur. Communities [Rep.] EUR EUR-4452 d-f-e* (1970).
50. Caswell, R. S. Deposition of energy by neutrons in spherical cavities. *Radiat. Res.* **27**, 92–107 (1966).
51. Caswell, R. S., and Coyne, J. J. Microdosimetric spectra and parameters of fast neutrons. *Proc. Symp. Microdosim., 5th, Verbania*, **1**, 97–123. *Comm. Eur. Communities [Rep.] EUR EUR-5452 d-e-f* (1976).
52. Caswell, R. S., and Coyne, J. J. Energy deposition spectra for neutrons based on recent cross section evaluations. *Symp. Microdosim., 6th, Brussels* **2**, 1159–1171. *Comm. Eur. Communities [Rep.] EUR EUR-6064 d-e-f* (1978).
53. Chmelevsky, D., Kellerer, A. M., Terrissol, M., and Patau, J. P. Proximity functions for electrons up to 10 keV. *Radiat. Res.* **84**, 219–238 (1980).
54. Berger, M. J. Spectrum of energy deposited by electrons in spherical regions. *Symp. Microdosim., 2nd, Stresa, Italy, 1969* pp. 541–559. *Comm. Eur. Communities [Rep.] EUR EUR-4452 d-f-e* (1970).
55. Paretzke, H. G. Advances in energy deposition theory. In “Advances in Radiation Protection and Dosimetry in Medicine” (R. H. Thomas and V. Perez-Mendez, eds.), p. 51, Plenum, New York, 1980.
56. Burger, G., Combecher, D., Kollerbaur, J., Leuthold, G., Ibach, T., and Paretzke, H. G. Experimental and theoretical ion track structure investigations and its implication for radiation quality. *Proc. Symp. Microdosim., 7th, Oxford, 1980* **1**, 537–547. *Comm. Eur. Communities [Rep.] EUR EUR-7147 d-e-f* (1981).
57. Wilson, W. E., and Paretzke, H. G. Spatial dependence of frequency distributions in ionization and energy imparted in nanometer volumes by 0.25 to 3 MeV protons. *Proc. Symp. Microdosim., 7th, Oxford*, **1**, 423–434. *Comm. Eur. Communities [Rep.] EUR EUR-7147 d-e-f* (1981).
58. Turner, J. E., Paretzke, H. G., Hamm, R. N., Wright, H. A., and Ritchie, R. H. Comparison of electron transport calculations for water in the liquid and vapor phases. *Proc. Symp. Microdosim., 8th, Brussels*, pp. 175–185. *Comm. Eur. Communities [Rep.] EUR EUR-8395* (1983).
59. Paretzke, H. G. Concepts of charged particle track structures. *Proc. Symp. Microdosim., 8th, Jülich*, pp. 67–77. *Comm. Eur. Communities [Rep.] EUR EUR-8395* (1983).
60. Wright, H. A., Turner, J. E., Hamm, R. N., and Ritchie, R. H. Physical and chemical evolution of an electron track in liquid water. *Proc. Symp. Microdosim., 8th, Jülich*, pp. 101–109. *Comm. Eur. Communities [Rep.] EUR EUR-8395* (1983).
61. Booz, J., and Coppola, M. Studies in radiation biophysics and microdosimetry. In “Annual Report of the Joint Research Center,” EUR-5260, p. 396. Comm. Eur. Communities, Luxembourg, 1974.
62. Chmelevsky, D. Distributions et moyennes des grandeurs microdosimétriques à l'échelle du nanomètre. *Rapp CEA-R—Fr., Commiss. Energ. At. CEA-R-4785* (1976).
63. Santaló, L. A. “Introduction to Integral Geometry.” Herman, Paris, 1953.
64. Serra, J. “Image Analysis and Mathematical Morphology.” Academic press, New York, 1982.
65. Chmelevsky, D., and Kellerer, A. M. Computation of microdosimetric distributions for small sites. *Radiat. Environ. Biophys.* **14**, 123–136 (1977).
66. Kliauga, P., and Dvorak, R. Microdosimetric measurements of ionization by monoenergetic photons. *Radiat. Res.* **73**, 1–20 (1978).
67. Coleman, R. “An Introduction to Mathematical Stereology,” Mem. Ser. Dep. Theor. Stat., Inst. Math., Aarhus Univ., Denmark, 1979.
68. Kellerer, A. M. Chord-length distributions and related quantities for spheroids. *Radiat. Res.*